SINGLE-WELL MODELING OF COALBED METHANE PRODUCTION

A Thesis

by

ELENA MARTYNOVA

Submitted to the Office of Graduate and Professional Studies of
Texas A&M University
in partial fulfillment of the requirements for the degree of

MASTER OF SCIENCE

Chair of Committee,	Peter P. Valko
Committee Members,	Walter B. Ayers
	Maria A. Barrufet
Head of Department,	A. Daniel Hill

May 2014

Major Subject: Petroleum Engineering

ABSTRACT

The presented study concerns the unconventional coal bed methane (CBM) fields that imply peculiarity of their evaluation. The theoretical basis of the CBM field development is briefly described, most widely known models of changes in the properties of the coal seam are considered.

The study objective was formulation of a computation framework based on material balance equation and incorporating non-equilibrium nature of gas desorption, matrix shrinkage and geomechanically dependent relative permeability curves. Further solution of a specific CBM single-well problem and parametric study for evaluation impact of separate parameters were conducted.

Focus of the studies was on well production forecasting, effect of mechanical properties of coal on production efficiency, comparison of the analytical models performance based on specific mathematical models for absolute and relative permeabilities and residual saturations.

Numerical simulation is not flexible and easy to understand, therefore other tools are needed in order to try out the newly proposed mathematical models of processes occurring during CBM production. For desorption controlled reservoirs, considering non-equilibrium nature of desorption has to be essential, otherwise the production can be significantly overestimated. The currently proposed models have significant drawbacks, since they have to be heavily adapted to give similar results, being based on experimental results with limited pressures.

DEDICATION

I lovingly dedicate this thesis to my parents, who have supported me each step of the way, and who truly believe this degree is important.

ACKNOWLEDGEMENTS

I would like to thank my committee chair, Dr. Valko, and my committee members, Dr. Ayers and Dr. Barrufet, for their guidance and support throughout the course of this research. Thanks also go to my TAMU friends and the department faculty and staff for making my time at Texas A&M University a great experience.

I also want to extend my gratitude to the faculty and staff of Gubkin University of oil and gas, who have provided me with a great educational basis and also helped me to go through with this research. My special thanks goes to Petr V. Pyatibratov, Maria P. Haidina, Natalya M. Zazovskaya and Anatoly B. Zolotukhin, who were willing to answer my questions and support me. I am very grateful for your participation.

Dear family and friends, some who have been waiting for me for so long back at home and others, who shared with me all the heartaches in College Station, - thank you for your patience, love and will to take me through this time.

TABLE OF CONTENTS

Page

ABSTRACT ii

DEDICATION iii

ACKNOWLEDGEMENTS iv

TABLE OF CONTENTS v

LIST OF TABLES vii

LIST OF FIGURES viii

CHAPTER I INTRODUCTION 1

Principal Concepts and Definitions 2
Objectives 11
Problem Statement 12

CHAPTER II LITERATURE REVIEW ON THE APPLIED CONCEPTS 14

Essential Theoretical Background on Absorption, Diffusion and Permeability 14
Material Balance Method as an Engineering Instrument 30
CBM Modeling Approaches 35

CHAPTER III PROBLEM STATEMENT AND SOLUTION DESCRIPTION 43

Framework for Model Developed 43
Model Comparison with Available Commercial Software 65

CHAPTER IV RESULTS AND DISCUSSION 69

Base Case Description and Results 69
Considering Different Shape Factor J Expressions 77
Considering the Impact of Non-Equilibrium Nature of Diffusion on Coal Deformation 80
Gas Production at Constant Pressure Drawdown, ($p-p_{wf}$) 84
Parametric Sensitivity Study 90
Possibility for Application in Optimization 119

Page

Results of Comparison Runs with F.A.S.T. CBM and the Proposed Single-Well Analytical Model 122
Discussion 131

CONCLUSIONS 134

NOMENCLATURE 136

REFERENCES 141

APPENDIX CODE FOR BASE CASE IN MATHEMATICA SOFTWARE PACKAGE 152

LIST OF TABLES

Page

Table 1. ASTM coal rank classification 4

Table 2. Coal seam vs. conventional reservoir (modified from Fekete associates, 2012). 12

Table 3. Comparison of permeability models (modified from Shi and Durukan, 2004) .26

Table 4. The comparison of F.A.S.T. CBM semi-analytical model and our model 68

Table 5. Input parameters used for the base case 70

Table 6. Properties variation 94

Table 7. Sensitivity summary 118

Table 8. OGIP estimations 125

LIST OF FIGURES

Page

Figure 1. Gas content of maturing coals (from Kim, 1977) 6

Figure 2. Coalbed methane gas storage mechanism and production (from Al-Jubori et al., 2009) 8

Figure 3. Example of a Langmuir Isotherm (modified from Mavor et al., 1996) 16

Figure 4. Desorption behaviour of under-saturated CBM reservoirs (modified from Morad et al., 2008). 51

Figure 5. Schematic representation of a) bundle of capillaries geometry (from Gates and Lietz, 1950); b) matchstick geometry (from Seidle et al., 1992) 57

Figure 6. Effect of permeability magnitude on typical shapes of capillary pressure curves (modified from Purcell, 1949) 59

Figure 7. Flowchart of the forecasting process realized 64

Figure 8. The applied Langmuir isotherm characterising gas content of coal 71

Figure 9. a) Gas and water rates (base case); b) Cumulative gas and water production (base case) 72

Figure 10. a) Gas and water relative permeabilities vs time (base case); b) Gas and water relative permeabilities vs water saturation (base case) 72

Figure 11. a) Absolute permeability change vs time (base case); b) Absolute permeability change vs average water pressure (base case) 73

Figure 12. a) Gas and water pressures (base case); b) Actual non-equilibrium cumulative desorbed gas volume (base case) 73

Figure 13. Residual and current water saturations (base case) 74

Figure 14. Relative permeability curves calculated for different times 76

Figure 15. Shape factor J approximations 78

Figure 16. Comparison of results from runs with application of different shape factor J trend lines 79

Page

Figure 17. a) Absolute permeability change for equilibrium-based volumetric strain change; b) Absolute permeability for equilibrium based volumetric strain change 82

Figure 18. a) Porosity (cleat) change for equilibrium-based volumetric strain change; b) Porosity (cleat) for equilibrium based volumetric strain change 82

Figure 19. Effect of including non-equilibrium nature of desorption in considering coal deformation 83

Figure 20. Comparison of constant wellbore flowing pressure and constant pressure drawdown regimes 86

Figure 21. a) Pressure drawdown; b) Effect of initial pressure drawdown on wellbore flowing pressure 88

Figure 22. Effect of initial pressure drawdown on a) gas rate; b) cumulative gas production 89

Figure 23. Effect of initial pressure drawdown on a) absolute permeability change; b) average water pressure 89

Figure 24. Effect of initial pressure drawdown on absolute permeability change vs average water pressure 90

Figure 25. Effect of diffusion time on gas rate 97

Figure 26. Effect of diffusion time on cumulative gas production 97

Figure 27. Effect of diffusion time on average water pressure 98

Figure 28. Effect of coal cleat compressibility on a) gas rate; b) cumulative gas production 100

Figure 29. Effect of coal cleat compressibility on absolute permeability as a function of a) average water pressure; b) time 100

Figure 30. Effect of coal cleat compressibility on average water pressure 101

Figure 31. The effect of Langmuir volumetric strain on a) gas rate; b) cumulative gas production 102

Page

Figure 32. Effect of Langmuir volumetric strain on a) absolute permeability; b) average water pressure 103

Figure 33. Effect of Poisson's ratio on a) gas rate; b) cumulative gas production 104

Figure 34. Effect of Poisson's ratio on absolute permeability change as a function of a) average water pressure; b) time 104

Figure 35. Effect of Poisson's ratio on average water pressure 105

Figure 36. Effect of Young's modulus on a) gas rate; b) cumulative gas production 106

Figure 37. Effect of Young's modulus on absolute permeability change as a function of a)average water pressure; b) time 107

Figure 38. Effect of Young's modulus on average water pressure 107

Figure 39. Effect of pore size distribution index on a) gas rate; b) cumulative gas production 108

Figure 40. Effect of pore size distribution index on a) permeability change; b) average water pressure 108

Figure 41. Effect of initial absolute permeability on a) gas rate; b) cumulative gas production 109

Figure 42. Effect of initial absolute permeability on absolute permeability change as a function of a) average water pressure; b) time 110

Figure 43. Effect of initial absolute permeability on average water pressure 110

Figure 44. Effect of initial residual water saturation on a) gas rate; b) cumulative gas production 111

Figure 45. Effect of initial residual water saturation on a) water rate; b) cumulative water production 111

Figure 46. Effect of initial residual water saturation on absolute permeability change as a function of a) average water pressure; b) time 112

Figure 47. Effect of initial residual water saturation on average water pressure 112

Figure 48. Effect of wellbore radius on a) gas rate; b) cumulative gas production 113

Page

Figure 49. Effect of wellbore radius on permeability change as a function of a) average water pressure; b) time 114

Figure 50. Effect of wellbore radius on average water pressure 114

Figure 51. Effect of skin-factor on a) gas rate; b) cumulative gas production 115

Figure 52. Effect of skin-factor on permeability change as a function of a) average water pressure; b) time 115

Figure 53. Effect of skin-factor on average water pressure 116

Figure 54. Effect of wellbore flowing pressure on a) gas rate; b) cumulative gas production 117

Figure 55. Effect of wellbore flowing pressure on a) permeability change; b) average water pressure 117

Figure 56. Wellbore flowing pressure optimization 120

Figure 57. Effect of dimensionless productivity index on a) gas rate; b) gas recovery 121

Figure 58. Langmuir isotherms constructed in a) proposed single-well analytical model; b) F.A.S.T. CBM 123

Figure 59. Permeability ratio constructed in F.A.S.T. CBM 124

Figure 60. Relative permeability applied in F.A.S.T. CBM simulation runs 125

Figure 61. F.A.S.T. CBM production forecast: a)gas and water rates; b) cumulative gas and water production 126

Figure 62. F.A.S.T. CBM production forecast: average reservoir pressure 126

Figure 63. Forecasted gas rate: F.A.S.T. CBM comparison with different runs of the single-well analytical model (variable τ, λ, η) 128

Figure 64. Forecasted gas rate: F.A.S.T. CBM comparison with different runs of the single-well analytical model (variable τ, λ, η) 129

Figure 65. Permeability change with pressure drawdown applied in F.A.S.T. CBM for run with c_f=0.1 MPa^{-1} 130

Page

Figure 66. Gas and water rates for c_f=0.1 MPa^{-1} runs predicted in a) the proposed single-well analytical model; b) F.A.S.T. CBM 131

CHAPTER I

INTRODUCTION*

In recent years, the energy industry has actively embraced unconventional resources. The future of these resources can be assessed in different ways, but it is undeniable that the development of this industry already has significantly affected the prices of hydrocarbons, and therefore, unconventional resources require proper attention.

Being dangerous to the coal mining industry, methane shows in coal have been known for a long time, and several methods for coal degasification have been used. However, CBM has only recently become an important commercial energy. Major CBM reserves occur in Russia, USA, China, Australia, Canada, UK, India, Ukraine and Kazakhstan. The largest, knowledgeable and most well-known centers of this sector, scientific and production, are situated in the USA, China, Australia and India.

Coal bed methane (CBM) is one type of unconventional resource. Huge reserves of coal occur around the world and are well described from a geological point of view, and most of these coals contain gas at different saturations. However, sufficient gas content for commercial production occurs only in appropriate geological settings (Al-Jubori et al., 2009).

Rapid development of technology to recover CBM in an economically efficient and environmentally safe manner will strongly impact the global energy industry. In the

*Part of the data reported in this chapter is reprinted with permission from "Coalbed Methane: Clean Energy for the World" by Al-Jubori et al, 2009. Oilfield Review, 21(2), p.7, Copyright 2009 by Schlumberger.

USA, CBM has already earned its place in the energy industry. The USA experience shows it is possible to profitably develop CBM projects. However, current CBM recovery technologies can be improved significantly. There is no common solution applicable to all fields, since each coal has unique properties that should be understood to apply appropriate development technology.

The first chapter includes principal concepts and definitions, comparison of coal beds and conventional gas reservoirs, and research objectives.

Principal Concepts and Definitions

By definition, coal is a rock having a concentration of organic compounds exceeding 50 % in weight and 70 % in volume, since the density of organics is lower than that of ash content. It is a heterogenous mixture of components, including organic matter, water, gas and mineral matter.

Over the years peat accumulates in low-energy environments such as marshes and swamps, where redundant organic matter is present. Peat is buried by sediments and with time is compacted by the weight of upper layers. Under the influence of pressure and temperature that increase with depth plant debris forms a friable combustible denser rock with different gas content depending on its maturity and quality. The combination of the chemical and physical processes changing the organic matter is referred to as coalification. As coal progresses in rank volatile matter is expelled. In the process of coalification the coal shrinks, forming coal blocks separated by the created natural fracture (cleat) system. The cleat system contains the primary face cleats and the right

angle secondary butt cleats. The microporous coal blocks are called the matrix. Understanding the spatial distribution and geometries of the natural fracture system is important because it provides the principal mechanism for permeability.

Being formed in variable conditions, coals may have very different characteristic environments and physical, mechanical, and chemical properties .

Depositional history of the coal beds affects their characteristics such as thickness and lateral extent; continuity of coal beds; coal properties (grade, type and rank); coal permeability (or natural fracturing).

Coals are usually classified into grades (according to relative percentage of organic to mineral components), types (according to organic component composition) and ranks (according to level of maturity).

1. *Coal grade* measures the coal quality and is defined by the ratio of the total organic content (TOC) to the mineral content. Only organic material has potential to adsorb significant quantities of gas.

2. *Coal type* is determined by the types of active organic carbons (macerals). The rest is mineral matter called ash that will not produce any hydrocarbons. Macerals are tiny organic particles of different origin, chemical composition and optical properties.

3. *Coal rank* represents the level of coalification or maturation. Coal rank gives the idea of gas content potential (storage capacity of coal), permeability, mechanical and physical properties of coal. Three properties are used to designate rank: carbon content, hydrogen content and volatile matter. Other valid measurements of coal rank include vitrinite reflectance, vitrinite being the most abundant maceral of coal.

Coal rank (Table 1) increases with growth in share of carbon present in it, which indicates greater modification of initial organic material. Therefore, coal rank is proportional to depth and time – being sensitive to temperature and pressure variation. As carbon content increases, hydrogen and oxygen decrease, defining natural processes of coal maturation. However, other variables may influence coal rank.

Table 1. ASTM coal rank classification

Class	Group	Abbreviation
Anthracitic	Meta-Anthracite	ma
	Anthracite	an
	Semianthracite	sa
Bituminous	Low Volatile	lvb
	Medium Volatile	mvb
	High Volatile A	hvAb
	High Volatile B	hvBb
	High Volatile C	hvCb
Sub-bituminous	Subbituminous A	subA
	Subbituminous B	subB
	Subbituminous C	subC
Lignitic	Lignite A	ligA
	Lignite B	ligB

Lignite is a coal in which organic matter has altered further than in peat, but not as significantly as in sub-bituminous coal.

Anthracite is a black coal with more than 92% of fixed carbon (dry, mineral matter-free) that typically has very low permeability due to the compaction increased with burial combined with the highest adsorbed gas content (Mavor et al., 1996).

Although gas storage capacity generally increases with coal rank, the permeability lowers with depth due to compaction and stress. Porosity tend to decrease with rank into the low-volatile bituminous stage of maturation and later to increase due to additional lost volatiles, that leave some pore space open. The pores in coal can be subdivided into macropores, mesopores and micropores. Sub-bituminous to low-volatile bituminous coals are considered to be optimum for commercial production since they combine acceptable reservoir properties with possible significant gas content (company, 2008). An idealized concept of the increase in gas content with rank was shown by Kim (1977) (Figure 1).

Methane and other gases that saturate coal may be generated from a biological process as a result of microbial action (anaerobic fermentation and CO_2 reduction) and from a thermal process as a result of increasing heat with increasing burial depth of the coal (if sufficient burial occurs) (Moore, 2012).

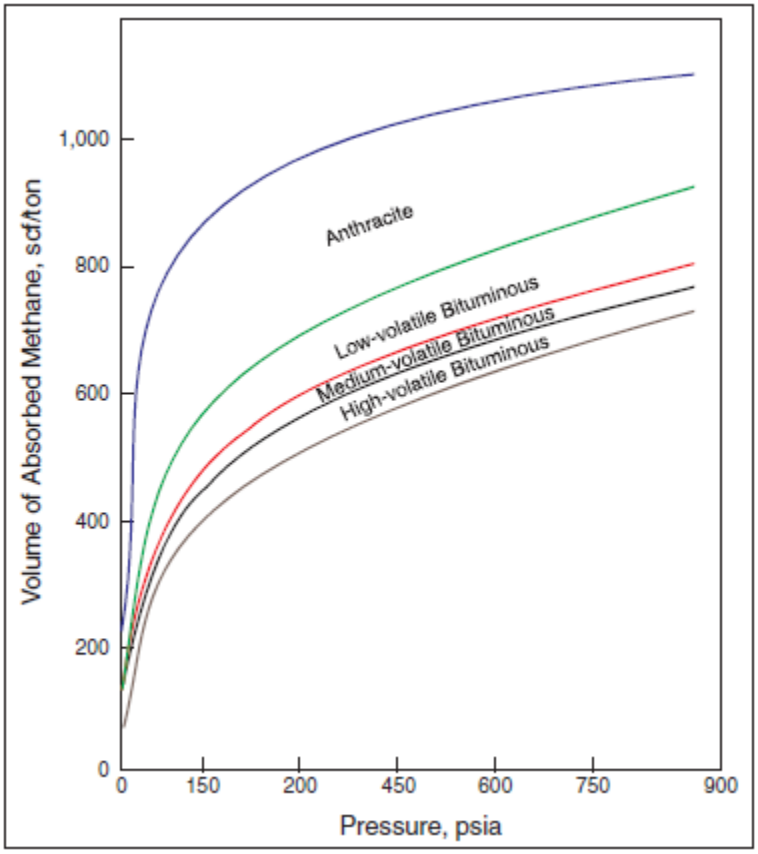

Figure 1. Gas content of maturing coals (modified from Kim, 1977)

Comparison of Coal Beds and Conventional Gas Reservoirs

Coalbed methane fields are the fields comprising continuous coal beds with considerable thickness. CBM reservoirs differ from conventional reservoirs in a number of ways: gas origin, structure, physical and mechanical characteristics, gas storage and transport mechanisms, production performance and behavior.

1. Gas origin.

First, coals may be self-sourcing reservoirs, meaning that secondary migration

is not required (similar to shales), unlike conventional reservoirs. Coal serves both as a source and as a reservoir. Conventional sandstone can only be reservoirs, since they do not contain organic matter, but do have significant porosity and permeability. Methane in coals is generated biogenically (by microbial activity) and by thermal maturation of organics. This characteristic makes understanding the geology of the coal particularly important for evaluating new areas or understanding the production characteristics of a developed area.

2. Gas storage.

One of the most important features distinguishing coal bed methane reservoirs is the gas storage mechanism. In sandstone and carbonate reservoirs, hydrocarbon-storage capacity is defined by porosity; oil and gas are stored in the void volume.

To introduce gas storage mechanism for CBM first we will refer to the internal structure of the coal and then turn to controls of gas storage capacity in coal.

a) Structure and liquid content of coals

Being naturally fractured, coals are usually characterized as dual-porosity systems. The coal matrix contains the primary microporosity, and the cleats provide the secondary macroporosity. Coal structure, gas storage and production mechanism are illustrated in Figure 2.

The coal cleat system generally is orthogonal with one direction terminating against the other. Coal cleat spacing and permeability matter immensely for methane production.

Coal also contains a very fine micropore and mesopore structure that has a very

low flow capacity compared to the coal cleats that have a much greater flow capacity.

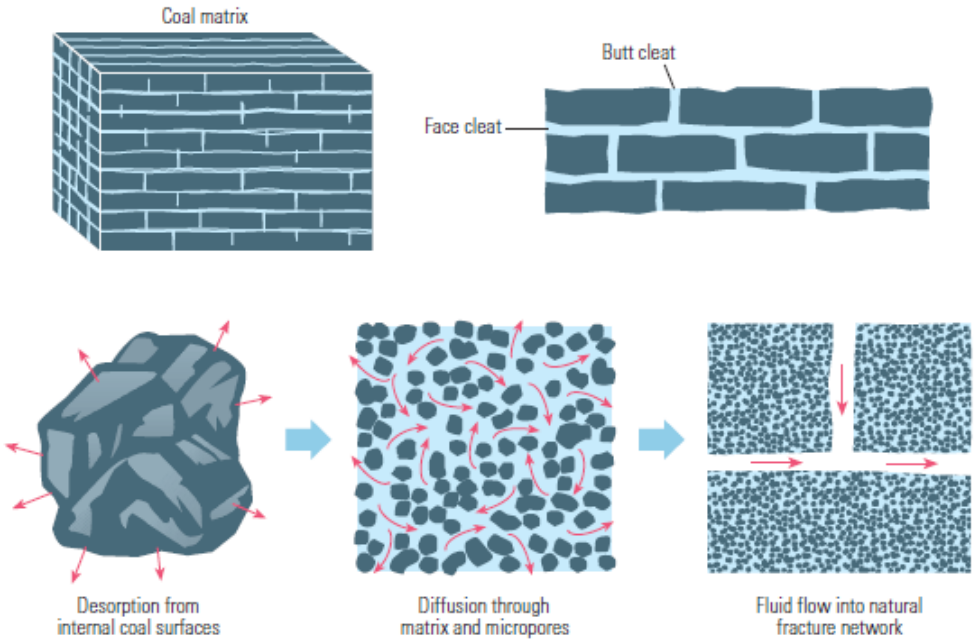

Figure 2. Coalbed methane gas storage mechanism and production (from Al-Jubori et al., 2009) **

The methane is stored in a coal seam in two ways. It can be present as an adsorbed layer on the internal surfaces of the coal micropores, in a near-liquid state, lining the inside of pores of the coal. As a result, coals have immense capacity for gas storage, being limited by actual internal surface area. More than 90% of gas in coal is held in adsorbed state. Additionally, gas can be present within the cleats as free gas within the fracture network (macropores) or gas dissolved in water which often exists in the cleats.

**Figure copyright Schlumberger. Used with permission.

Adsorbed methane (and other gases, since the composition of produced gas is more complex than pure methane, being mixed with heavier hydrocarbons, nitrogen and carbon dioxide) is bound to the organics by Van-der-Waals weak intermolecular forces. Storage capacity in coal is related to the pressure, and adsorbed storage capacity usually described by the Langmuir sorption isotherm that can be determined from crushed samples. Several factors affect adsorption: temperature, moisture content, ash content and gas composition. Those parameters should be accounted for when performing measurements to get trustworthy results. Moisture and ash have negative impact on adsorption. Heavier hydrocarbons and CO_2 are adsorbed more strongly than methane, which makes CO_2 sequestration in coal effective.

Water is stored in coals in two ways: as bound water in the coal matrix and as free water in the coal cleat system. The bound water in coals is formed as a by-product of the coalification process. Matrix bound water is not mobile and has not been shown to significantly affect methane recovery from coal. The free water contained in the cleat system is mobile at high water saturations (greater than thirty percent). Many coal beds are active aquifer systems and thus are 100% water saturated in the cleat system. Coals that are not aquifers may have initial water saturations less than 100 %.

Coal has large gas storage capacity but low matrix permeability, whereas cleats have small gas storage capacity and high permeability. Usually, permeability of coals is defined as the permeability of the cleats, since matrix has negligible permeability.

b) Coal properties

The main properties of the coal influencing its gas storage capacity are the following: coal grade, coal type and coal rank.

For most coal seams, the quantity of gas held in the coal is primarily a function of coal rank, ash content, moisture content, temperature and the pressure of the coal seam.

3. Gas transport mechanism.

In conventional reservoirs gas flow to wellbore is controlled by pressure gradient. In coalbeds gas movement also is a function of concentration. First the desorbed gas diffuses through the coal matrix and enters the cleats and then - driven by pressure gradient - it reaches the wellbore (Figure 2).

4. Production profiles.

Development of CBM fields starts with water production. Gas production commences after dewatering of the reservoir that provides necessary pressure depletion to release gas from the coal surface. Then, the gas diffuses through the matrix, migrates into the fractures, flowing through them to the wellbore. Conventional reservoirs gas production rate is greatest upon initial completion. Water (in case of aquifer support) is produced simultaneously, with rates increasing with time and depletion of the reservoir. Coals, on the contrary, have a "negative decline curve."

5. Physical and mechanical characteristics.

Coal is more compressible than conventional reservoir rocks. The permeability of the CBM formation is more dependent on the stress state and

adsorbed gas.

6. CBM production behavior is difficult to predict or analyze due to its complexity. Partly, because production is governed by the interaction of single-phase gas diffusion through the matrix connected with desorption process and two-phase (gas and water) Darcy flow through the cleat system. Therefore, conventional reservoir engineering techniques cannot be used to predict CBM production behavior, and permeability models need to be improved to incorporate various effects that take place in coals.

More generally the differences between conventional and CBM reservoirs are presented in Table 2.

Objectives

The objective is to develop a CBM simulation software that incorporates the peculiarities of CBM production. The study will result in formulation of a computation framework based on material balance equation and incorporating non-equilibrium nature of gas desorption, matrix shrinkage and geomechanically dependent relative permeability curves. The study performed will allow seeing how seemingly small variation in input parameters and assumptions applied may result in significant variance of forecasted values, therefore outlining the importance of adequate determination of coal properties. For brevity, we refer to the developed software as "single well analytical model."

Table 2. Coal seam vs. conventional reservoir (modified from Fekete associates, 2012)

Parameter	CBM reservoir	Conventional reservoir
Gas generation	Gas is generated and trapped within the coal	Transfers from source rock to lower pressure areas until it is trapped
Structure	Cleats are uniformly-spaced	Fractures, if existing, are spaced uniformly
Gas storage mechanism	Mostly adsorption	Compression
Gas transport mechanism	Combination of concentration and pressure gradients	Pressure gradient
Production performance	Negative decline curve (gas rate increases with time then declines); Gas-water ratio increases with time	Gas rate declines with time; Gas-water ratio decreases with time
Depth of commercial deposits	Shallow	Can be shallow or deep
Number of wells	Large number of wells	Small amount of wells
Extraction principles	Artificial lift is used to dewater the reservoir and reach gas desorption conditions	Natural drainage mechanism can usually be used

Problem Statement

Models of CBM reservoirs are designed differently from those applied for conventional oil and gas fields. Specialized software packages have been created for production modeling. These packages take into account physical and technical peculiarities of coals and the gas extraction process. Simulator development (e.g. conventional: Eclipse (Schlumberger), Landmark VIP (Halliburton), GEM (Computer Modeling Group), or special CBM: F.A.S.T. CBM (Fekete), COMET, etc.) has been carried out by leading companies over decades. The software packages incorporate many options, allowing engineers to handle any element of the field development –

from well perforation zone to gathering and processing facilities. This enables the solution of a large variety of problems – from well placement optimization to the choice of well stimulation and enhanced recovery methods and comparison of different production options.

Models used for CBM are complex, since they must include additional gas storage mechanisms (such as adsorption), coal deformation and the non-equilibrium nature of the degasification process (Wei et al., 2007; King et al., 1986). Modeling reservoirs is still challenging, since applicability of the models and limitations on their use have not been sufficiently studied. Each existing software uses a different approach and simplifies the various mechanisms in different ways, while the proposed mathematical descriptions are constantly being updated and advanced. Ongoing theoretical and experimental research addresses the need for improved understanding of the processes associated with the production of methane from coal beds. Therefore the use of commercial software is limited by two factors: some specific details important for CBM modeling may be not included, and the time and effort needed to set up a problem and investigate the effect of various parameters may be overwhelming. Therefore, there is a need for specific models incorporating the necessary concepts, but in a manner to allow for quick evaluation.

CHAPTER II

LITERATURE REVIEW ON THE APPLIED CONCEPTS

Essential Theoretical Background on Absorption, Diffusion and Permeability

Accounting for dual porosity of coal gas movement is understood as a combination of three processes: 1) gas desorption from internal micropore surfaces in coal matrix; 2) diffusion of gas through the coal matrix governed by concentration gradient; and 3) laminar Darcy's flow through cleats that is provided by permeability (King, 1985; King et al., 1986).

Adsorption

Coal is capable of storing a significant volume of gas by adsorption. Adsorption is collecting and holding of gas on the surface of a solid. Attached molecules of gas exist as a single layer in near-liquid state on the surfaces of coal. Desorption is the process when gas molecules are released from the surface area of the material. In coals desorption is initiated with reservoir pressure reduction, when gas storage capacity of coal decreases. Quantitively, the relationship between pressure and amount of gas adsorbed is described by an isotherm. The adsorbed gas volume may be influenced by a number of factors, including pressure, temperature, coal rank, ash content, gas composition, moisture content, etc. (Levy et al., 1997).

The adsorbing capacity of a coal seam varies non-linearly as a function of

pressure at a specific temperature that is usually described by Langmuir isotherm (formulated by Langmuir in 1918). This model is based on some general assumptions:

- only one gas molecule is adsorbed at a single site;
- adsorbed molecules do not affect each other;
- sites are indistinguishable by the gas molecules; and
- adsorption takes place on an open surface and nothing limits the gas access to sites (Daniels and Alberty, 1957).

Although the applicability of those assumptions to coal may be questionable, the model still represents the adsorption phenomena adequately. Typically, the empirical Langmuir isotherm relationship is expressed in the following way:

$$V_E(p) = \frac{V_L p}{p + P_L}, \tag{2.1}$$

where $V_E(p)$ – gas storage capacity; p – pressure; V_L – Langmuir volume constant; P_L – Langmuir pressure constant.

Langmuir volume constant characterizes the maximum amount of gas that can be adsorbed at infinite pressure, and Langmuir pressure constant is the pressure at which ½ V_L is adsorbed. P_L affects the shape of the isotherm, while V_L controls the volume reached asymptotically.

The Figure 3 shows the typical form of Langmuir isotherm.

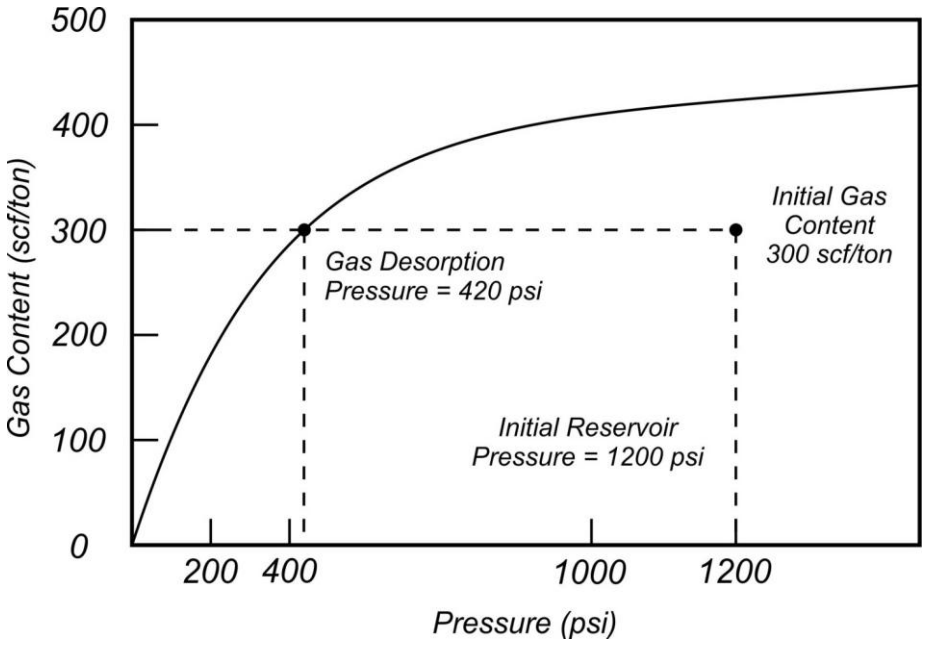

Figure 3. Example of a Langmuir Isotherm (modified from Mavor et al., 1996)

Initial reservoir pressure and gas content define the point on the plot which is located on the isotherm curve if the coal is saturated with gas or below it for undersaturated conditions (where the pore space is completely filled with water). To obtain gas production from undersaturated reservoir, it should be depleted (to some extent) by dewatering, until the pressure reaches the value on the curve – desorption pressure – corresponding to the actual adsorbed gas content. Afterwards, the gas is desorbed from the coal and is produced. Gas production continues until the pressure reaches abandonment value. Total gas to be produced can be estimated by the difference between initial and abandonment adsorbed gas values (though a more precise approach should also consider the change in the free gas content between these two states).

Langmuir volume and pressure constants and gas content are determined from adsorption test data. Desorption measurements, in turn, identify initial gas content of the

coal. Other models of adsorption have been developed on the basis of Brunauer, Emmet and Teller (BET) theory and Polanyi's potential theory (Harpalani et al., 2006).

Since coal beds do not hold pure methane, but rather a mixture of gases including nitrogen, carbon dioxide and heavier hydrocarbons the Langmuir adsorption model has been extended to include the effect of multicomponent adsorption. This extended model is addressed as Extended Langmuir Isotherm ("ELI") (Ruthven, 1984; Harpalani and Parity, 1993). ELI is especially useful when considering secondary enhanced recovery by CO_2 or N_2 injection. However this theory has some drawbacks and is not very accurate, especially at higher pressures. There are some variations of the adsorption model to include coefficients for moisture and ash content, in addition to accounting for different components in the gas.

Diffusion

After gas starts desorbing from the matrix and molecules detached from the internal surface of the coal matrix micropores, molecular diffusion through the matrix into the fractures begins. Diffusion is the process of molecular motion governed by gas concentration gradient. It is governed by a combination of three mechanisms: bulk; Knudsen-type; and surface diffusion (Smith and Williams, 1984). Surface diffusion occurs in pseudo-liquid molecular layer, when the molecules move along the micropore surface. Bulk diffusion happens in the gas phase and is governed by concentration gradient. Finally, Knudsen-type diffusional flow accounts for movement of gas in

smaller capillaries, when collision with the walls happens more often than collision with other gas molecules.

Mathematically diffusion through the coal matrix is described by Fick's Law (Fick, 1855):

$$F = D \, {dC}/{dx}\,, \tag{2.2}$$

where F – diffusion flux; D – diffusion coefficient; dC/dx – concentration gradient.

The diffusion coefficient is a function of temperature, pressure, pore length, pore diameter, and water content and should reflect all three diffusion mechanisms mentioned above (Olague and Smith, 1989). It can be determined experimentally by desorbing methane from a core sample in the laboratory while measuring the desorption rate as a function of time.

Various models have been proposed to describe diffusion in coal. Originally, diffusion was described as a single step process (single-pore size in coal (unipore model), but later it was proposed that better results could be achieved using a two-step approach (bidisperse model) (Siemons et al., 2003; Ruckenstein et al., 1971; Cui et al., 2004; Shi and Durucan, 2003a, 2003b). Comparison of the models was presented in (Wei et al., 2007). In addition, empirical relations have been documented for the diffusion of desorbed methane through coal particles (Airey, 1968).

For convenience of calculations, King and Ertekin (1991) gave an equation of the rate of diffusion for a unit of the reservoir, under the driving force of a concentration gradient :

$$\frac{dV}{dt} = -Da(V - V_E), \tag{2.3}$$

where dV/dt – volumetric gas flow per unit time; D – diffusion coefficient; a – Warren and Root shape factor (influences flow through matrix between micropores and macropores); V – adsorbate volumetric concentration; V_E – equilibrium sorption isotherm volume.

Warren and Root shape factor may be replaced by the following relation:

$$a = \frac{8\pi}{S^2}, \tag{2.4}$$

where S – spacing between cleats (size of block).

Sawyer et al. (1987) introduced the concept of sorption time (sometimes also referred as diffusion time):

$$\tau = \frac{1}{Da}, \tag{2.5}$$

Sorption time (τ) is the time required to desorb 63.2 % of the initial gas volume. It characterizes the diffusion effects and generally is determined experimentally. This is the characteristic time the gas needs to reach the macropores. In coals, sorption time varies significantly from less than 1 day to more than 300 days, depending on coal rank, composition and cleat spacing (Boyer et al., 1990).

Substituting (2.5) into (2.4) we get:

$$\frac{dV}{dt} = -\frac{1}{\tau}(V - V_E), \tag{2.6}$$

The equation 2.6 allows us to calculate volumetric flow rate of methane to the cleats, in terms of the difference of actual and equilibrium adsorbate concentrations.

Permeability

Permeability is an intrinsic parameter of porous formations. It is increasingly important in coal, where the gas content is determined by microporosity, whereas the transportability of gas is dependent on macroporosity. Correct determination of coal permeability is highly important, since it controls the deliverability of the well (Connell and Detournay, 2009). Two kinds of permeability may be present in coal reservoirs: matrix permeability and cleat permeability. While matrix permeability is too low for commercial production (Ayers, 2002), it is important for better understanding of the transport mechanisms and reservoir behavior (Moore, 2012).

The natural cleat and artificial hydraulic fracture network must supply the equivalent permeability for commercial flow rates of methane. Unfortunately, it is extremely difficult to evaluate equivalent permeability, due to the complexity of the processes taking place in coal reservoirs. Permeability in coal is a dynamic property, which may change due to three mechanisms: Klinkenberg effect; matrix shrinkage; and effective stress during the production period (company, 2008). Klinkenberg effect increases the equivalent permeability at lower reservoir pressure due to slippage near the walls of the cleats (Patching, 1965). Matrix shrinkage – due to desorption - also increases the permeability. The simultaneous increase in effective stress, however, decreases the permeability.

Coals respond greatly to stress changes, due to their high compressibility in comparison with conventional sandstone reservoirs (Ayers, 2002; Warpinski and Teufel, 1990). Overburden stress tends to decrease reservoir permeability; therefore, deep coals

usually cannot be commercially produced (Moore, 2012). Increase in horizontal stress also results in lower permeability value, due to cleats closure. Effective stress has also been proven to affect permeability (Sparks et al., 1995). With a 7 MPa increase in effective stress, permeability may decrease by more than 10 times. Some empirical models for the relationship between permeability and variation in effective stress have been proposed (Somerton, 1975; Harpalani and Schraufnagle, 1990; Liu and Harpalani, 2012).

Theoretically, production from coal beds should increase the horizontal stress, closing the cleats. However, laboratory and field evidence indicate that at higher effective stress a rebound in permeability occurs. This has been attributed to matrix shrinkage that results from active gas desorption from coals, when the effective stress increase is achieved by decreasing the pore pressure at fixed absolute stress (Mavor, 1997; Palmer and Mansoori, 1996; Harpalani and Schraufnagle, 1990). Matrix shrinkage effect causes coal cleats to widen, allowing for greater permeability to occur (Gray, 1987). An experimental study of the effect of methane desorption on coal permeability was undertaken (Harpalani and Schraufnagle, 1990). Coal matrix shrinkage has been documented to significantly increase permeability below desorption pressure. They have also shown that the increase in permeability caused an enhancement in gas production. Understanding and accounting for this positive effect when forecasting production from coal seams is crucial, since it may dominate over the negative effect of effective stress increase (Wang and Ward, 2009).

Description of dynamic permeability changes in coal has been ongoing. Several attempts have been made to describe coal permeability changes mathematically, utilizing both experimental and theoretical/numerical approaches. Gray (1987) was the first one to explain that permeability changes during pressure depletion are a result of two opposing effects – effective stress increase and matrix shrinkage due to gas desorption. He also proposed an empirical exponential relationship for calculation of permeability at positive effective stress.

Another model for permeability accounting for coal matrix shrinkage and compressibility was developed for the COMET simulator (ARI model) (Sawyer et al., 1990). The ARI model uses gas concentration to calculate the changes of permeability according to matrix shrinkage, which is theoretically more correct than relating both effects to pore pressure.

Seidle et al. (1992) proposed a model based on matchstick geometry, instead of the widely used bundle of capillaries geometry for porous media. Their equation is similar to one proposed earlier by McKee et al. (1988). It is formulated as:

$$k = k_0 e^{-3c_f(\sigma-\sigma_0)}, \tag{2.7}$$

where c_f is cleat volume compressibility in 1/MPa; σ is hydrostatic stress in MPa and k is cleat permeability. Subscript 0 indicates the initial state of the parameter. This equation is useful when fitting experimental data to acquire the value of cleat volume compressibility, which otherwise was determined experimentally in a complicated and expensive way (Seidle and Huitt, 1995). Another equation was proposed to quantify the permeability increase due to matrix shrinkage. Seidle and Huitt (1995) proposed a

permeability based on sorption induced strain, where permeability is a function of initial porosity and pressure.

Another analytical model based on fundamental rock mechanic principles was introduced by Palmer and Mansoori (1996). It allowed to model permeability changes in terms of the stress effects and matrix shrinkage. Their equations for pore volume compressibility (cleat volume compressibility) and permeability are also dependent on effective stress and matrix shrinkage. The Palmer and Mansoori model is based on the Langmuir strain relationship, and it appears to allow micro-pore shrinkage even when no gas is desorbed (Wei and Zhang, 2010).They also used a cubic relationship between porosity and permeability. This model presented a permeability rebound at lower pressure, when significant amount of gas has desorbed (Palmer and Mansoori, 1996).

A more general form of Palmer and Mansoori equation, allowing to calculate volumetric strain with different models, was proposed by Clarkson et al. (2008). The Palmer and Mansoori (1996) expression was modified by Mavor and Gunter (2004) to include enhanced recovery from coal beds and CO_2 storage.

Pekot and Reeves (2003) compared the ARI model and Palmer and Mansoori model and confirmed that they had given similar results in most cases, however ARI model is preferential for undersaturated coals, while in cases of swelling not proportional to gas concentration Palmer and Mansoori model yields better results.

Another model based on relation between permeability and stress by Seidle et al. (1992) was developed by Shi and Durucan (2003c). The Shi and Durucan model improves upon the Palmer and Mansoori model so that the micro-pore shrinkage occurs

only in the case of gas desorption (Shi and Durucan, 2003c, 2004, 2005, 2009, 2010, 2003a, 2003b; Shi et al., 2008).

Cui and Bustin (2005) used constitutive equation for porous media to derive permeability model. Their study showed that for coals with a higher Young's modulus and Poisson's ratio the rebound pressure is higher.

Robertson and Christiansen (2008) criticized models of Shi and Durucan and Palmer and Mansoori stating that they overestimate the permeability increase in coals due to matrix shrinkage. They proposed a permeability model for coal based on cubic geometry model (instead of matchstick geometry). Robertson and Christiansen (2008) hypothesized that three factors may affect cleat width: fracture compressibility, mechanical elasticity and sorption-induced strain. A sensitivity analysis demonstrated that input variables can have a significant impact on the calculated permeability values as a function of changing pore pressure.

Volumetric balance between the bulk coal, solid grain/matrix and cleat/fracture pores was applied in derivation of a simplified permeability model by Ma et al. (2011), using coal volume assumption. The grain/matrix volume dynamically changes with reservoir depletion resulting in cleat aperture change from assuming matchstick geometry. In this model the accent is on the change of grain volume, that is later converted to cleat volume change, instead of pore volume compressibility.

All of these models (ARI, Palmer and Mansoori, Shi and Durucan) are empirically derived and assume the conditions of constant overburden stress and uniaxial strain.

However the assumption of uniaxial strain may not be accurate (Connell and Detournay, 2009), therefore other coupled fluid-flow and geomechanics theoretical models have also been proposed, resolving the apparent contradiction that drawdown reservoir deformation equations imply zero horizontal strain at the outer reservoir boundary and unchanged overburden stress at the same time.

In the triple-porosity/ dual-permeability model proposed by Wei and Zhang (2010), the Klinkenberg effect on permeability is considered in both the macropore system and the fracture system. Besides, the swelling/shrinkage effect is also taken into account in the micro porosity.

Another theoretically sound formulation of porosity and permeability change was given by Zheng and Lili (2011). Their 3D model includes matrix shrinkage effect, dual porosity, single permeability, non-equilibrium adsorption, two-phase flow, high velocity non-Darcy flow, threshold pressure and slippage effect.

Recently Geilikman and Wong (2012) applied fluid and solid mass as elementary variables to directly impact the variation of strain and stress as production continues. Wang et al. (2009) accounted for permeability anisotropy. Gu and Chalaturnyk (2010) considered discontinuities in the coal formation. Table 3 provides a summary of various permeability/porosity models.

Table 3. Comparison of permeability models (modified from Shi and Durukan, 2004)

Authors	Model
Gray (1987)	$\sigma - \sigma_0 = -\frac{\nu}{1-\nu}(p - p_0) + \frac{E}{1-\nu}\frac{\Delta\varepsilon_s}{\Delta p_s}\Delta p_s$ $k = 0.001013e^{-0.714\sigma}$ where k – permeability; p - pressure; Δp_s – change in equivalent sorption pressure; ν - Poisson's ratio; E - Young's modulus; $(\sigma - \sigma_0)$ – stress change; $(\Delta\varepsilon_s)/(\Delta p_s)$ – strain caused by a unit change in equivalent sorption pressure.
	Matrix shrinkage is proportional to reduction in equivalent sorption pressure.
Harpalani and Zhao (1989)	$k = \frac{A}{P} + B + CP$ where *A, B, C* - constants; P - pressure.
	Empirical
Sawyer et al. (1990)	$\phi = \phi_i[1 + C_p(P - P_i)] - C_m(1 - \phi_i)(\frac{\Delta P_i}{\Delta C_i})(C - C_i)$ where ϕ - porosity; C_p – pore volume compressibility; C_m – matrix shrinkage compressibility; C – average matrix gas concentration; P - pressure; ΔP_i – maximum pressure change based on initial desorption pressure; ΔC_i – maximum concentration change based on initial desorption pressure. $\frac{\Delta P_i}{\Delta C_i} = \frac{P_{di} - 14.7}{C(P_{di}) - 14.7}$ where P_{di}– initial desorption pressure; $C(P_{di})$ – concentration at initial desorption pressure.
	Combines compressibility and shrinkage/swelling factors

Table 3. Continued

Authors	Model
Seidle and Huitt (1995)	$$\frac{\phi}{\phi_0} = 1 + \left(1 + \frac{2}{\phi_0}\right)\varepsilon\left(\frac{Bp_0}{1+Bp_0} - \frac{Bp}{1+Bp}\right)$$ $$\frac{k}{k_0} = \frac{\phi^3}{\phi_0^3}$$ $$k = k_0 e^{-3c_f(\sigma-\sigma_0)}$$ where $\frac{\phi}{\phi_0}$ - porosity ratio; p - pressure; k - permeability; C_m - matrix swelling coefficient; V_E – amount of adsorption at infinite pressure; B – Langmuir constant; $\varepsilon = C_m V_m$ – strain due to matrix shrinkage. $$\frac{k}{k_0} = \left[1 + \left(1 + \frac{2}{\phi_0}\right) C_m V_E \left(\frac{Bp_0}{1+Bp_0} - \frac{Bp}{1+Bp}\right)\right]^3$$
	Includes matrix shrinkage effect only. Assumes: Swelling is proportional to amount of gas adsorbed; Coal is represented my matchstick geometry.
Palmer and Monsoori (1996)	$$\phi - \phi_0 = \frac{1}{M}(p - p_0) - \left(1 - \frac{K}{M}\right) \times \varepsilon_L \left(\frac{p}{p + P_\varepsilon} - \frac{p_0}{p_0 + P_\varepsilon}\right)$$ $$\frac{k}{k_0} = \frac{\phi^3}{\phi_0^3}$$ $$M = \frac{E(1-\upsilon)}{(1+\upsilon)(1-2\upsilon)}, \quad K = \frac{E}{3(1-2\upsilon)}$$ where ϕ – coalbed porosity, fraction; K – bulk modulus; M – constrained axial modulus; E –Young's modulus; ε_L, P_ε – Langmuir type parameters. Second term – mechanical strain due to changes in pressure; Last term – effect of the sorption induced strain.
	Permeability can rebound at lower drawdown pressures if the matrix shrinkage is strong enough; Field permeability sometimes did not match unless permeability loss associated with increased effective stress was neglected (Palmer, 2004)
Gilman and Beckie (2000)	$$k = k_0 \exp\left(\frac{3\nu}{1-\nu}\frac{p - p_0}{E_F}\right) \exp\left(-\frac{3\alpha E}{1-\nu}\frac{\Delta S}{E_F}\right)$$ where α – volumetric swelling coefficient; ν - Poisson's ratio; ΔS - change of the adsorbate mass; E_F - some analog of Young's modulus for a fracture.
	The parameter EF is not specified.

Table 3. Continued

Authors	Model
Cui and Bustin (2005)	$k = k_0 \exp\left\{\frac{3}{K_p}\left[\frac{(1+\nu)}{3(1-\nu)}(p - p_0) - \frac{2E}{9(1-\nu)}(\varepsilon_\nu - \varepsilon_{\nu 0})\right]\right\}$ where ν - Poisson's ratio; E - Young's modulus; K_p - modulus of pore volume, reciprocal of pore volume compressibility; $(\varepsilon_\nu - \varepsilon_{\nu 0})$ - the change in sorption-induced volumetric strain.
	K_p is considered to be constant during CBM production
Shi and Durucan (2005)	$\sigma - \sigma_0 = -\frac{\nu}{1-\nu}(p - p_0) + \frac{E}{3(1-\nu)}\varepsilon_L\left(\frac{p}{p+P_\varepsilon} - \frac{p_0}{p_0+P_\varepsilon}\right)$ $k = k_0 e^{-3c_f(\sigma-\sigma_0)}$ where c_f – cleat compressibility; $(\sigma - \sigma_0)$ – difference in effective horizontal stress; ν – Poisson's ratio; E – Young's modulus; ε_L- Langmuir volumetric strain constant; P_ε – Langmuir strain constant at ½ ε_L; k - permeability.
	Based on Seidle et al. (1992)
Robertson and Christiansen (2006)	$k = \frac{w^3}{12a}$ where w – cleat width; a – cleat spacing. $\frac{k}{k_0} = e^{3\left\{c_0\frac{1-e^{\alpha(p-p_0)}}{-\alpha} + \frac{3}{\phi_0}\left[\frac{1-2\nu}{E}(p_r - p_0) - \frac{\varepsilon_{max}}{p_L+p_0}ln\left(\frac{p_L+p_r}{p_L+p_0}\right)\right]\right\}}$ where α - rate of change of fracture compressibility; E – Young's modulus; ν – Poisson's ratio; ε_{max} – linear strain at infinite pore pressure on unconstrained sample; p_L – Langmuir pressure.
	3 factors influencing change in cleat width: pore volume compressibility, matrix compressibility governed by mechanical elastic moduli, sorption induced strain.

Table 3. Continued

Authors	Model
Ma et al. (2011)	$\frac{\Delta a}{a} = -1 + \sqrt{1 + \varepsilon_L(\frac{p_0}{P_L + p_0} - \frac{p}{P_L + p})} + \frac{1 - \nu}{E}(p - p_0)$ where Δa/a - the horizontal strain in a single matchstick; ε_L - Langmuir volumetric strain constant; P_L - Langmuir pressure constant; p - pressure; ν – Poisson's ratio; E – Young's modulus; k – permeability; ϕ_0- initial porosity.
	$\frac{\mathrm{k}}{k_0} = \frac{\left(1 + \frac{2}{\phi_0}\frac{\Delta a}{a}\right)^3}{1 - \frac{\Delta a}{a}}$
	Overall matchstick strain resulting from matrix shrinkage and decrease in reservoir pressure.

Relative Permeability

Another way permeability change may be included in modeling is phase relative permeability (Gray, 1987). As other properties, relative permeabilities may change significantly from one coal to another and the laboratory derived curves may be very different from the ones obtained from history-matching (Clarkson et al., 2010; Zuber and Olszewski, 1992). It is hard to acquire adequate experimental relative permeability data due to difficulties in establishing consistent experimental conditions and realistic representation of the cleat network by a small core (company, 2008). This leads to difficulties in predicting relative permeability and production behavior during the period of two-phase flow.

A work by Reznik et al. (1974) indicated that coal relative permeabilities were strong functions of stress.

A systematic investigation of controls on coal relative permeabilities shape was attempted by Clarkson et al. (2010). They believed that understanding those controls would be a big step to improve the forecasting capacity. The significant impact of absolute permeability change on relative permeability curves was identified.

Chen et al. (2012) studied the effect of relative permeability curves, showing that phase production rate is proportional to phase relative permeability.

Zuber et al. (1987) also mentioned that the simulated production rates were highly dependent on relative permeability curves applied. However, they stated that reliable data on relative permeabilities was hard to obtain.

Recently, a model has been proposed that considers the changes in relative permeability curves as the consequence of the same processes affecting absolute permeability and porosity during CBM production (Chen et al., 2013). Relative permeabilities are described as binary functions of water saturation and porosity change.

Material Balance Method as an Engineering Instrument

Material balance equation was derived by Schilthuis (1936). This equation represents volumetric balance, realized by equalizing the observed cumulative production expressed in terms of collected volume modified to in-situ conditions with volumetric gain of fluids owning to their expansion in the reservoir due to pressure drawdown (Grishin, 1985). The simplest interpretation of the given formula is that

supposing produced fluid measured on the surface was placed back into the reservoir at reduced pressure, it would occupy the space equal to the sum of complete expansion water influx.

Volumetric material balance method is an important instrument of understanding formation properties and hydrocarbon reserves estimation. This method radically differs from numerical modeling of reservoirs (computer simulation) – modern widely used practice of reservoir engineering, since numerical modeling uses an algorithm assuming division of pay zone into a large number of discrete cells. With fragmentation of reservoir arises the problem of reservoir characterization at every cell and accounting for fluid cross-flow between blocks (with use of relative permeabilities), which increases the number of assumptions being taken and enhances uncertainty when attempting to describe system behavior (Dake, 2001).

Material balance method is built upon analysis of liquid and gas in place physical properties change at pressure variation during reservoir depletion (Zhdanov, 1962).

Mostly this method is being applied for quantification of hydrocarbon reserves on the basis of field data like amount of produced gas and liquid, as well as PVT-properties (Zheltov, 1985).

Material balance method implies integration of in-situ conditions and reservoir properties. Formation is considered to be zero-dimensional black box (tank), which may contain fractures, heterogeneities, significant anisotropy of properties, horizontal wells, etc. The key advantage of the given technique appears to be the possibility to evaluate original oil in place and drive mechanisms, although specifically for coal beds expulsion

mechanism is different from conventional reservoirs, as the formulation of material balance itself is, as given by different researchers.

There are certain benefits and drawbacks of material balance method. Material balance method places certain limitations on engineers' actions in comparison with numerical modeling. In numerical modeling it is possible to change values of certain characteristics in every grid block for the purpose of reaching better history match, while with material balance this cannot be done. Numerical methods handle formation heterogeneity and anisotropy better than material balance method.

Given that pressure drop in the reservoir is uniform, forecasting techniques may be employed in material balance. In the reversed situation (non-uniform pressure drop) benefits of material balance equation significantly decrease.

For a long period of time material balance equation has been one of the main instruments used by reservoir engineers for interpreting and forecasting reservoir behavior. Later on it has begun to lose its popularity to more advanced techniques of numerical simulation. However, with numerical modeling on the stage of history matching (while adjusting reservoir parameters on the basis of comparison of simulation results and actual field data) considerable human factor can often be observed (Dontsov, 1977).

Supposing pattern of pressure change is known, one may apply material balance equation using characteristics of production change and PVT fluid properties. In that case there is no need to restrict the use of certain geometric models, which means that material balance equation can be used for calculating original oil in place, model

adaptation as well as defining expulsion mechanisms. Given technique is not only the most reliable since it implies the least number of assumptions for reservoir engineering, but also one of the most straightforward and clear for interpretation, even trivial, when applied for gas reservoirs. On the contrary, building a hydrodynamic model using geologic maps and petrophysically defined properties of the formation implicates that original reserves are known (Dake, 1983).

Numerical modeling and use of analytic calculations based on material balance may complement each other to acquire adequate results. The following sequence of steps would be optimal: on the ground of material balance system properties are estimated that are later used as input data in numerical model. The concept of material balance is appropriate for history matching based on the most general production data. It should be noted that on the step of preliminary reservoir property evaluation it is preferential to employ numerical modeling, since in that case material balance equation itself carries uncertainty.

Application of Material Balance Equation

With the help of material balance method a wide range of oil, gas and gas condensate field development objectives may be solved. Traditionally, it is applied to determine initial reserves and establish the volume of water influx into the formation from an aquifer.

If reserves are known with reasonable accuracy from geologic materials analysis and applications of methods not related to material balance calculations, then it is

possible to study the influence of current production/injection rates on average reservoir pressure. One may establish the activity of a particular draining mechanism of production zone. Thus, assuming no water invaded successively initial reserves are estimated. Constant value of the calculated reserves suggests volumetric draining condition, while continuously increasing reserves indicate water drive (in the absence of other complicating factors) (Gimatudinov, 1983).

In a CBM reservoir the production behavior will depend heavily on the interrelation of the nonlinearities involved in the effect of pressure depletion on porosity, absolute permeability and relative permeabilities, in addition to the nonlinerity inherent with the volumetric behavior of gas. To investigate these effects, a simple tank model has advantages compared to reservoir simulation, because a reservoir simulator may not be prepared to accept all the effects. But even if a reservoir simulator is formally capable of handling all those effects, it might encounter serious convergence problems. A CBM model is always “stiff”, because the pore space has small storage capacity, compared to the adsorption capacity of the matrix. Stiff nonlinear partial differential equations are difficult to solve numerically.

Several modifications of material balance technique had been undertaken in order to make material balance equation application and analysis possible in CBM reservoirs.

King presented a material balance technique for estimating the original gas in place and predicting well performance for unconventional gas reservoirs (King, 1990; King, 1993). This method is the most comprehensive from the ones applied for CBM, it uses the traditional assumptions for the material balance approach but also considers the

effects of adsorbed gas. King assumes equilibrium between free gas and absorbed gas in the coal and pseudo-steady state process during adsorption, it also includes the water compressibility and water influx. This work provided a procedure of gas in place estimation by using the p/z method and prediction of future production performance based on the existing material balance techniques. The method is applied in F.A.S.T. CBM software, can be used for original gas in place estimation and production prediction.

Seidle (1999) and Jensen and Smith (1997) presented modifications (simplifications) to King's method. Seidle's method suggests using constant water saturation and also assumes formation and water compressibilities to be negligible. This eliminates mathematical problems from the original method.

Jensen and Smith's method assumes the gas stored in the cleat system is negligible; therefore, water saturation effects are omitted.

When a dedicated tank model is written, it is not necessary to use simplifications in the nonlinearities and convergence can be enforced more effectively than in a numerical simulator.

CBM Modeling Approaches

Describing CBM production performance has been a developing field for quite some time. Different approaches have been proposed to solve reserves estimation problems and production forecasting.

One of the early works on fluid flow in CBM reservoirs was done by Cervik (1967). He presented a basic concept of transport phenomenon for gas at free gas and desorption state. He presented the fact that desorption in coal depends on coal particles size, equilibrated pressure and diffusivity coefficient. Based on his study, it was not recommended to use the same basic concept for conventional gas reservoir engineering in a coalbed methane reservoir model, since the Darcy's law and Fick's law govern overall mass transport phenomenon in coals.

Zuber et al. (1987) pointed out that history matching analysis utilizing laboratory, geologic and production data can be used to determine CBM reservoir flow parameters and predict performance by using a two-phase, dual porosity finite difference simulator modified to include gas storage and flow mechanisms applicable to coal.

A proposal that conventional reservoir simulators, modifying data input, could be used for modeling CBM production came later from Seidle and Arri (1990). This approach is equilibrium, which means that desorption from micropores in coal matrix to cleats happens instantaneously and diffusion is neglected. The key to include adsorption to the model is in including a miniscule amount of immobile oil with high gas content, and the solution gas oil ratio is calculated using the Langmuir isotherm. Input data (like porosity and gas-water relative permeability curves) has to be shifted in order to account for the presence of non-physically existent immobile oil. However, no code modifications in the simulator are required, which makes the application quite easy. Applications of this method in combination with conventional black oil simulator verified the method. The results were compared with special CBM reservoir simulators.

Several authors proposed application of material balance method for CBM production description (King, 1993; King, 1990; Seidle, 1999; Jensen and Smith, 1997).

Papers by Law et al. (2002); Hower (2003); Jalali and Mohaghegh (2004) showed how numerical compositional simulators with additional features can be used for coalbed methane production simulation.

Law et al. (2002) presented a comparative study using numerical simulation for modeling enhanced recovery in CBM reservoirs with CO2 injection. Enhanced production simulation is more complicated since it has to include multicomponent effects of adsorption, diffusion, shrinkage, dual porosity nature of coal. They compared both conventional and special CBM simulators. Conventional oil or gas compositional simulators were used to model CBM recovery processes by using a single porosity approach assuming that the gas diffusion from matrix to fractures is instantaneous.

An alternative technique was proposed by Aminian et al. (2004) to predict CBM production performance. The technique uses a set of gas and water type curves, applies dimensionless rate and time for water and gas. Their study concluded that type curves could be successfully used for production history matching to determine initial matrix content and cleat porosity. This technique generates production forecasts. Besides this, a correlation for peak gas rate was developed in this study for production predictions .

The triple-porosity dual-permeability mathematical model for desorption-controlled reservoir was introduced by Reeves and Pekot (2001). It is based on Warren and Root (1963) dual-permeability approach for fractured reservoirs. It contested the results of existing dual-porosity single-permeability model when forecasting CBM

reservoir performance. Reeves and Pekot showed that the actual gas production (field data) appeared to be much higher than the simulated values. The third porosity was introduced in the matrix block system to provide free gas and water storage capacity for the modification of material balance techniques. Decoupled models of a desorption process from a matrix block and the diffusion process through a micropermeability matrix were introduced. This way mass transport could be explicitly determined. A comparison of existing models and the one proposed was performed proposing that the results of a new model were a better match with field data. This work also introduced a new coalbed methane simulator, COMET2 with some modifications in the fundamentals of the fluid flow and desorption process.

Tan (2002) revised the approach of Seidle and Arri. This work used independent implementation on commercial simulator to model CBM reservoirs. This work illustrated pressure dependent porosity and permeability phenomenon with some comparative runs. Tan's work also suggested the dual grid approach to gain a more accurate result in a matrix-fracture model. They compared the results with ones published by Paul et al. (1990) and received excellent match, however the results were not consistent with the ones of Seidle.

Guo et al. (2003) created a 3D two-phase flow CBM numerical reservoir simulator. This new simulator was more complicated. The new simulator improved CBM reservoir characterization by including transport phenomena in the coal micropores and fracture system. The gas resulting from the desorption process was calculated with a sorption isotherm curve from the experiments and calculation.

Therefore, an equilibrium state of desorption process was applied (instantaneous diffusion).

Good reviews on numerical simulation of coalbed recovery process were presented by Wei et al. (2007); King et al. (1986).

Sensitivity Studies

The relative importance of reservoir parameters on the efficiency of methane extraction from coal was assessed by Remner et al. (1986). They addressed well interference, absolute and relative permeabilities, sorption time and water production. They noted that early gas production values depended on diffusion time and water permeability. A positive well interference effect on gas rate has also been spotted.

Derickson et al. (1998) presented a sensitivity study result for CBM reservoir production performance in Huaibei, China. After an investigation of some fundamental coal properties variation and their effect on the production rate they concluded that coal permeability, gas content, initial water saturation, and coal thickness were the most influential.

Roadifer et al. (2003)conducted a massive comprehensive parametric study with Monte Carlo simulation. Relative importance of each parameter, like reservoir properties, geological data, completion and operation constraints were calculated. The sensitivity study was completed by changing one value while keeping the other values constant. On the contrary, a parametric study was realized by applying all possible

combinations of each parameter at every value (e.g. minimum, most likely, and maximum).

Young et al. (1991) presented a parametric study for San Juan basin area. The basin area was divided into three parts depending on properties variation and sensitivity study on permeability, porosity, fracture half-length, coal compressibility, gas content and drainage variation was performed.

Software

The methods described above are applied in a number of reservoir simulators and semi-analytic software programs that are available in the industry to perform reserves estimation and CBM reservoir performance forecasting.

All the simulators, although solving the same problems, apply different approaches and assumptions. Therefore, simulators have some variety in their input data, description of the physical problem, and calculation techniques.

Commercial reservoir simulators like GEM (by Computer Modeling Group) and Eclipse (by Halliburton) have integrated sorption and diffusion processes, coal shrinkage, compaction effects, and under-saturated coals, which they apply to their dual porosity models to allow CBM reservoir modeling. They are capable of handling multicomponent gas effects (typically CO2 and methane), which is useful for enhanced production modeling. Different well geometries and completions are available, including hydraulic fractured and horizontal multi-branch wells. Those commercial simulators apply dual porosity models (modified from Warren and Root, 1963), coal gas storage

capacity is considered to be a function of pressure and is described by Langmuir Isotherm, gas diffusion from matrix to cleats is governed by Fick's law and permeability change due to matrix shrinkage is included via Palmer and Mansoori method (Palmer and Mansoori, 1996). They may generate simulated relative permeability curves or use the input values.

COMET3 numerical simulator by Advanced Resources International, Inc. is capable of modeling triple porosity, dual permeability naturally fractured reservoirs with matrix porosity and multicomponent gas adsorption. It also allows simulating enhanced CBM production.

A new simulator was designed for independent producers by Jalali and Mohaghegh (2004) from West Virginia University to make the application of simulation technology available for a wider range of producers. This single-well radial model generates production forecasts and volumetric calculations. It is based on mathematical formulation by King (1985).

Semi-analytical software programs are also available for modeling CBM wells. Those programs apply the same equations used for conventional reservoirs to predict CBM performance, with an exception of production from the matrix being a function of the Langmuir isotherm. The semi-analytical software programs as a rule consider equilibrium adsorption (consider diffusion negligible and desorption instantaneous), therefore sorption time is not an input for CBM reservoir analysis in these programs.

Fekete Associates Inc. created F.A.S.T. CBM, which is a part of Harmony package and which is a semi-analytic model. This program also allows reserves

estimation, production forecasting (history-free and history-matched), decline curve analysis, etc. For modeling CBM wells, this program combines additional gas storage mechanism – adsorption, and equations for conventional gas reservoirs. Matrix shrinkage option is available with a choice of Palmer and Mansoori, Shi and Durucan or Seidle and Huitt theories. The software also includes decline analysis for alternative estimation of gas in place and material balance calculations using different techniques (King, 1993; Seidle, 1999; Jensen and Smith, 1997). In addition, it has numerical modeling option, which allows more flexibility in history-matching and performance analysis of horizontal wells, multi-layer analysis and non-equilibrium sorption (diffusion time included).

Rapid Technology Corporation introduced PRODESY, which is also a semi-analytic software, which allows to model horizontal wells in coal seams and includes adsorption mechanism.

Another specialized software program available in the industry is PROMAT (Schlumberger). This software allows to model dry coal reservoirs, where cleats are not water saturated.

CHAPTER III

PROBLEM STATEMENT AND SOLUTION DESCRIPTION*

This chapter will present the framework and theory applied in the program realization of the material balance method for single-well production behavior modeling in Wolfram Mathematica software.

Framework for Model Developed

Scope

The single-well analytical model was created in the software system Mathematica (by Wolfram Research).

To estimate original gas in place and acquire the production forecast we use a pseudo-steady state non-equilibrium tank model coupled with geomechanical effects (compressibility and matrix shrinkage).

The following general assumptions are applied:

- Darcy flow in cleats;
- Reservoir is isothermal;
- No water influx (no aquifer action);

*Part of the data reported in this chapter is reprinted with permission from "Capillary Pressures – Their Measurement Using Mercury and the Calculation of Permeability Therefrom" by Purcell, 1949. Journal of Petroleum Technology, 1(2), p.44, Copyright 1949 by SPE. Further reproduction prohibited without permission.

Part of the data reported in this chapter is reprinted with permission from "Application of Matchstick Geometry to Stress Dependent Permeability in Coals" by Seidle et al., 1992. Conference Proceedings of SPE Rocky Mountain Regional Meeting, 1992, Casper, Wyoming, p.444, Copyright 1992 by SPE. Further reproduction prohibited without permission.

- Uncompressible water;
- Pseudo-steady state inflow equation (uses constant average pressure during a given time step);
- Details of the geometry are represented by the Productivity Index;

The approach is based on the widely used Shi and Durucan model (Shi and Durucan, 2003c, 2004, 2005, 2009, 2003a, 2003b; Shi et al., 2008), describing the relation between effective horizontal stress and permeability. It is combined with the form proposed by Chen et al. (2013), considering relative permeability as a binary function of saturation and porosity change. This model allows investigation of the effects of matrix shrinkage that occur in coal as a result of desorption and compression.

The proposed solution includes non-equilibrium quasi-steady state description of the diffusion process in coal. In many existing simulation software packages diffusion is not considered; desorption described as an equilibrium process without time delay. In this work a time constant (τ) will be used to address the non-equilibrium nature of the process.

The model created in this research also takes into consideration the effects of stress dependence of relative permeabilities, commonly neglected in reservoir simulators. Although relative permeabilities have been proved to change as a result of different in-situ processes, due to lack of research on the topic, most models consider them constant. In contrast, our model will address the shifts of the relative permeability curves for coal caused by changes in porosity/permeability due to the varying stress state during depletion of the pore pressure (Chen et al., 2013).

Principal difference of the proposed solution from similar previous models is in accounting for the non-equilibrium nature of desorption in deformation-dependent characteristics like permeability, porosity and phase relative permeabilities. This is made possible by considering stresses and strains depending on both gas phase pressure and adsorbed amount of gas.

Production forecasting is performed applying deliverability and material balance equations at each step. The method is implicit in pressure and explicit in saturation.

On the basis of known initial reservoir properties, we will solve the material balance equation to produce a pressure decline curve and production profile that are agreeable with the above mentioned relations and laws, specific for coal reservoirs. We will consider a case in which gas and water are extracted from the system, resulting in the drop of the average reservoir pressure, causing the deformation of pore structure. Pressure change in the drainage zone is accompanied by coal deformation, resulting in porosity and permeability change. The absolute and effective phase saturation change then results in change in the relative permeability curves.

Material Balance

The framework is based on gas material balance equation in the following generalized form:

$$G_p = OFGIP - G_F/B_g + G_D \,, \tag{3.1}$$

where G_p – cumulative gas produced at standard conditions; *OFGIP* – original free gas in place at standard conditions; G_D – cumulative volume of gas that desorbed and

diffused into cleats at standard conditions; G_F – currently free gas in cleats at reservoir conditions; B_g – gas formation volume factor.

The definition of gas volume factor is:

$$B_g = \frac{p_{st}}{p}\frac{T_{res}}{T_{st}}Z\,, \tag{3.2}$$

where Z - compressibility factor; T_{res} - reservoir temperature; T_{st} - temperature at standard conditions; p_{st} - pressure at standard conditions.

Original free gas volume converted to standard conditions is given as:

$$OFGIP = \frac{Ah\phi_i(1 - S_{wi})}{B_{gi}}\,, \tag{3.3}$$

where A – area; h – thickness; S_w - initial water saturation.

Applying the relation between gas and water saturation (3.4) the expression for in-situ pore volume occupied by free gas may be written as (3.5).

$$S_w + S_g = 1\,, \tag{3.4}$$

$$G_F = V_p - \left(V_{wi} - W_p\right), \tag{3.5}$$

where V_p – cleat volume; V_{wi} – initial water content; W_p – cumulative water produced; S_w - water saturation; S_g - gas saturation.

Initial water content is described as follows:

$$V_{wi} = Ah\phi_i S_{wi}\,, \tag{3.6}$$

where ϕ_i - initial porosity.

Cleat volume changes accordingly to the effects of matrix shrinkage and compressibility during production and will be discussed later in this chapter.

Unlike traditional gas material balance equation it includes the term, accounting for additional storage mechanism for coal - adsorption. Therefore total in-situ amount of gas at every time step can be defined as the sum of gas adsorbed in coal matrix and free gas in cleats. When production commences it results in pressure drawdown that induces gas desorption.

Gas adsorption is described by Langmuir Isotherm, which gives equilibrium gas content at standard conditions:

$$\mathrm{V_E}(\mathrm{p_g}) = \frac{\mathrm{V_L}\,\mathrm{p_g}}{\mathrm{p_g} + \mathrm{P_L}}\ , \tag{3.7}$$

To calculate the total volume of gas adsorbed at equilibrium by coal mass being drained at specified pressure the gas content in equilibrium with cleat gas pressure given by Langmuir Isotherm for 1 kg should be multiplied by coal mass (3.9), that can be calculated from density and reservoir dimensions:

$$G_A(p_g) = m_c V_E(p_g)\ , \tag{3.8}$$

$$m_c = Ah\rho_c\ , \tag{3.9}$$

where m_c - coal mass, ρ_c - coal bulk density.

Original gas in place, OGIP, can be determined by adding the gas volume adsorbed at initial pressure and initially free gas value:

$$OGIP = G + OFGIP\ , \tag{3.10}$$

where $G = G_A(p_{gi})$ – adsorbed gas at initial pressure.

Desorption is considered to be a non-equilibrium process, therefore diffusion time constant is applied to slow down the entrance of desorbed gas into cleats. This

complicates the desorbed volume calculation, which depends on the concentration of gas currently in matrix (which is not equal to equilibrium gas content calculated by Langmuir isotherm) and gas content at equilibrium with new cleat gas pressure.

To determine G_D, the cumulative volume of gas that desorbed and diffused from coal matrix on the (n+1)-th time step, the desorbed gas that entered the cleats on the n-th time step should be added to the difference of currently adsorbed value on the n-th time step and the equilibrium gas content at new gas pressure, divided by the diffusion time constant:

$$G_D^{n+1} = G_D^n + \left(G_{ads}^n - G_A(p_g)\right)\frac{\Delta t}{\tau} \ , \tag{3.11}$$

The new volume of gas in matrix, G_{ads}, can then be calculated.

Volume of gas in matrix, G_{ads}, is acquired as the difference of initially adsorbed volume and cumulative volume that has desorbed and entered the cleat system by that moment (diffused to cleats):

$$G_{ads}^n = G - G_D^n \ , \tag{3.12}$$

The volume of gas currently in matrix is important for our framework, since we consider that coal deformation happens according to non-equilibrium nature of desorption. Therefore permeability, residual phase saturations and phase relative permeabilities depend on it.

Permeability Model

In this work Shi and Durucan (2003c) permeability model is applied. This model links horizontal stress dependent on rock mechanical properties and volumetric

swelling/shrinkage strain change to permeability via relation proposed earlier by Seidle et al. (1992).

$$\sigma - \sigma_i = -\frac{\upsilon}{1-\upsilon}(p - p_i) + E\frac{\Delta\varepsilon_s}{3(1-\upsilon)} \ , \tag{3.13}$$

$$k = k_i e^{-3c_f(\sigma-\sigma_i)} \ , \tag{3.14}$$

where $(\sigma - \sigma_i)$ – horizontal stress change; υ - Poisson's ratio; E - Young's modulus; $\Delta\varepsilon_s$ - volumetric strain change; k - permeability; p - pressure; p_i - initial pressure; c_f - coal cleat volume compressibility.

The first term in equation 3.13 represents lateral stress change due to compression from pore pressure drawdown. The second term represents the indirect effect of coal swelling/shrinkage on lateral stress change.

Volumetric strain is described by the Langmuir type equation (Pan et al., 2010; Chen et al., 2013; Levine, 1996) so volumetric strain change is:

$$\Delta\varepsilon_s = \frac{\varepsilon_L p}{p + P_\varepsilon} - \frac{\varepsilon_L p_i}{p_i + P_\varepsilon} \ , \tag{3.15}$$

where ε_L - Langmuir volumetric strain; P_ε - pressure at $\frac{1}{2}\varepsilon_L$.

Due to non-equilibrium nature of desorption in coal, the current volumetric strain is controlled by the actual volume of gas currently in matrix (3.12). This makes sure that actual amount of gas that desorbed causes strain, not the amount that would have desorbed at equilibrium in accordance to current pressure.

Incorporating the concept that volumetric strain corresponds to current adsorbed content rather than to current pressure, the equivalent pore pressure is determined inverting the Langmuir Isotherm (3.7) in the following manner:

$$p_{ads} = \frac{p_L V_{ads}}{V_L - V_{ads}} \ , \tag{3.16}$$

At this pressure 1 kilogram of coal at equilibrium adsorbs the volume V_{ads}, which corresponds to the total gas currently in the matrix:

$$V_{ads} = \frac{G_{ads}}{m_c} \ , \tag{3.17}$$

Therefore in our formulation volumetric strain change in equation 3.15 is a function of p_{ads}: $\Delta\varepsilon_s(p_{ads})$.

Substituting $\sigma - \sigma_i$ in equation 3.14 with a combination of 3.13, 3.15, 3.16 and rearranging the resulting equation for permeability change as a function of pressure and currently adsorbed volume would be:

$$\frac{k}{k_i} = e^{-3c_f\left(-\frac{v}{1-v}(p-p_i)+E\frac{\frac{\varepsilon_L p_L V_{ads}}{(V_L - V_{ads})\left(\frac{p_L V_{ads}}{V_L - V_{ads}}+P_s\right)} - \frac{\varepsilon_L p_i}{p_i + P_s}}{3(1-v)}\right)}, \tag{3.18}$$

Currently, the software proposed cannot be used for undersaturated reservoirs – reservoirs that contain less gas than proposed by Langmuir Isotherm at initial pressure as illustrated in Figure 4 (Morad et al., 2008). If we wanted to apply it for a reservoir where initial pressure exceeds critical desorption pressure dewatering stage would have to be calculated first. The value of critical desorption pressure can be acquired from laboratory measurements.

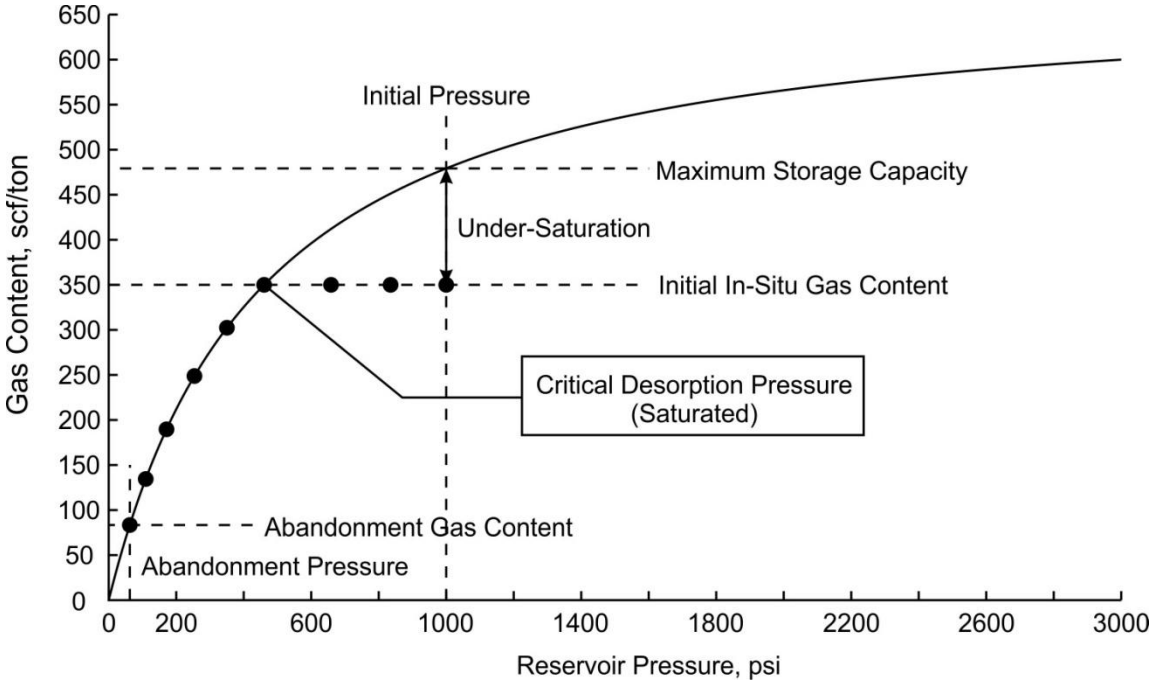

Figure 4. Desorption behavior of under-saturated CBM reservoirs (modified from Morad et al., 2008).

Effective horizontal stress calculation would be different in two production periods, according to Shi and Durucan permeability model (Shi and Durucan, 2004; Shi et al., 2008):

$$\sigma - \sigma_i = -\frac{\upsilon}{1-\upsilon}(p - p_i), \qquad p_d < p \le p_i \ , \tag{3.19}$$

$$\sigma - \sigma_d = -\frac{\upsilon}{1-\upsilon}(p - p_d) + \frac{E}{3(1-\upsilon)}\varepsilon_L\left(\frac{p}{p+P_\varepsilon} - \frac{p_d}{p_d+P_\varepsilon}\right),$$

$$0 < p \le p_d \ , \tag{3.20}$$

where p_d is critical desorption pressure.

Equation 3.19 characterizes the dewatering period before desorption commences. Equation 3.19 shows horizontal stress change when pressure drops below critical desorption pressure.

However, equation 3.20 does not consider the non-equilibrium nature of desorption and would have to be rearranged in accordance with our understanding for $0 < p \leq p_d$:

$$\sigma - \sigma_d = -\frac{\upsilon}{1-\upsilon}(p - p_d) + \frac{E}{3(1-\upsilon)}\varepsilon_L\left(\frac{p_{ads}}{p_{ads} + P_\varepsilon} - \frac{p_d}{p_d + P_\varepsilon}\right), \tag{3.21}$$

Initial Porosity and Porosity Change

In this research it is assumed that the initial porosity of coal may be calculated. It is the minimal porosity necessary to comprise the maximum adsorbed amount given by the Langmuir Isotherm. The adsorbed gas in coal is present in pseudo-liquid state, therefore it still takes some volume – or causes similar amount of matrix- swell. The Langmuir volume of gas in pseudo-liquid state in 1 kilogram of coal would occupy the following volume:

$$V_{Lg-l} = \frac{V_L \rho_g}{\rho_{g-l}}\ , \tag{3.22}$$

where ρ_{g-l} - density of adsorbed gas in pseudo-liquid state, ρ_g - density of gas at standard conditions.

Subtracting the volume that is occupied by gas in pseudo-liquid state at initial conditions, we get the volume that has to be available in 1 kilogram of coal for maximum adsorption to be possible:

$$V_{pore\ i} = \frac{(V_L - V_E(p_i))\rho_g}{\rho_{g-l}}\ , \tag{3.23}$$

Dividing it by the volume of 1 kilogram of coal we acquire the minimal necessary porosity at initial conditions:

$$\phi_i = \frac{V_{pore\ i}}{1/\rho_c}\ , \tag{3.24}$$

This calculation seems reasonable, independently of the details of how one accounts for the storage of the CH_4 being in pseudo-liquid state. Whether one considers that CH_4 will occupy additional space from the macroporosity, or one thinks that the CH_4 will penetrate the matrix causing its swelling, the bottomline is the same: the ϕ_i should be available at the initial state.

The analytical model based on material balance method calculates a new value of porosity using both compressibility effect and swelling and shrinkage mechanisms applicable for coal beds. The derivation of the model for porosity change is based on the uniaxial strain assumpsion (the deformation is laterally constrained) during pore pressure change.

The elastic properties of rocks affect the redistribution of pressure in the reservoir in the process of exploitation. Linear elasticity assumes a linear and unique relationship between stress and strain. Isotropic linear elastic materials are characterized by two independent constants: Young's modulus, E and Poisson's ratio, ν that are introduced by describing the deformation resulting from application of stress on a cylindrical sample.

Young's modulus is proportional to axial stress and inversely proportional to caused axial strain:

$$E = \frac{\sigma_1}{\Delta\varepsilon_1} \ , \tag{3.25}$$

Axial strain is given as:

$$\Delta\varepsilon_1 = \frac{l_i - l}{l_i} \ , \tag{3.26}$$

where l – is the resultant length and l_i – the initial length prior to stress application.

Poisson's ratio, ν constant is defined as the ratio of lateral expansion to longitudinal contraction, since when a rock specimen is compressed in one direction it deforms in two directions:

$$\nu = -\frac{\Delta\varepsilon_2}{\Delta\varepsilon_1} \ , \tag{3.27}$$

Lateral expansion is given as:

$$\Delta\varepsilon_2 = \frac{d_i - d}{d_i} \ , \tag{3.28}$$

where d – is the resultant diameter and d_i – the initial diameter prior to stress application.

If we assume that in the process of sedimentation compression of rock occurred only in the vertical direction and the horizontal direction strains did not occur, then:

$$\Delta\varepsilon_{\text{horizontals}} = 0 \ , \tag{3.29}$$

$$\Delta\sigma_{horizontals} = \Delta\sigma_{vertical} \frac{\upsilon}{1-\upsilon} \ , \tag{3.30}$$

$$\Delta\varepsilon_{\text{vertical}} = \frac{\Delta\sigma_{\text{vertical}}}{\text{E}\,(1-\upsilon)/((1+\upsilon)(1-2\upsilon))} \ , \tag{3.31}$$

Equation 3.31 may be rewritten as follows:

$$\Delta\varepsilon_{\text{vertical}} = \frac{(p - \text{p}_\text{i})}{\text{E}\,(1-\upsilon)/((1+\upsilon)(1-2\upsilon))} \ , \tag{3.32}$$

That represents uniaxial strain condition (Economides and Kenneth, 2000). Equation 3.30 is derived in the absence of horizontal deformation and not considering the plasticity of the coal. In real reservoirs that assumption is not always valid, and therefore more complex definitions of tension state of the rocks may be required.

In accordance with the concept of effective stresses applied to describe the elastic deformation of porous elastic media, rock deformation is determined mainly by changes in its pore volume, that is, the above expression for strain 3.32 actually represents a reduction of porosity due to its resilient compression.

The strain resulting from pressure drop represented in equation 3.32 equally affects total and solid volume and represents the effect of compression.

Solid volume changes as a result of volumetric strain due to desorption and compression.

After pressure drop the new fraction of volume occupied by solid according to equations 3.32, 3.15 and 3.16 can be calculated:

$$\mathrm{sol} = \frac{\mathrm{sol_i} + \Delta\varepsilon_s(p_{ads}) + \frac{p - \mathrm{p_{wi}}}{\mathrm{E}\,(1-\upsilon)/((1+\upsilon)(1-2\upsilon))}}{1 + \frac{p - \mathrm{p_{wi}}}{\mathrm{E}\,(1-\upsilon)/((1+\upsilon)(1-2\upsilon))}}\ , \tag{3.33}$$

where $\mathrm{sol_i}$ – is fraction of volume occupied by solid at initial state.

The numerator gives new solid volume after compaction and swelling/shrinkage strain, while denominator represents the new total volume after compaction.

The relation of porosity and fraction of volume occupied by solid is:

$$1 = sol + \phi\ , \tag{3.34}$$

Fraction of volume occupied by solid at initial state, sol_i and current porosity can be acquired from equation 3.34.

Applying equation 3.34 porosity change is defined as:

$$\frac{\phi}{\phi_i} = \frac{1 - sol}{1 - sol_i} \ , \tag{3.35}$$

The change in porosity may be positive or negative, depending on the impact of compaction and desorption terms. When a lot of gas desorbs and matrix shrinks significantly it results in porosity increase. On the contrary, when less gas desorbs, or when matrix shrinkage is physically less influential at higher pressure the porosity decreases.

Capillary Pressure and Relative Permeability Model

Permeability model is linked with capillary pressure and relative permeability models developed by Chen et al. (2013). Chen et al. in their research paper addressed the changes of relative permeability that are commonly not accounted for.

The derivation of relative permeability model for coal was done through the integration from the capillary pressure model by Purcell method (Purcell, 1949) adjusted for its application with matchstick geometry. Coal structure is better represented by matchstick geometry, than bundle of capillary tubes (schematic representations given in Figure 5 based on Seidle et al. (1992); Gates and Lietz (1950)). This structure describes the fluid flow as flow between parallel plates (Harpalani and McPherson, 1986; Seidle et al., 1992).

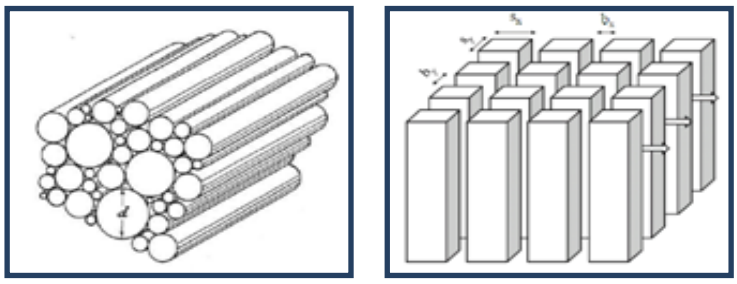

a) b)

Figure 5. Schematic representation of a) bundle of capillaries geometry (from Gates and Lietz, 1950); b) matchstick geometry (from Seidle et al., 1992)***

The derived models also account for coal deformation during production. The porosity change which is a result of compressibility and matrix shrinkage becomes one of the factors influencing capillary pressure and as a consequence relative permeability.

Curvature of capillary pressure curves and residual phase saturations may be affected by the abovementioned mechanisms. Chen et al. propose to make relative permeabilities binary functions of both water saturation and porosity change with pressure. This is achieved by introducing a residual phase saturation model and a shape factor as functions of permeability ratio, since porosity and permeability are related through the cubic relation often used for coal (McKee and Hanson, 1975; Gu, 2009; Liu and Harpalani, 2012; Palmer and Mansoori, 1996; Cui and Bustin, 2005):

$$\left(\frac{k}{k_i}\right) = \left(\frac{\phi}{\phi_i}\right)^3, \tag{3.36}$$

*** Figure is reprinted with permission from "Application of Matchstick Geometry to Stress Dependent Permeability in Coals" by Seidle et al., 1992. Conference Proceedings of SPE Rocky Mountain Regional Meeting, 1992, Casper, Wyoming, p.444, Copyright 1992 by SPE. Further reproduction prohibited without permission.

Residual phase saturation model in this work is derived modifying the approach of Chen et al. (2013) to include the proposed porosity change model that accounts for non-equilibrium desorption (see equation 3.33, 3.35). Applying the assumption that residual amount of water remains the same in the new pore volume and regarding water density as constant the residual water saturation is:

$$S_{wr} = S_{wri}\left(\frac{\phi}{\phi_i}\right)^{-1}, \tag{3.37}$$

where S_{wr} - residual water saturation; S_{wri} – initial residual water saturation.

Applying the gas compressibility in a similar manner residual gas saturation is written as:

$$S_{gr} = S_{gri}\left(\frac{\phi}{\phi_i}\right)^{-1}\left(\frac{\rho_g}{\rho_{gi}}\right)^{-1}, \tag{3.38}$$

where S_{gr} - residual gas saturation; S_{gri} – initial residual gas saturation.

The change in residual phase saturation is included in capillary pressure and relative permeability models by incorporating residual saturation terms in normalized water saturation expression that defines the fraction of mobile water.

Normalized water saturation is given as:

$$S_w^* = \frac{S_w - S_{wr}}{1 - S_{wr} - S_{gr}}, \tag{3.39}$$

After substituting residual saturations the equation becomes:

$$S_w^* = \frac{S_w - S_{wri}\left(\frac{\phi}{\phi_i}\right)^{-1}}{1 - S_{wri}\left(\frac{\phi}{\phi_i}\right)^{-1} - S_{gri}\left(\frac{\phi}{\phi_i}\right)^{-1}\left(\frac{\rho_g}{\rho_{gi}}\right)^{-1}}, \tag{3.40}$$

Curvature of capillary pressure curve is controlled by pore size distribution index, λ, in Brooks-Corey model (Brooks and Corey, 1966):

$$p_c = p_e (S_w^*)^{-1/\lambda} \ , \qquad (3.41)$$

where p_e – entry capillary pressure.

It is logical, however, that porosity/permeability change occurring in coal would affect that factor. Purcell (1949) showed how the capillary pressure curves shift at different orders of magnitude of permeability. That is illustrated in Figure 6.

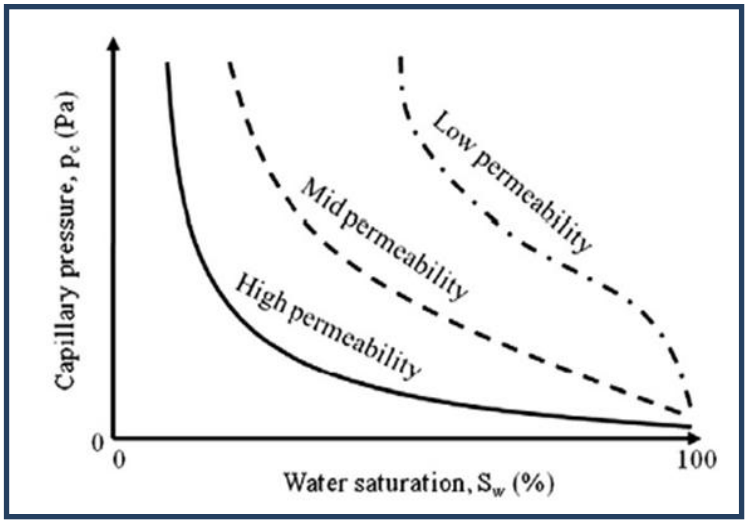

Figure 6. Effect of permeability magnitude on typical shapes of capillary pressure curves (modified from Purcell, 1949)****

As follows from Figure 6 depending on the nature of $p_c = f(S_w)$ is to a large extent determined by the permeability of porous media. Obviously, other rock properties

*** Figure is reprinted with permission from "Application of Matchstick Geometry to Stress Dependent Permeability in Coals" by Seidle et al., 1992. Conference Proceedings of SPE Rocky Mountain Regional Meeting, 1992, Casper, Wyoming, p.444, Copyright 1992 by SPE. Further reproduction prohibited without permission.

and fluid parameters also affect the shape of the curves. (Leverett, 1941) was the first to attempt to take into account the effect of the properties of rocks and fluids and summarize the dependence of the capillary pressure on saturation for different formations in a single relationship.

In our case to consider the effect of porosity change on the curvature of capillary pressure curve and correct the pore size distribution index accordingly an additional shape parameter is introduced, *J*. Shape factor *J* is a function of porosity/permeability change and currently is an empirical relation based on experimental research of Pittsburgh coal (Dabbous et al., 1976; Dabbous et al., 1974; Reznik et al., 1974).

The capillary pressure model applied for integration 3.41 is extended to include shape factor J and becomes:

$$p_c = p_e (S_w^*)^{-1/J \cdot \lambda} \ , \tag{3.42}$$

Capillary pressure model allows to link gas and water pressures, which is relevant for rate and PVT calculations:

$$p_c = p_g - p_w \ , \tag{3.43}$$

where p_g – gas pressure; p_w – water pressure.

Modifying Brooks-Corey capillary pressure model used to integrate relative permeability model with a shape parameter *J*-factor that is a function of porosity/permeability change results in a new formulation of relative permeability model based on matchstick geometry:

$$k_{rw} = k_{rw}^* (S_w^*)^{\eta+1+2/J\lambda} \ , \tag{3.44}$$

$$k_{rg} = k_{rg}^{*}(1 - S_w^{*})^{\eta}\left(1 - (S_w^{*})^{1+2/J\lambda}\right) , \quad (3.45)$$

where λ is pore size distribution index; η – tortuosity coefficient; k_{rw} - water relative permeability; k_{rg} - gas relative permeability; k_{rw}^{*} - end-point water relative permeability; k_{rg}^{*} - end-point gas relative permeability.

Deliverability

Fluid flow in cleats is considered to obey Darcy's law. Gas rate is calculated through gas pseudopressure function proposed by Al-Hussainy et al. (1966) which is presented below:

$$m(p) = 2\int_0^p \frac{p}{\mu Z} dp , \quad (3.46)$$

where μ - gas viscosity; $m(p)$ - gas pseudopressure.

The following deliverability equations are applied for production forecasting:

$$q_g = \pi k k_{rg} h \frac{T_{st}}{p_{st} T_{res}} J_D \left(m(p) - m(p_{wf})\right) , \quad (3.47)$$

$$q_w = \frac{2\pi k k_{rw} h}{\mu_w} J_D (p_w - p_{wf}) , \quad (3.48)$$

where J_D - dimensionless productivity index; p_{wf} - wellbore flowing pressure; μ_w - viscosity of water.

They are written in consistent system of units and represent the rates at surface conditions.

J_D – dimensionless productivity index is calculated as:

$$J_D = \frac{1}{\left(ln\frac{r_e}{r_w} - 0.75 + s\right)}\ , \tag{3.49}$$

where r_e - drainage radius; r_w - wellbore radius; s - skin-factor.

Drainage radius r_e is defined as:

$$r_e = \sqrt{\frac{A}{\pi}}\ , \tag{3.50}$$

Forecast Procedure

To perform the production forecast, material balance equation is combined with deliverability equations.

Shortly the procedure may be described by 3 steps:

1. Calculate gas and water rates based on current average pressure and PVT properties, known from the material balance equation and cumulative production.

2. Assume the rates constant for the specified time period and calculate the cumulative production by adding the produced volumes:

$$G_p^{n+1} = G_p^n + q_g \Delta t \ , \tag{3.51}$$

$$W_p^{n+1} = W_p^n + q_w \Delta t \ , \tag{3.52}$$

3. Calculate new average pressure from material balance equation. Repeat the procedure.

Given the described material, based on the above formulas an algorithm for creating production forecasts and calculating reservoir properties was developed. Flowchart in Figure 7 illustrates the algorithm.

The algorithm is implemented in program package Mathematica (by Wolfram Research).

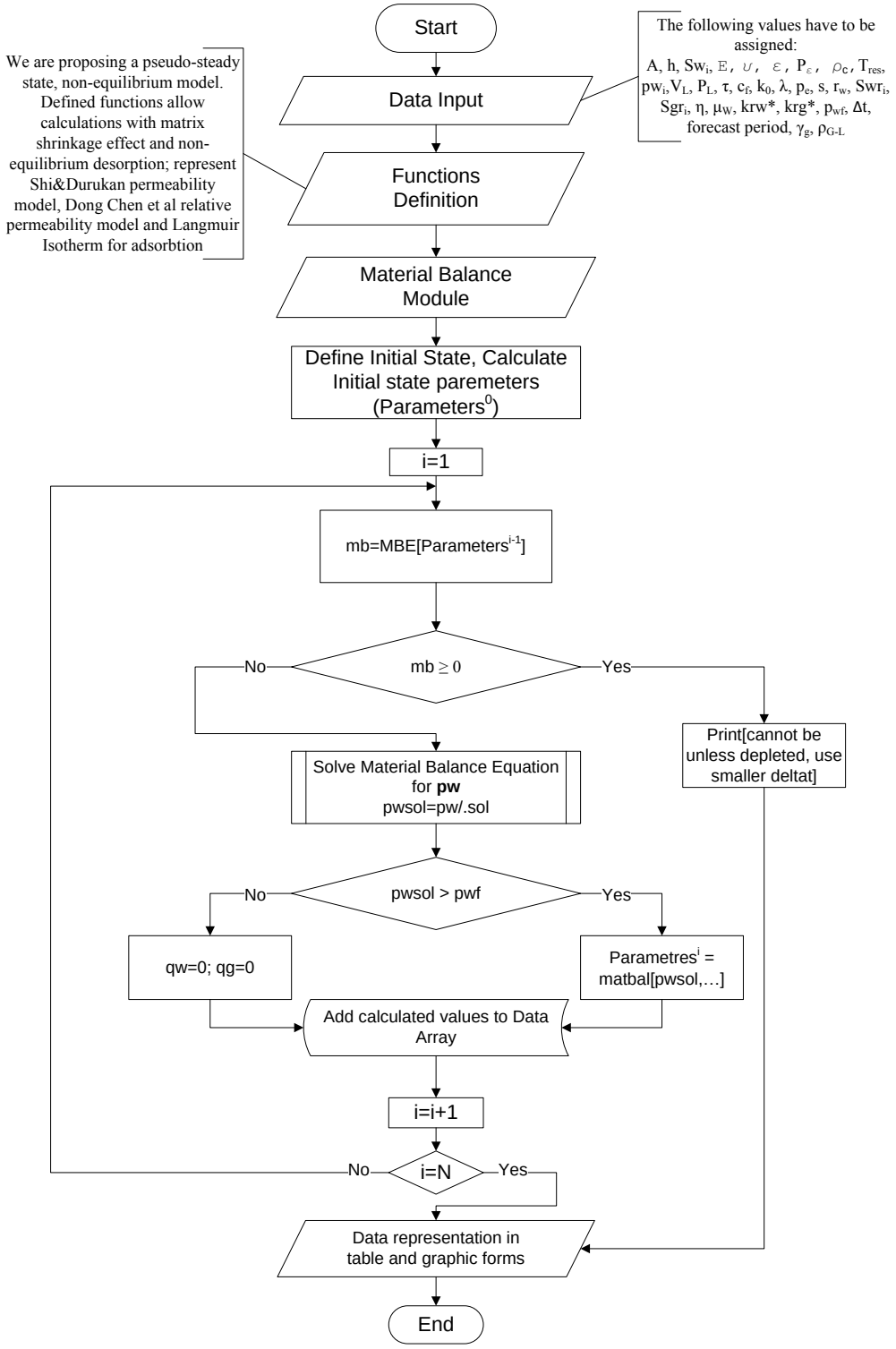

Figure 7. Flowchart of the forecasting process realized

Model Comparison with Available Commercial Software

For comparison, F.A.S.T. CBM (Fekete Associates Inc.) software was used. The software package used contains analytical as well as numerical simulation capability. We applied the pseudo-steady state history-free analytical forecast mode that is most similar to the proposed single-well analytical model.

In order to compare the results it is important to understand the theoretical differences and similarities that exist between F.A.S.T. CBM and the written software.

F.A.S.T. CBM applies King version of material balance (King, 1993; Fekete Associates Inc., 2012). It is different in some aspects from the version of material balance equation that we are applying. Also accounting for free gas content in cleats and gas adsorbed in matrix in addition F.A.S.T. CBM includes water compressibility effects.

Gas adsorption is described by the Langmuir Isotherm and equilibrium desorption is considered. Water saturation, porosity and gas formation volume factor are pressure dependent and permeability can optionally change due to matrix shrinkage effect.

The following general form of material balance equation is used that is the same that we use:

$$G_p = G + OFGIP - G_A(p) - G_F(p)\,, \tag{3.53}$$

F.A.S.T. CBM, as the majority of commercial software applies relative permeability curves that are not dependent on in-situ changes. It may use either Corey, Honarpour or generalized Corey correlations or curves, acquired by history matching

(Fekete Harmony online help). We chose to use generalized Corey correlation, which is expressed as:

$$k_{rg} = k_{rg}^{*}\left(\frac{S_g - S_{gr}}{1 - S_{gr} - S_{wr}}\right)^{n_g}, \tag{3.54}$$

$$k_{rw} = k_{rw}^{*}\left(\frac{S_w - S_{wr}}{1 - S_{wr}}\right)^{n_w}, \tag{3.55}$$

where S_{gr} – residual (critical) gas saturation; S_{wr} – residual (irreducible) water saturation; k_{rgcw} – End-point gas relative permeability (Gas-relative permeability at connate water saturation); k_{rwgc} – End-point gas relative permeability (Gas-relative permeability at connate water saturation); n_g – gas exponent; n_w – water exponent.

Including geomechanical effects of matrix shrinkage in F.A.S.T. CBM is optional. There is a choice of Seidle and Huitt, Palmer and Mansoori or Shi and Durucan permeability models. In order to be consistent with the proposed program we apply Shi and Durucan model.

Another difference lies in the units applied in calculations. All the equations in F.A.S.T. CBM use the input in field units.

Therefore, the deliverability and other applied equations contain conversion factors. Well deliverability is calculated in field units through pseudopressure function mentioned earlier in equation 3.46 . Radial flow is considered.

The applied deliverability equations are written as follows:

$$q_g = \frac{k_g h\left[m(p) - m(p_{wf})\right]}{1422T\left[ln\left(\frac{r_e}{r_w}\right) - 0.75 + s\right]}, \tag{3.56}$$

$$q_w = \frac{k_w h[p - p_{wf}]}{141.2\mu_w B_w \left[ln\left(\frac{r_e}{r_w}\right) - 0.75 + s\right]}\ , \tag{3.57}$$

where h – net pay (ft); k_g – gas effective permeability (mD); m(p) – gas pseudopressure (psi^2/cp); p – average reservoir pressure (psia); p_{wf} – bottomhole flowing pressure (psia); q_g – gas rate (MSCFD); r_e – external radius of the reservoir (ft); r_w – wellbore radius (ft); s – skin; T – temperature (^oR); B_w – water formation volume factor (bbl/stb); k_w – water effective permeability (mD); q_w – water rate (bbl/d); μ_w – water viscosity (cp);

Table 4 summarizes the differences between the proposed single-well analytical model and F.A.S.T. CBM.

Table 4. The comparison of F.A.S.T. CBM semi-analytical model and our model

F.A.S.T. CBM Model	**Our Model**
Assume constant average pressure at a given time step at all points of the drainage volume (pseudo-steady state tank models).	
Forecast is performed combining deliverability and material balance equations at each step.	
Fracture can be modeled by decrease in skin-value.	
The gas diffusion from matrix is always assumed at instantaneous equilibrium.	Can model transport mechanism to cleats assuming pseudo- steady state, non-equilibrium desorption.
Includes water compressibility effects.	Considers water incompressible.
Constant relative permeability curves	Improved relative permeability model, relative permeability is a binary function of water saturation and permeability change
Calculations are performed in field units, with the possibility to present data in either metric or field units	Calculations are performed in SI units, but the output may be modified to be in either SI or field units.

CHAPTER IV

RESULTS AND DISCUSSION

This chapter presents the cases that were realized and examined in this research. The results will be illustrated and analyzed.

Base Case Description and Results

The single-well analytical model was designed specifically for coalbed methane reservoirs for all well performance forecasts presented in this paper. This simulator models the processes of Darcy flow, Fickian diffusion, and methane desorption, which are the mechanisms that characterize the behavior of coalbed methane reservoirs.

We considered a coal model with area 10,000 m^2 and pay thickness 2 m. The base case option is based on constant wellbore flowing pressure assumption and includes the modified Shi and Durucan (2003c) permeability, modified Chen et al. (2013) relative permeability and specially designed for this program porosity models with deformation being a function of reservoir pressure and the actual desorbed and diffused gas volume. The production forecast was performed for a one year period.

The input parameters used in the base case calculation are in Table 5. Listed parameters were obtained from the literature (Chen et al., 2013; Palmer and Mansoori, 1996; Shi and Durucan, 2004; Shi et al., 2008; Pan et al., 2010; Billemont et al., 2013; Economides et al., 2013).

Table 5. Input parameters used for the base case

Parameter	**Value**	**Unit**
Area, A	10000	m^2
Thickness, h	2	m
Coal density, ρ_c	1600	kg/m^3
Initial water saturation, S_{wi}	0.95	%
Young's modulus, E	2900	MPa
Poisson's ratio, ν	0.35	-
Langmuir volumetric strain constant, ε_L	0.01266	-
Langmuir pressure constant at ½ ε_L, P_ε	4.31	MPa
Adsorbed gas density, ρ_{g-l}	414	kg/m^3
Reservoir temperature, T_{res}	305.15	K
Specific gravity of gas (pure methane), γ_g	0.55	-
CO_2 concentration	0	-
N_2 concentration	0	-
H_2S concentration	0	-
Initial water pressure, p_{wi}	6.41	MPa
Gas Langmuir volume constant, V_L	0.027	m^3/kg
Gas Langmuir pressure constant at ½ V_L	2.96	MPa
Diffusion time, τ	50	days
Coal cleat compressibility, c_f	0.2	1/MPa
Initial permeability, k_i	2	mD
Pore size distribution index, λ	0.22	-
Entry capillary pressure, p_e	0.006	MPa
Skin factor, s	0	-
Initial residual water saturation, S_{wri}	0.84	-
Initial residual gas saturation, S_{gri}	0	-
Tortuosity coefficient, η	1	-
Viscosity of water, μ_w	$6.5 * 10^{-4}$	Pa*s
End-point relative permeability of water, k_{rw}*	1	-
End-point relative permeability of gas, k_{rg}*	1	-
Bottom hole pressure, p_{wf}	0.3	MPa

Our model is limited to single well. No water influx is assumed (there is no aquifer available, no water coming out of matrix). Gas storage is limited by coal mass and Langmuir Isotherm. The applied Langmuir Isotherm is shown in Figure 8. Since our reservoir is saturated, the initial point is directly on the curve, therefore desorption has

already commenced (critical desorption pressure was reached) and the flow will be two-phase from the beginning of production. Initial condition with regard to gas content is shown on Langmuir Isotherm in Figure 8.

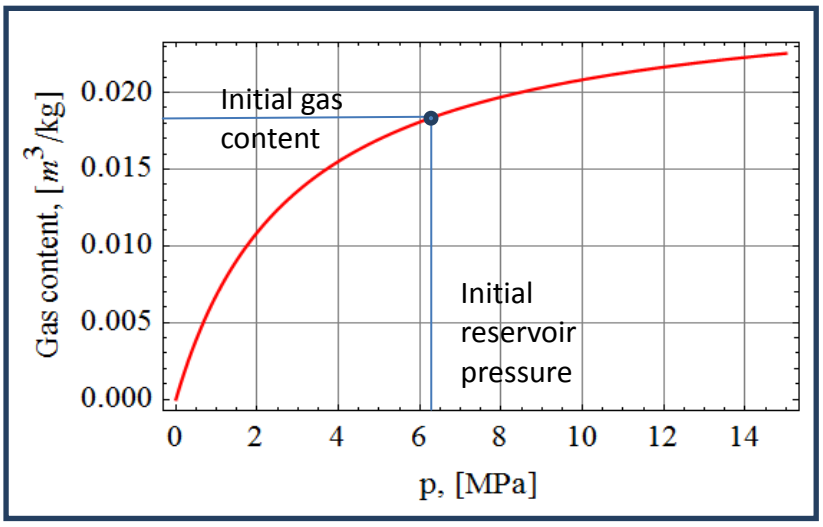

Figure 8. The applied Langmuir isotherm characterising gas content of coal

The estimated OGIP value is 593 000 m^3.

Figure 9 - Figure 13 represent the production performance predicted.

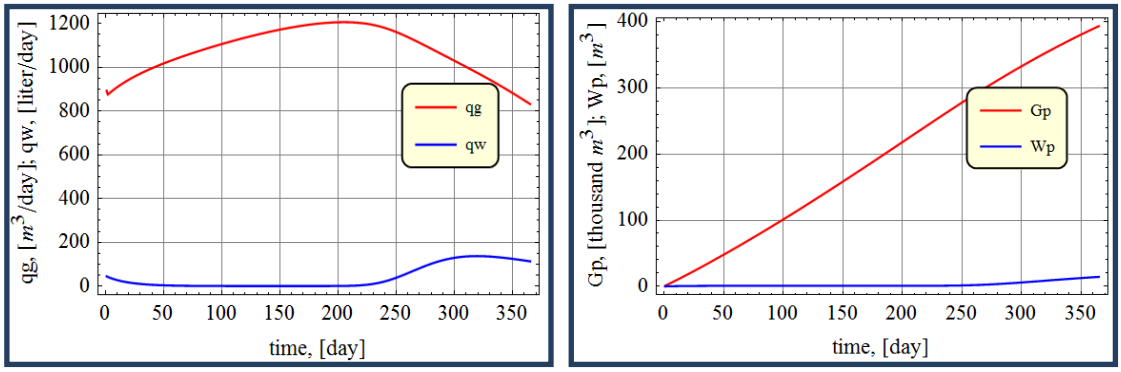

a) b)

Figure 9. a) Gas and water rates (base case); b) Cumulative gas and water production (base case)

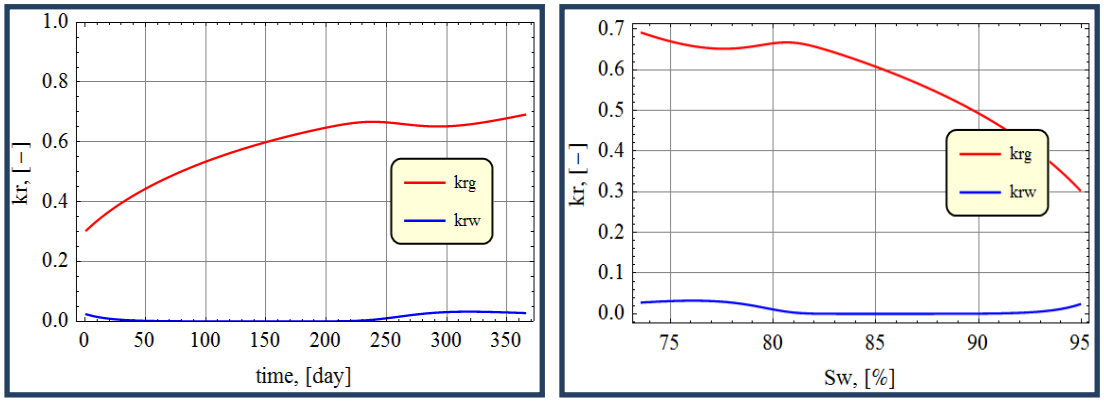

a) b)

Figure 10. a) Gas and water relative permeabilities vs time (base case); b) Gas and water relative permeabilities vs water saturation (base case)

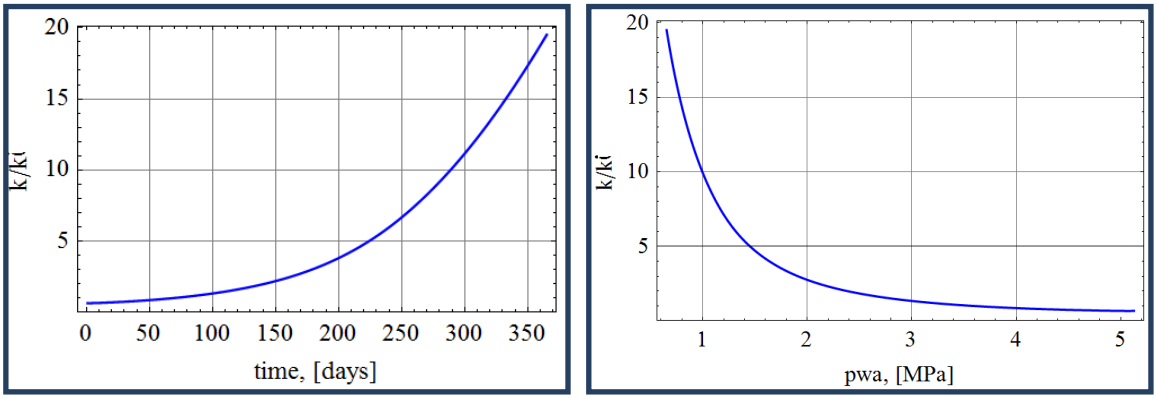

a) b)

Figure 11. a) Absolute permeability change vs time (base case); b) Absolute permeability change vs average water pressure (base case)

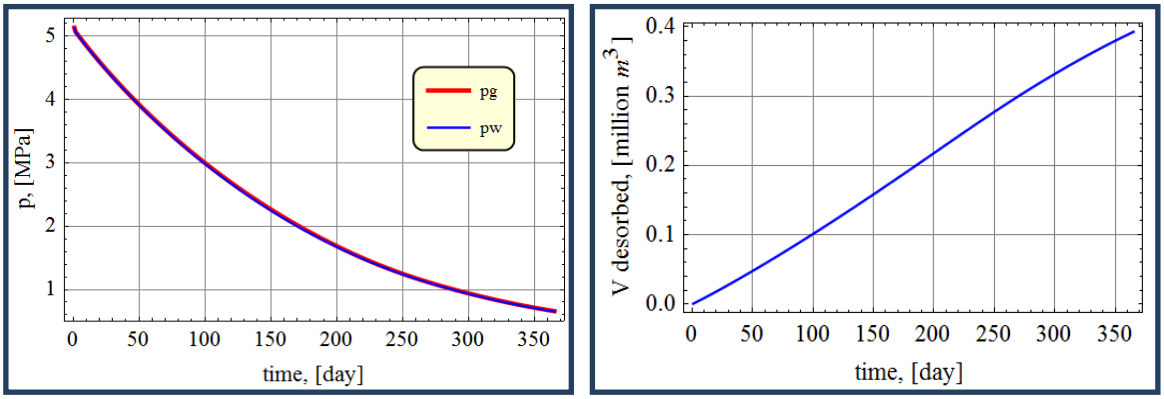

a) b)

Figure 12. a) Gas and water pressures (base case); b) Actual non-equilibrium cumulative desorbed gas volume (base case)

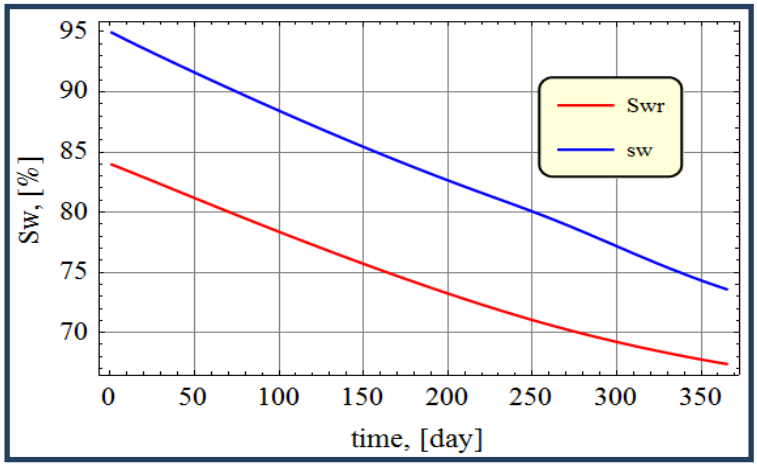

Figure 13. Residual and current water saturations (base case)

Our initial state parameters imply that the reservoir is saturated, therefore gas production starts with no delay for dewatering to depressurize the coal seam to critical desorption pressure.

Production controlled by pressure gradient causes the reduction in average reservoir pressure. As pressure declines the gas starts desorbing in non-equilibrium manner, controlled by diffusion mechanism. Gas desorption causes matrix shrinkage, decrease in effective horizontal stress and consequently increase in permeability. Therefore we see a significant increase in gas rate that peaks after 200 days of production. That is an illustration of typical negative decline curve behavior of CBM reservoirs. The period of "negative" decline corresponds to an increasing gas desorption rate associated with pressure drawdown and coalbed dewatering. After gas rate reaches its peak the production declines, since the pressure gradient is lower compared to beginning of production and less gas is desorbing (according to Langmuir Isotherm).

Water behavior is more peculiar and is a direct result of the applied porosity, permeability and relative permeability models. Water production continues as long as conditions are appropriate – that is current water saturation is higher than residual and water relative permeability is sufficient. In this model relative permeabilities are binary functions of saturation and permeability change. Their curvature can be found on Figure 10 and related to water production.

Figure 13 illustrates how the residual water saturation changes as a result of gas desorption and compression effects on porosity. Change of residual water saturation is related to the change of the pore volume, that is, with increasing volume of macropores (cleats) due to the effect of matrix shrinkage with gas desorption a reduction of the residual water saturation at constant volume occupied by water takes place. In other words at constant volume of residual water, its share in pore volume (water saturation) decreases.

Permeability ratio plotted against pressure in Figure 11 is a representation of the Shi and Durukan permeability model applied as described in Chapter III. It considers coal deformation corresponding to compression and matrix shrinkage as a result of the non-equilibrium desorption process.

In this model relative permeabilities are binary functions of saturation and porosity change. Therefore at every timestep only one value of relative permeability exists. We have plotted permeability curves at different times, and porosities consequently. They are shown in Figure 14. In the process of production the values of the residual saturations change and so do relative permeability curves. Change of

residual water saturation is related to the change of the pore volume, that is, with increasing volume of macropores (cleats) due to the effect of matrix shrinkage with gas desorption a reduction of the residual water saturation at constant volume occupied by water takes place. In other words at constant volume of residual water, its share in pore volume (water saturation) decreases.

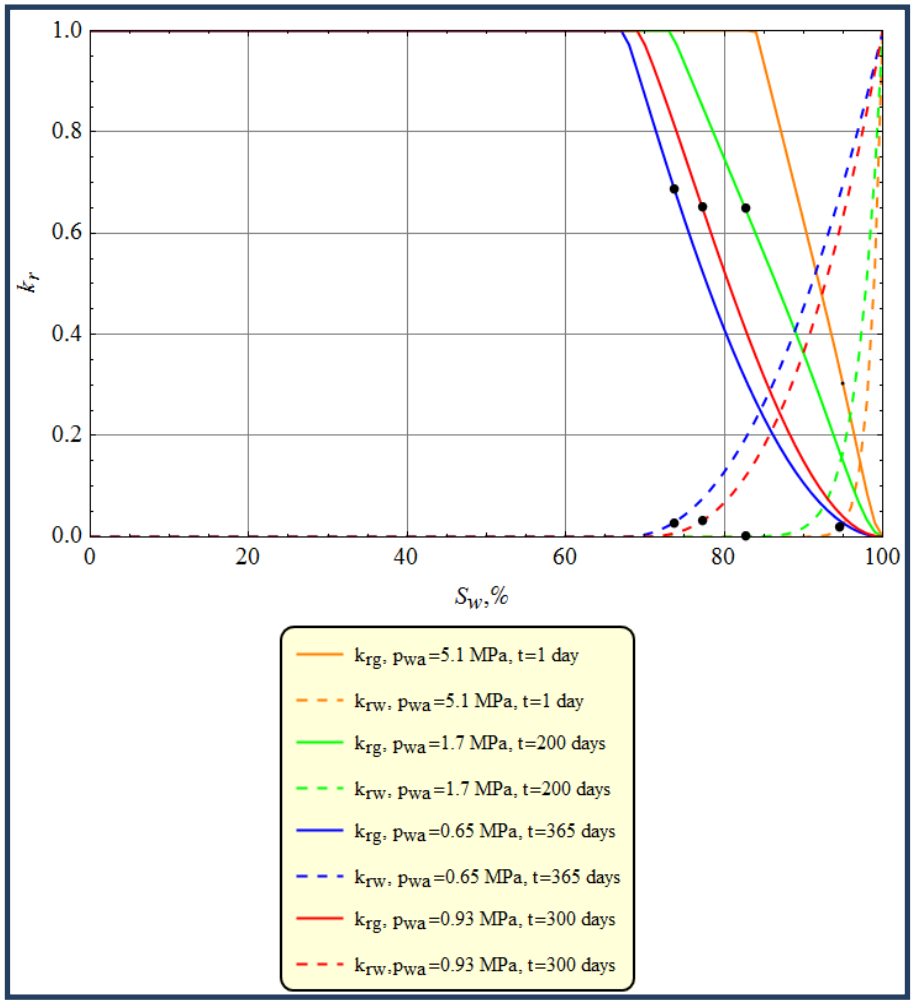

Figure 14. Relative permeability curves calculated for different times

Considering Different Shape Factor J Expressions

Chen et al. (2013) introduce a shape factor J that is dependent on permeability ratio. As shown in Purcell (1949) capillary pressure is greatly affected by permeability magnitude, this should not be neglected when performing studies of flow through coal seams. Shape factor J provides means of incorporating the effect of porosity change to the form of relative permeability curves. Since pore size distribution index (λ) originally controls the curvature of capillary pressure curves at constant porosity, additional coefficient representing its change with flexible porosity values is needed. Capillary pressure consequently affects relative permeability, resulting in production changes. Due to lack of data on the matter, Chen et al. (2013) are using an empirical approximation based on experimental data of Pittsburgh coal by Dabbous et al. (1976); Dabbous et al. (1974) and Reznik et al. (1974). Currently used J factor, being a function of permeability change k/k_i , may only be considered as an illustration of behavior for one type of coal and more robust interpretation following an excessive study is needed to allow a general use of J. The plot provided for fitting in Chen et al. (2013), as seen in Figure 15 is based on 3 points only. That makes the approximation highly uncertain. Therefore, we have run additional options with rough linear and power trend lines as shown in Figure 15. The results will be compared to each other and base case.

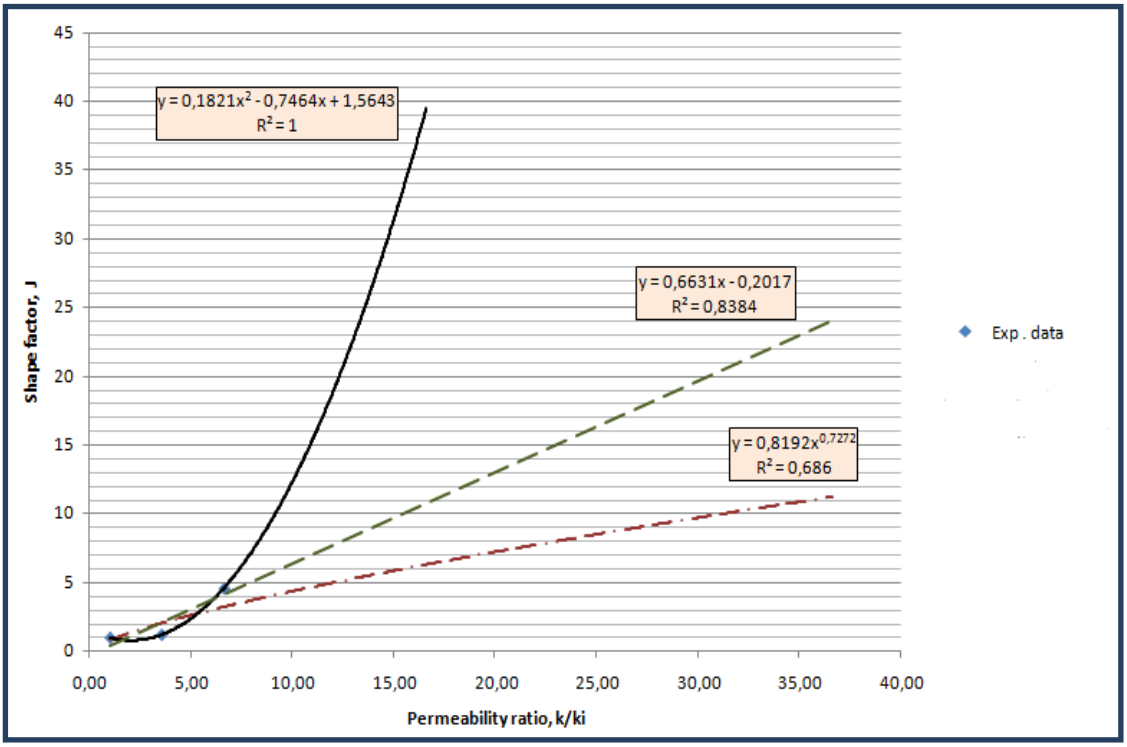

Figure 15. Shape factor J approximations

Currently, end-point relative permeability changes with porosity variation are not accounted for, since it has not been widely studied experimentally. However, it is assumed that the change of general curvature has a more significant effect than end-point changes on methane flow rate (Karacan, 2008; Young et al., 1992).

As mentioned earlier J-factor controls relative permeabilities. A difference in water production behavior was identified as a result of simulation runs. Roughly, it can be said that linear approximation of shape factor function could be considered as pessimistic in comparison with the optimistic parabolic case. The results of runs with different shape factor J expressions are presented in Figure 16.

Quadratic trend J-function	Linear trend J-function	Power trend J-function
Gas and water rates		
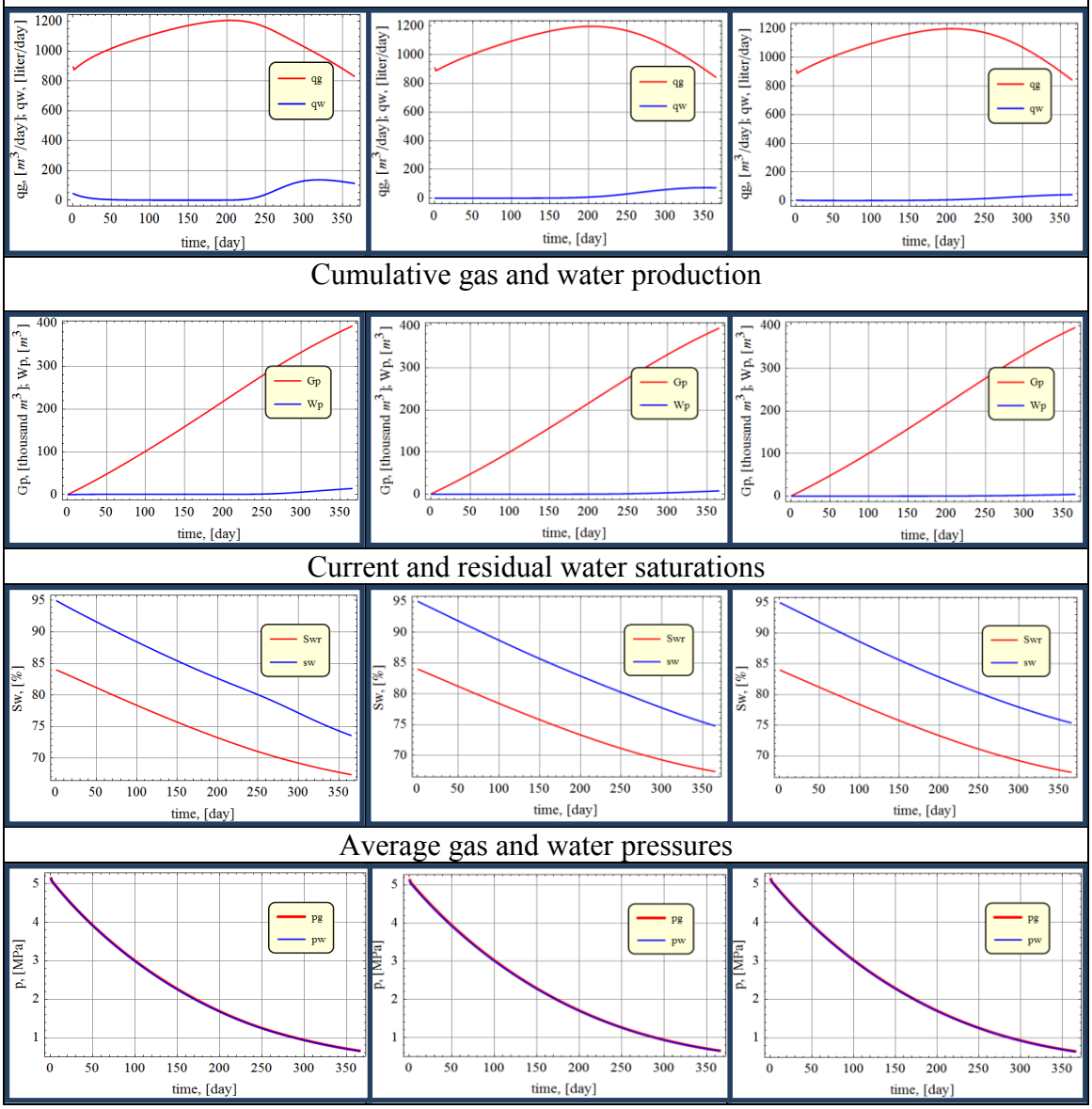		
Cumulative gas and water production		
Current and residual water saturations		
Average gas and water pressures		

Figure 16. Comparison of results from runs with application of different shape factor J trend lines

Quadratic trend J-function	Linear trend J-function	Power trend J-function
Actual non-equilibrium cumulative desorbed gas volume		
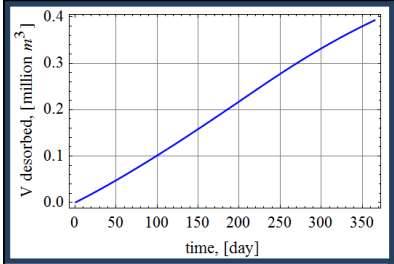	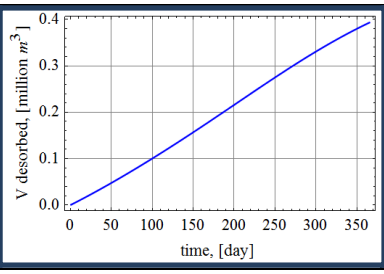	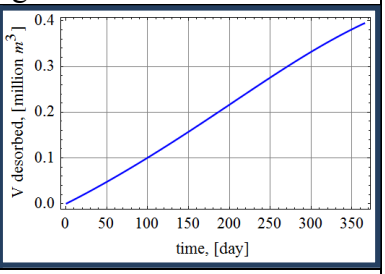
Absolute permeability change vs time		
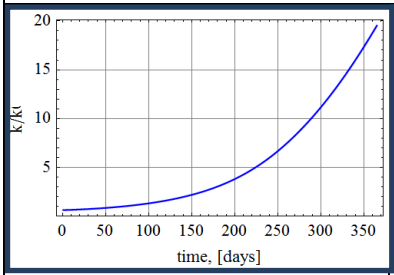	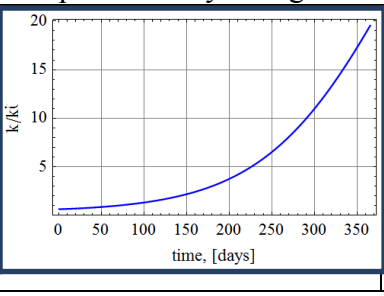	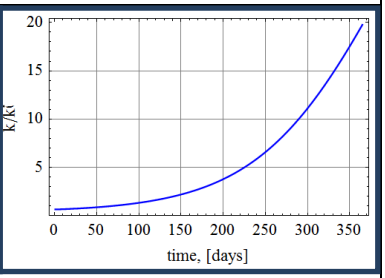
Relative gas and water permeabilities vs time		
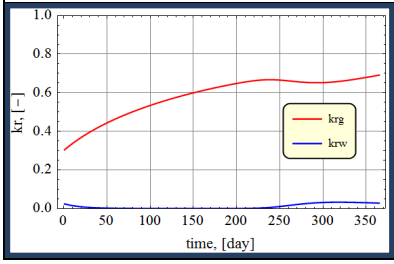	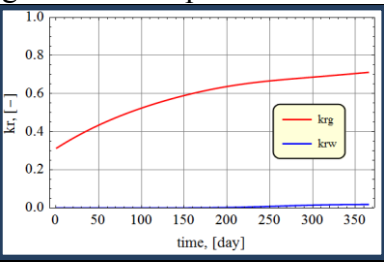	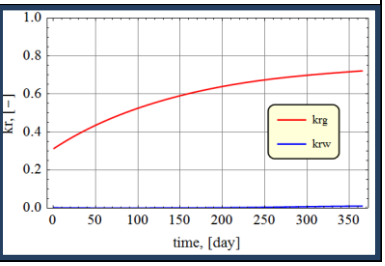

Figure 16. Continued

Considering the Impact of Non-Equilibrium Nature of Diffusion on Coal Deformation

As described in CHAPTER III the proposed solution applies an improved version of porosity and permeability models in regards of non-equilibrium nature of desorption. The original formulations seemingly lacked accounting for the impact continuous process of diffusion. The proposed solution makes the deformation dependent on the

actual desorbed volume in contrast to pressure dependent value of strain that represents volume that desorbs at equilibrium with pressure in question. The proposed model is more consistent for large values of diffusion constant especially. Since at large values of diffusion constant τ gas movement is slowed down significantly and the actual released gas volumes are smaller than those proposed by Langmuir Isotherm the current adsorbed gas content is larger and therefore the deformation is supposed to be proportional. It may be said that in previous formulations matrix shrinkage was considered proportional to desorption, while we made it proportional to both desorption and diffusion.

In order to perform the assessment of the impact of including diffusion-related effects on coal mechanics we performed a run that does not account for them. It will be compared to base case later in this chapter.

Base case considers permeability, porosity and relative permeability as functions of pressure and current volume adsorbed in non-equilibrium conditions. When that option is dropped, permeability and porosity changes can be calculated based on pressure change only regardless of the actual desorbed amount, volumetric strain being calculated for equilibrium conditions. Therefore it is possible to predict the filtration and capacitive characteristics of the formation based on pressure change. This results in permeability and porosity changes that can be acquired prior to performing production forecasts and follow in Figure 17 - Figure 18.

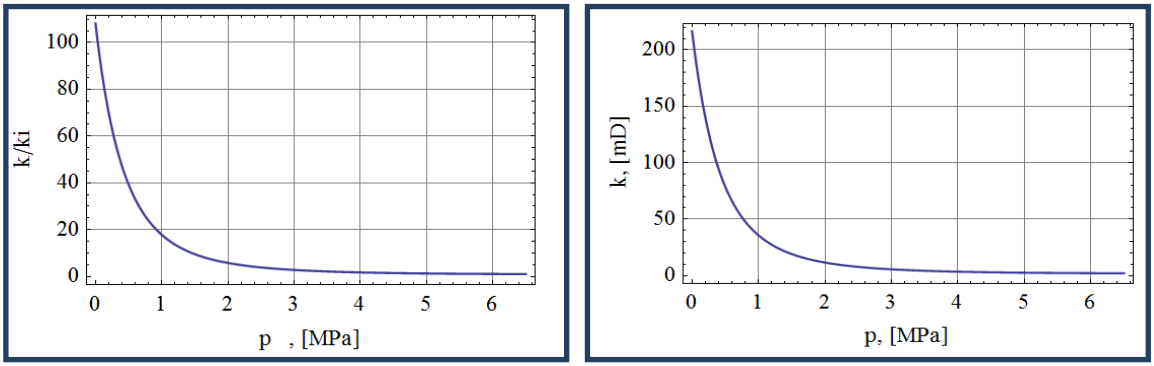

a) b)

Figure 17. a) Absolute permeability change for equilibrium-based volumetric strain change; b) Absolute permeability for equilibrium based volumetric strain change

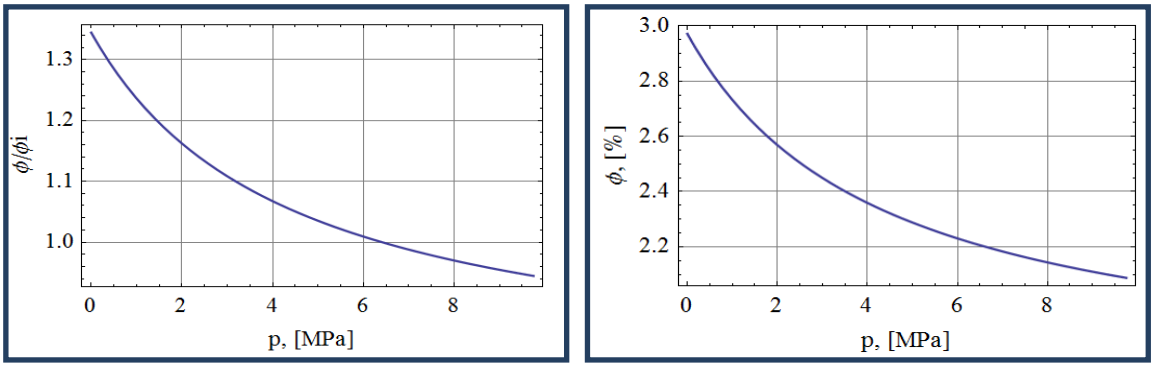

a) b)

Figure 18. a) Porosity (cleat) change for equilibrium-based volumetric strain change; b) Porosity (cleat) for equilibrium based volumetric strain change

The comparison of well performance in the case being described to base case may be done on the basis of Figure 19.

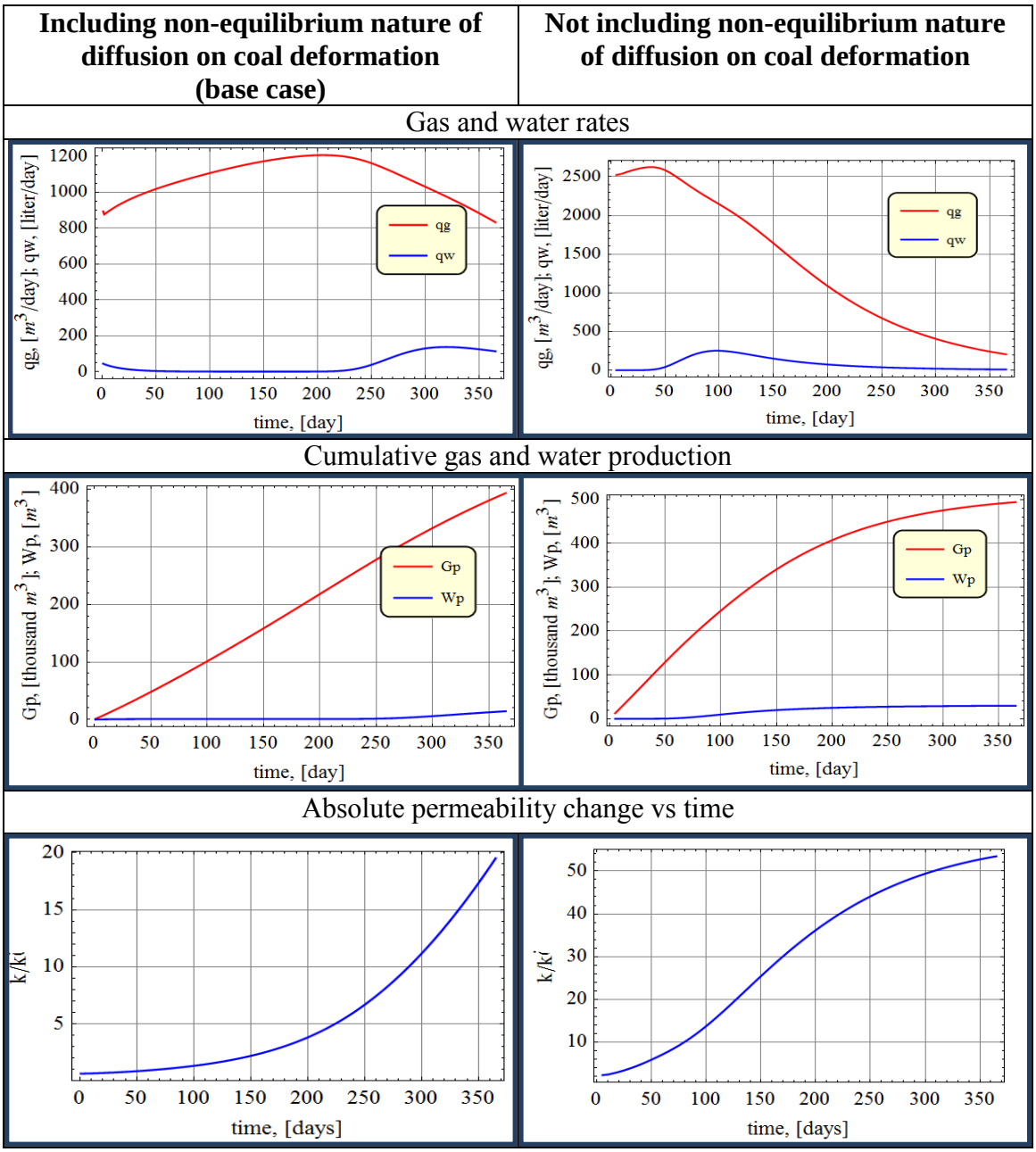

Figure 19. Effect of including non-equilibrium nature of desorption in considering coal deformation

Including non-equilibrium nature of diffusion on coal deformation (base case)	Not including non-equilibrium nature of diffusion on coal deformation
Relative gas and water permeabilities vs time	

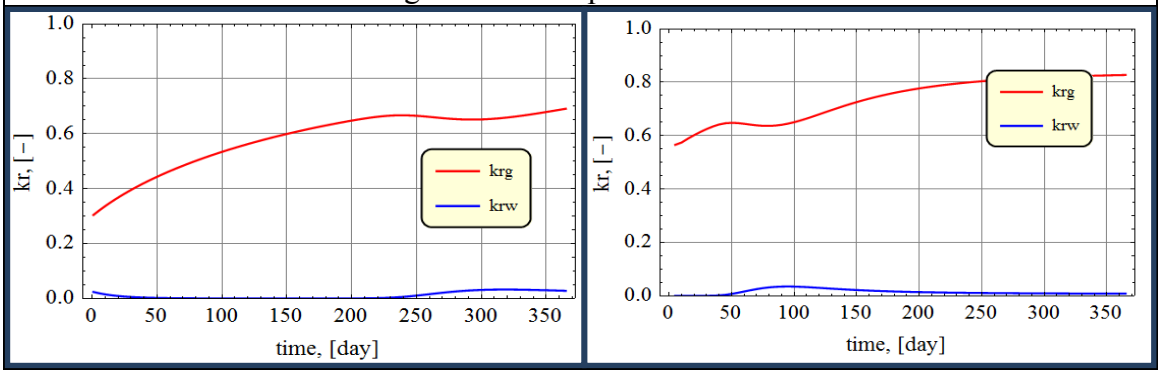

Figure 19. Continued

The performed calculations support that not accounting for the fact that gas desorbs continuously in calculating the volumetric strain change due to matrix shrinkage results in significant overestimation of gas rates. This is to be expected since when higher gas content in matrix is accounted for the calculated volumetric strain change is lower and therefore porosity and permeability enhancement due to matrix shrinkage are less significant; that is illustrated with the base case. Lower permeability does not allow high production rates, so the pressure declines at slower rate.

Gas Production at Constant Pressure Drawdown, ($p-p_{wf}$)

Production rate is proportional to drawdown, defined as average pressure in the reservoir minus wellbore flowing pressure. Base case calculation uses constant wellbore flowing pressure as input. However, it order to control the production of CBM it is

possible to set variable wellbore flowing pressure. The scope of this research did not suggest the detailed study of possible well exploitation regimes. However, by analogy with conventional gas reservoirs we tried to investigate the effect of constant pressure gdrawdown on production. Depending on operational conditions there may be various reasons for pressure drawdown limitation. For example, high pressure drawdown values may cause unwanted deformation of porous media causing conduction disturbances of natural fracture system in coal, creating negative permeability effect.

The input had to be modified to include the value of desired values of pressure drawdown Δp and minimal wellbore flowing pressure $p_{wf\ min}$. The calculation of wellbore flowing pressure was therefore performed at every time step in the following way:

$$p_{wf} = p_w - \Delta p\ , \qquad (p_w - \Delta p) > p_{wf\ min}\ , \tag{4.1}$$

$$p_{wf} = p_{wf\ min}\ , \qquad (p_w - \Delta p) \leq p_{wf\ min}\ , \tag{4.2}$$

Minimal wellbore flowing pressure $p_{wf\,min}$ was set 0.3 MPa in all the runs.

We will address the effect of different choice of pressure drawdowns on production as well as compare constant wellbore flowing pressure and constant pressure drawdown regimes.

There may be various reasons for the choice of either constant wellbore flowing pressure or constant pressure drawdown well exploitation regime. The results of comparison of those regimes are rather trivial, since we are not considering the possible negative effects of high pressure drawdowns on fracture conductivities that would lead

to decision of limiting the wellbore flowing pressure. The production performance comparison is illustrated in Figure 20.

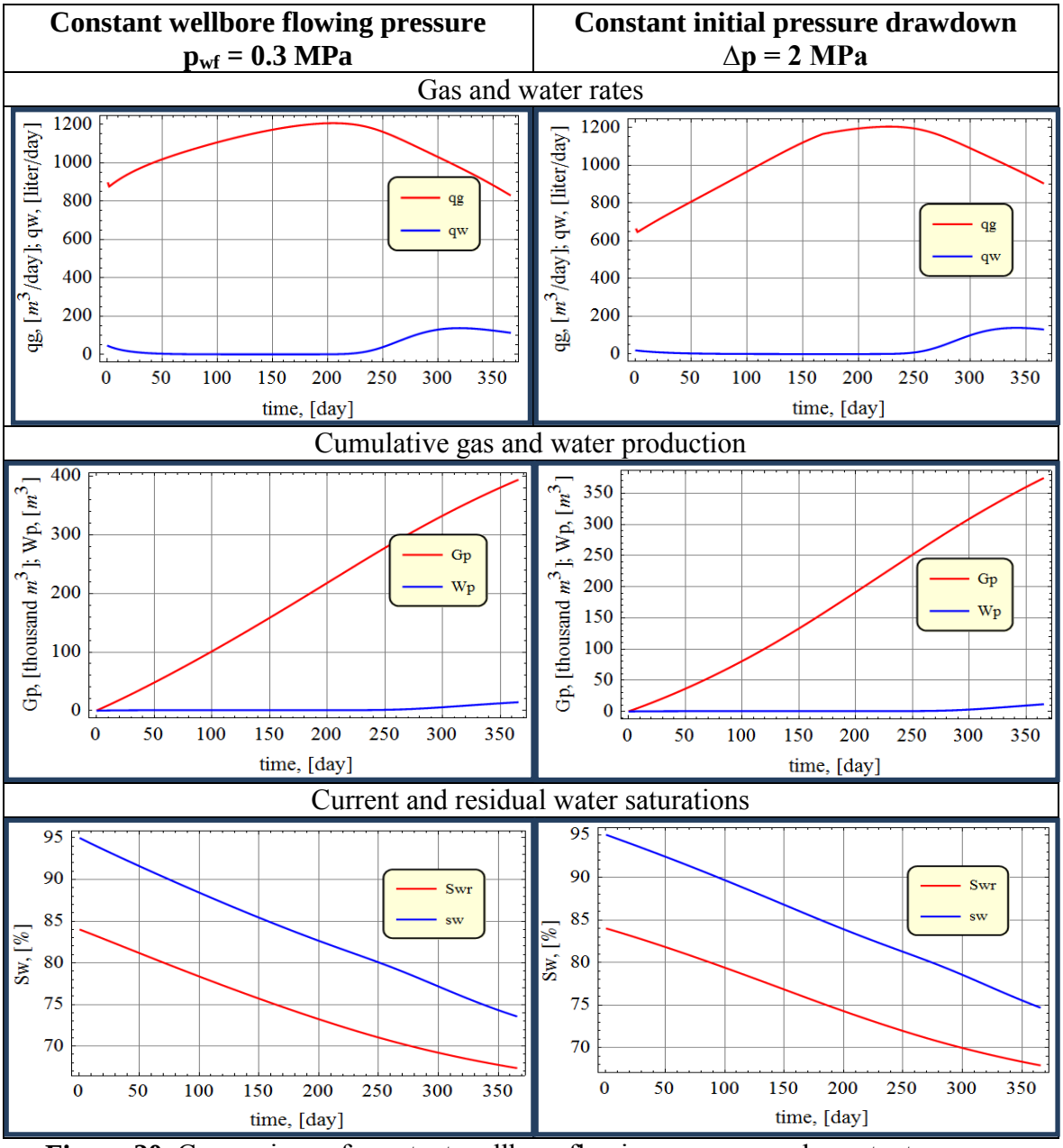

Figure 20. Comparison of constant wellbore flowing pressure and constant pressure drawdown regimes

Constant wellbore flowing pressure p_{wf} = 0.3 MPa	**Constant initial pressure drawdown Δp = 2 MPa**

Average gas and water pressures

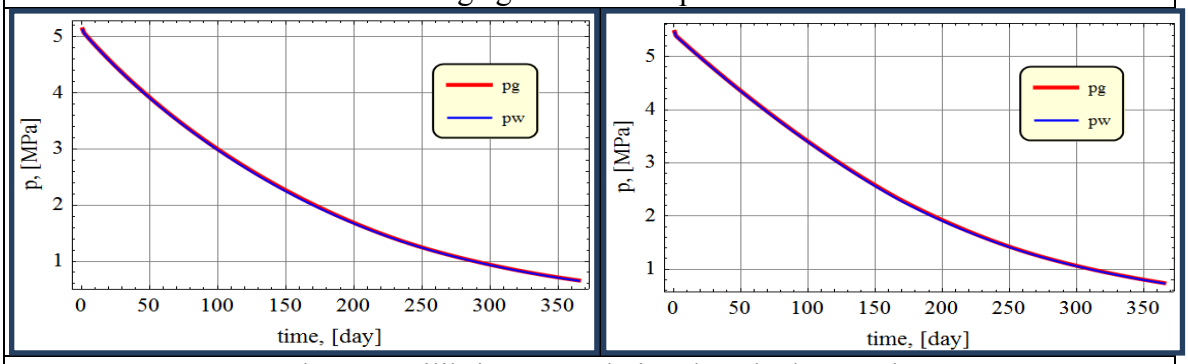

Actual non-equilibrium cumulative desorbed gas volume

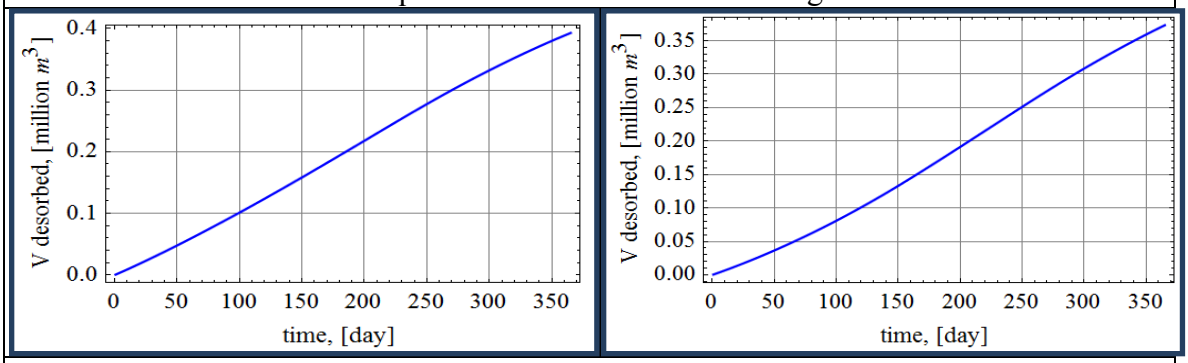

Absolute permeability change vs time

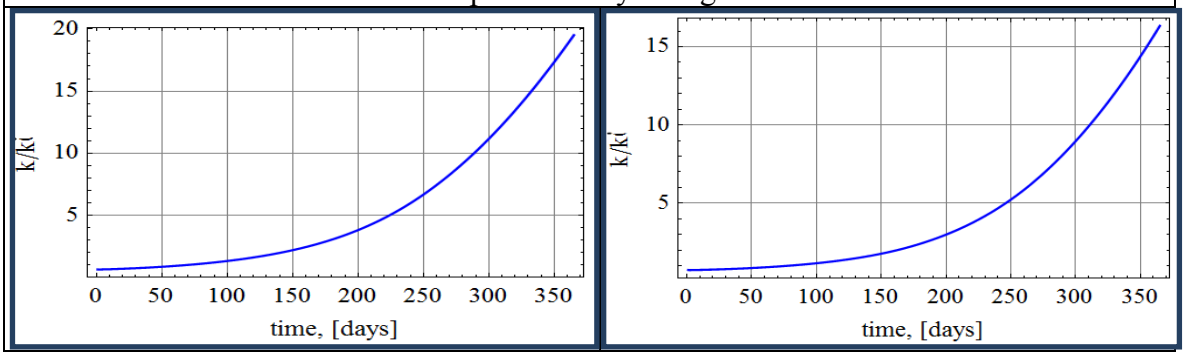

Figure 20. Continued

Constant wellbore flowing pressure p_{wf} = 0.3 MPa	Constant initial pressure drawdown Δp = 2 MPa
Relative gas and water permeabilities vs time	

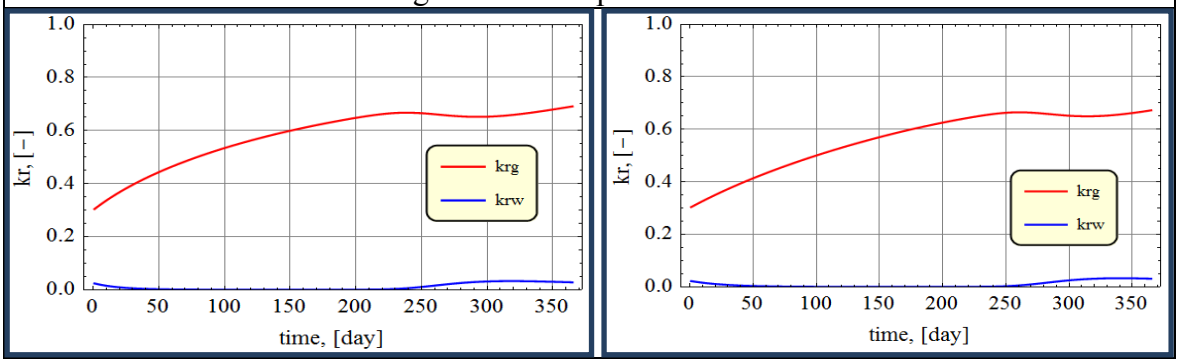

Figure 20. Continued

Initially higher wellbore flowing pressure for constant pressure drawdown case causes reservoir pressure to decrease at slower rate and leads to lower production rates. As a result during the same time period the cumulative gas production reached is lower.

Figure 21 - Figure 24 show the comparison results using different choices of pressure drawdown.

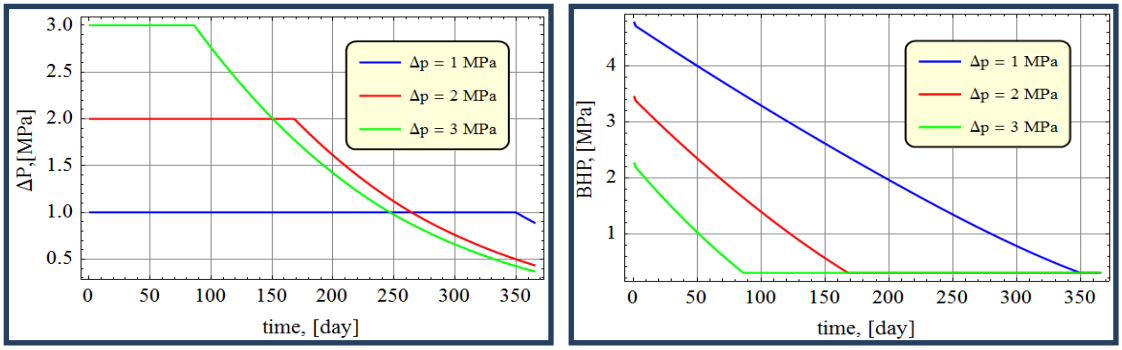

a) b)

Figure 21. a) Pressure drawdown; b) Effect of initial pressure drawdown on wellbore flowing pressure

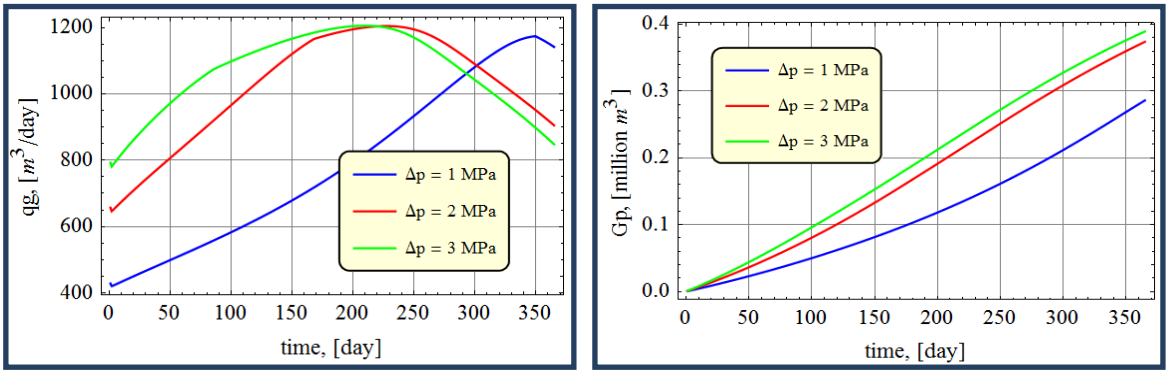

a) b)

Figure 22. Effect of initial pressure drawdown on a) gas rate; b) cumulative gas production

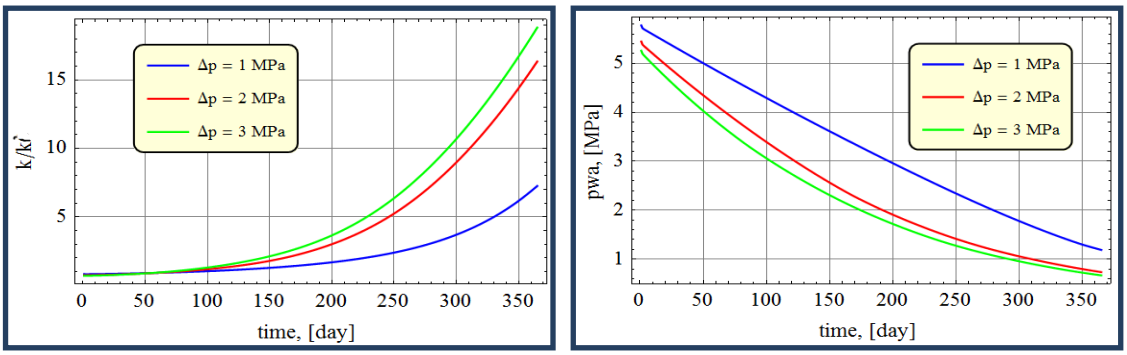

a) b)

Figure 23. Effect of initial pressure drawdown on a) absolute permeability change; b) average water pressure

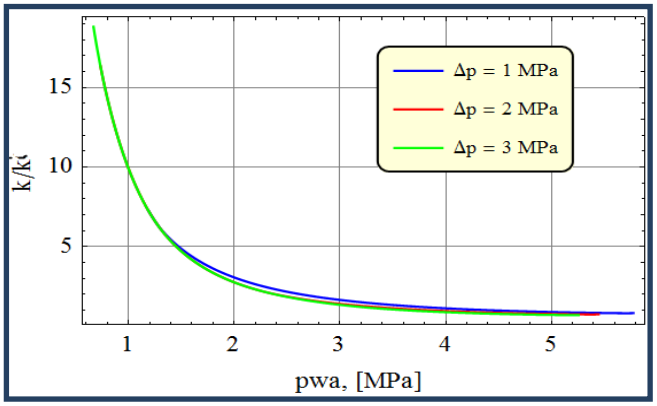

Figure 24. Effect of initial pressure drawdown on absolute permeability change vs average water pressure

The peak gas rate is reached later for lower values of pressure drawdown (Figure 22a) and the production continues longer. By analogy with what has been said earlier, the cumulative gas production reached by the end of a one year period is lower for lower pressure drawdowns (Figure 22b). All of the illustrated differences may be explained by the behavior of the reservoir pressure. Absolute permeability changes as a function of pressure and volume adsorbed at non-equilibrium conditions. The effect of non-instantaneous diffusion is reflected in the slight difference of the curvature of absolute permeability curve plotted as a function of pressure that would be absent was that effect not included.

Parametric Sensitivity Study

A "parametric study" approach was implied to investigate the relative importance of some properties used as input for CBM single-well analytical model. The variation of

predicted well performance can be analyzed, resulting from independent changes (all other values remaining equal) of each reservoir property based on the base case.

In this study coalbed parameters that control gas storage and flow were considered to be independent parameters, so that it would be possible to evaluate the significance of separate effects. Strictly speaking that is not accurate, since coal seams are bound systems and their properties come as a complete set of porosity (both micro and macro), stress conditions, elastic properties, saturations, etc. As a result every coal is unique and its behavior in changing conditions is unique. However, lack of convenient data sets puts us in a situation where we have to vary the properties according to separate property measurements for different coals available in literature. Although it would be preferential to compare models based on complete data sets, it would also be harder to interpret the separate effects since all the parameters would be different at every run. While keeping constant every parameter but one allows producing clear results for quality understanding. As a result we can estimate relative importance of parameters of reservoir engineering, gas flow and storage for predicting methane and water production behavior.

Understanding of relative contribution of separate input parameters is important since it allows to understand how much measurement bias errors may reflect on production performance forecasting; help assessment of the forecast reliability, major prediction uncertainties and identifying the most influential parameters.

We investigated the reservoir behavior under constant producible gas volume conditions, therefore we kept the reservoir dimensions, initial reservoir pressure, initial

porosity and adsorption parameters constant. We performed a sensitivity study on the following parameters: wellbore flowing pressure p_{wf}, coal cleat compressibility c_f, Langmuir volumetric strain ε_L, initial permeability k_i, Poisson's ratio ν, pore size distribution index λ, wellbore radius r_w, skin-factor s, residual water saturation at initial conditions S_{wri}, diffusion time τ and Young's modulus.

Most of these parameters are characteristics of coal and cannot be controlled, therefore representing the possible values for coals of different age and geologic setting. This allows us to study the performance of different coals at similar production conditions.

CBM property variation intervals to assess the sensitivity of the results of calculation of technological parameters to the input data were justified based on literature review.

Chen et al. (2012) presented a useful summary of possible variation in coal properties based on extensive amount of literature sources. Paper by Robertson and Christiansen (2008) also presents a table summarizing the coal properties cited in different papers.

A methodology for measuring various coal properties needed for application of Palmer and Mansoori or Shi and Durucan permeability models was created by Pan et al. (2010). It was tested on bituminous coal from Bulli seam - Australian coal from South Sydney basin. This study stated that permeability models that include matrix shrinkage are highly sensitive to initial value of porosity. They measured pressure dependence of

cleat compressibility, however it is not very significant: decreases from 0.0507 1/MPa to 0.0366 1/MPa for increasing pore pressure for methane.

It can be noted that very different compressibility values are reported in literature for coal. The order of magnitude changes significantly for every specific coal. Harpalani (1999) reported an experimental method to measure coal compressibilities, including pore compressibility. The paper, however, stressed that the described procedure yields uncertain results and more robust techniques are needed. This study also noted that matrix shrinkage effect could dominate over pore volume compressibility effect resulting in a possibility of permeability increase.

Due to complexity of experimental determination of pore volume compressibility, Seidle et al. (1992) proposed a successful analytical technique to fit experimental data and estimate cleat volume compressibility - c_f.

The possible data for different coals according to literature review can be found in Table 6.

Table 6. Properties variation

Parameter	Values	References
Initial water saturation	40 % - 100 %	Karacan (2008); Chen et al. (2012); King et al. (1986); King (1993); King (1990); Remner et al. (1986)
Initial pressure	1.03 MPa - 10.77 MPa	Karacan (2008); Chen et al. (2012); King et al. (1986); Spencer et al. (1987); Guo et al. (2003); Young et al. (1991); King (1993); King (1990)
Diffusion Time	0.083 day – 925.93 days	Karacan (2008); Spencer et al. (1987); Chen et al. (2012); Young et al. (1992); King (1993); King (1990)
Langmuir Volume	0.002 m^3/kg – 0.031 m^3/kg	Chen et al. (2012); Karacan (2008); Pan et al. (2010); Remner et al. (1986); Young et al. (1991); Young et al. (1992)
Langmuir Pressure	0.18 Mpa – 5.8 MPa	Chen et al. (2012); Karacan (2008); Pan et al. (2010); Remner et al. (1986); Young et al. (1991); Young et al. (1992)
Porosity	0.05 % - 30 %	Robertson and Christiansen (2008); Karacan (2008); Chen et al. (2012); King (1993); King (1990); King et al. (1986); Remner et al. (1986); Spencer et al. (1987); Young et al. (1991); Young et al. (1992);Guo et al. (2003)
Residual water saturation	10 % - 82 %	King (1990); Karacan (2008); Chen et al. (2012); Remner et al. (1986); Guo et al. (2003)
Irreducible gas saturation	0 % - 3 %	Remner et al. (1986); King (1993); King (1990); Chen et al. (2012)
End-point gas relative pemeability	0.35 – 1	Karacan (2008); King (1993); King (1990)

Table 6. Continued

Parameter	Values	References
Langmuir volumetric strain	0.0019 - 0.03	Pan et al. (2010); Shi and Durucan (2004, 2010) Chen et al. (2012); Robertson and Christiansen (2008)
Langmuir pressure at ½ Langmuir volumetric strain constant	2.07 MPa - 12 MPa	Robertson and Christiansen (2008); Chen et al. (2012); Pan et al. (2010); Shi and Durucan (2004, 2010)
Coal cleat compressibility	0.0011 MPa^{-1} - 0.59 MPa^{-1}	Pan et al. (2010); Harpalani (1999); Spencer et al. (1987); Seidle et al. (1992); Young et al. (1991); Young et al. (1992); Guo et al. (2003); Robertson and Christiansen (2008); Shi and Durucan (2004, 2010); Roadifer et al. (2003); King (1993); King (1990); Sparks et al. (1995)
Permeability	0.05 md – 50 md	Spencer et al. (1987); Chen et al. (2012); Young et al. (1992); Guo et al. (2003); King (1993); King (1990)
Young's modulus	700 MPa – 7000 MPa	Chen et al. (2012); Seidle et al. (1992); Robertson and Christiansen (2008); Shi and Durucan (2004, 2010)
Poisson's ratio	0.2 – 0.5	Chen et al. (2012); Seidle et al. (1992); Robertson and Christiansen (2008); Shi and Durucan (2004, 2010)
Bottom hole pressure	0.1 MPa – 1.7 MPa	Chen et al. (2012)

Effect of Diffusion Time Constant

The total amount of available gas (gas content in coal corresponding to a sum of free gas in macropore space and all the adsorbed gas saturating coal matrix) and its volume desorbing at a particular pressure are controlled by Langmuir isotherm, that is,

the parameters of adsorption. In addition to this the mechanism of diffusion delays the appearance of desorbed gas in cleats for the corresponding number of days.

With pressure drawdown gas desorbs from micropore and mesopore surfaces in coal matrix and starts moving towards macropores – cleats system – under the influence of a methane concentration gradient. This flow is defined by a combination of 3 mechanisms – Knudsen-type, bulk and surface diffusion processes, each describing movement in different size capillaries (Smith and Williams, 1984; Kolesar and Ertekin, 1986). In other words, the desorbed gas is not released immediately but with regard to its diffusional flow. Later free gas molecules may commence their movement in cleats towards the well as proposed by the mathematical description of the process. This leads to a continuing production caused by the appearance in a cleat system of the delayed gas.

In our model we apply unsteady-state diffusion effects by specifying diffusion time τ, in Fick's law. It is time constant regulating the speed of gas release to macropores.

According to literature the diffusion for small values of τ is faster and a higher cumulative gas production and a higher production rate peak is to be expected (Remner et al., 1986; Spencer et al., 1987). We have run six cases for desorption times of 0.25, 1, 9, 50, 100 and 150 days. The production behavior for those cases is illustrated in Figure 25 - Figure 27.

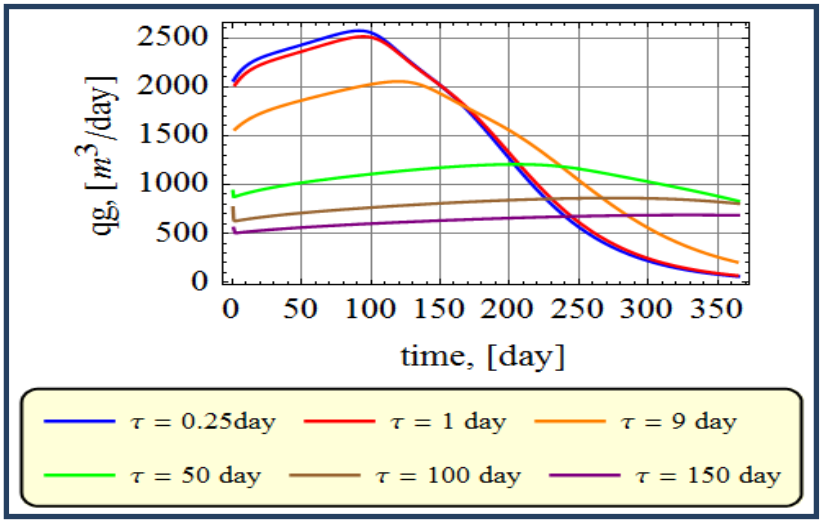

Figure 25. Effect of diffusion time on gas rate

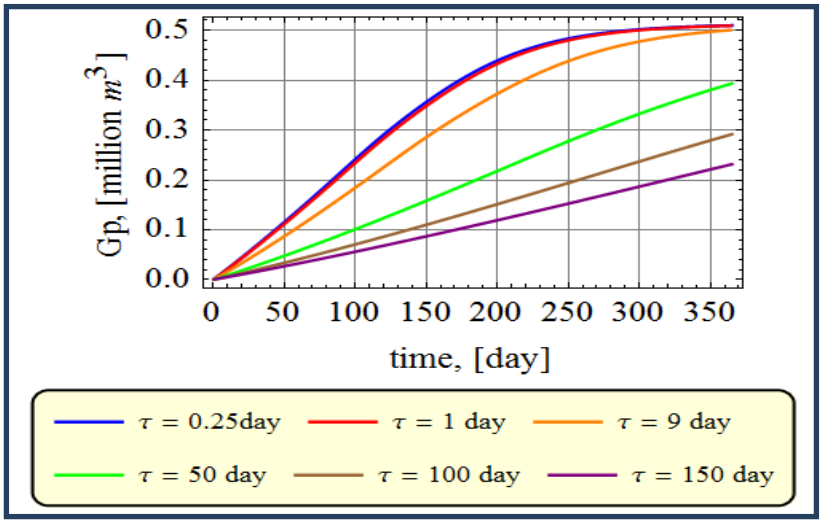

Figure 26. Effect of diffusion time on cumulative gas production

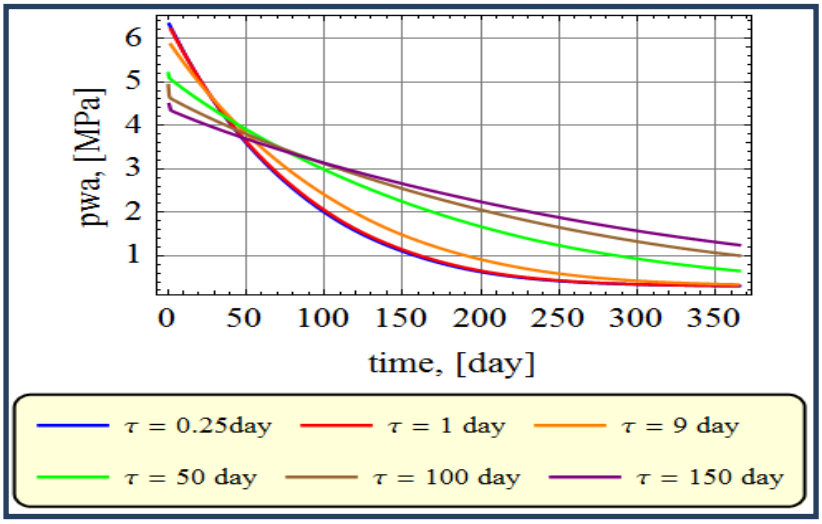

Figure 27. Effect of diffusion time on average water pressure

In our production forecasts we see that increase in desorption time increases production period as expected. Increase in desorption time means that smaller fraction of desorbed gas is available at cleats at every time unit.

In this case the ingress of gas into the cracks is delayed. Thus it can be seen that at the later stage production is carried out by the ongoing diffusion. In other words later in the life of coal seam an internal pressure maintenance mechanism may be represented by a combination of diffusion time and desorption.

Coal Cleat Compressibility

Coal cleat compressibility coefficient is mostly identified through the process of adaptation of the model to real data, since experimental measurements are highly complicated, expensive and hard to interpret. The performed study proposes that with increase in coal cleat compressibility the maximum gas rate growth and production

period shortening can be observed. This is due to higher increase in permeability due to gas desorption, since permeability and effective horizontal stress are related according to equation 3.14 as described by Seidle et al. (1992).

When pressure drop is not significant and compression dominates effective horizontal stress is increasing. As a result the more compressible coal cleats are the less permeable the rock becomes. As with time more gas desorbs and effective horizontal stress starts decreasing the cleats widen making the formation more permeable. In that case permeability grows proportionally to the value of coal cleat compressibility. Consequently, gas relative permeability is also increasing. A combination of those two parameters being part of productivity equations results in higher rates. Higher production rates at large permeabilities stipulate increase in rate of pressure drop and production period shortens.

In other words, additional factor for pressure drop is that at greater magnitude of cleat compressibility the macropore volume growth intensifies. Cumulative production during the same time period is larger for maximum for coals with larger cleat compressibility, therefore they may be more profitable to recover in short term.

Figure 28 - Figure 30 illustrate the changes that occur when different values of coal cleat compressibility are applied. The results confirm that increased coal cleat compressibility c_f causes steeper permeability growth, faster permeability decline and higher value of peak gas production.

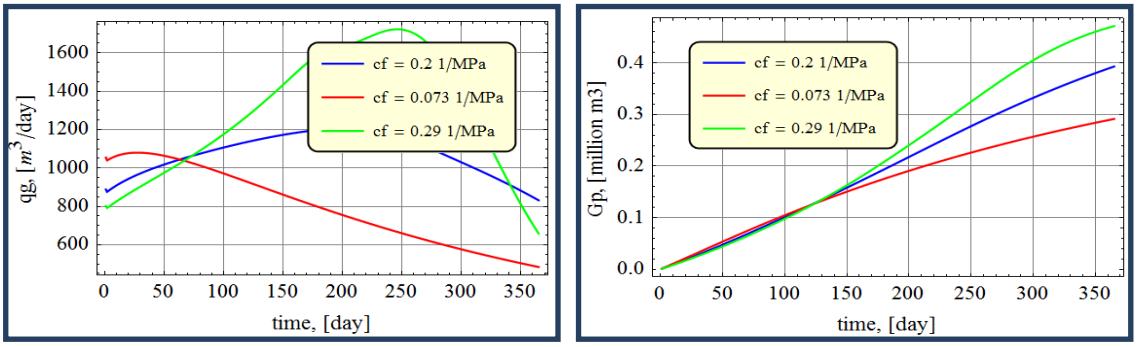

a) b)

Figure 28. Effect of coal cleat compressibility on a) gas rate; b) cumulative gas production

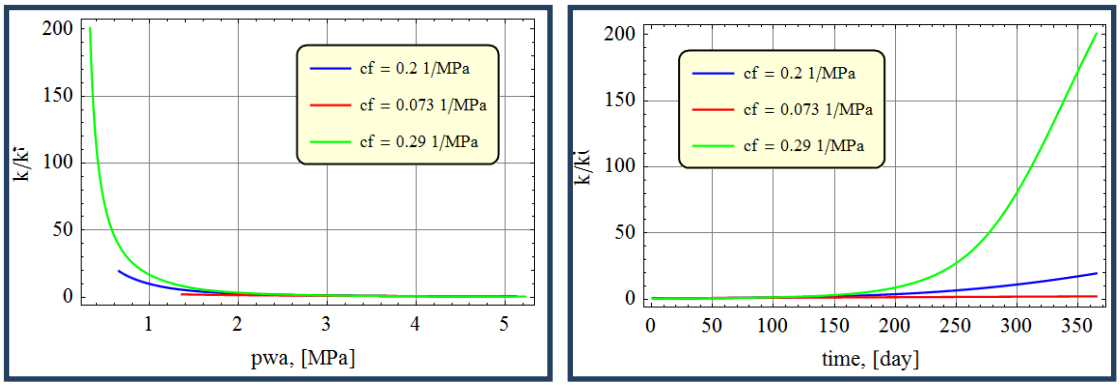

a) b)

Figure 29. Effect of coal cleat compressibility on absolute permeability as a function of a) average water pressure; b) time

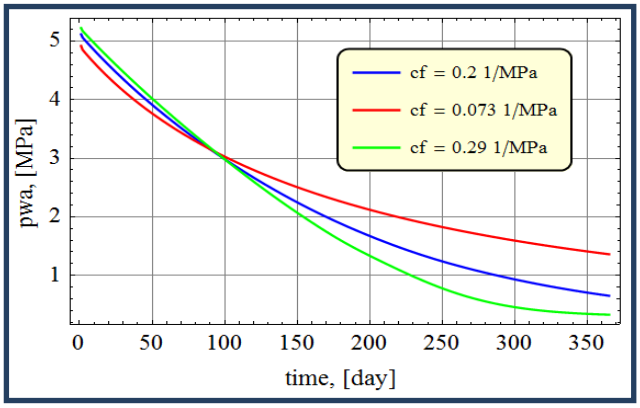

Figure 30. Effect of coal cleat compressibility on average water pressure

Effect of Langmuir Volumetric Strain Constant

This scenario was performed to examine the influence of coal swelling/shrinkage capacity on CBM production. To account for the effect of matrix shrinkage Shi and Durucan (2003c) model refers to total volumetric swelling/shrinkage strain change that is expressed through a Langmuir type equation in accordance with laboratory evidence (Harpalani and Chen, 1995; Seidle and Huitt, 1995; Levine, 1996). One of the constants used is Langmuir volumetric strain constant. This constant defines the maximum value of volumetric strain (in unit fraction) that can be approached at infinite pressure – when coal is saturated with gas down to the limit. The higher the coefficient value the more dramatically coal matrix deforms with gas desorption. When gas is adsorbed on micropore surfaces matrix swells significantly and as it is being released it becomes more compact.

Results shown in Figure 31 - Figure 32 propose that with higher matrix shrinkage capacity (higher Langmuir volumetric strain) the maximum gas rate and cumulative gas

production over the equal time periods are higher. Such behavior is not unexpected since it was earlier said that high volumetric strain values describe the coals where the matrix would shrink more significantly with gas desorption providing wider cleat openings and increased permeabilities. The influence of shrinkage capacity becomes more significant with time as the desorption induced permeability increase grows, which corresponds with findings of others researchers (Robertson and Christiansen, 2007; Wei and Zhang, 2010).

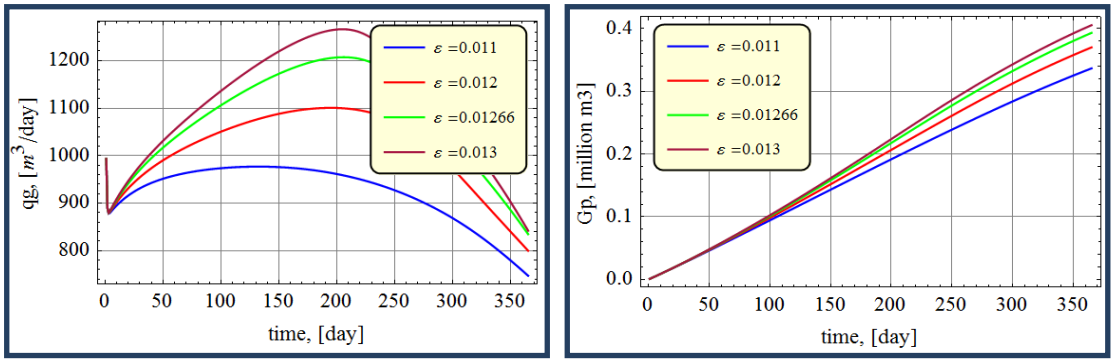

a) b)

Figure 31. The effect of Langmuir volumetric strain on a) gas rate; b) cumulative gas production

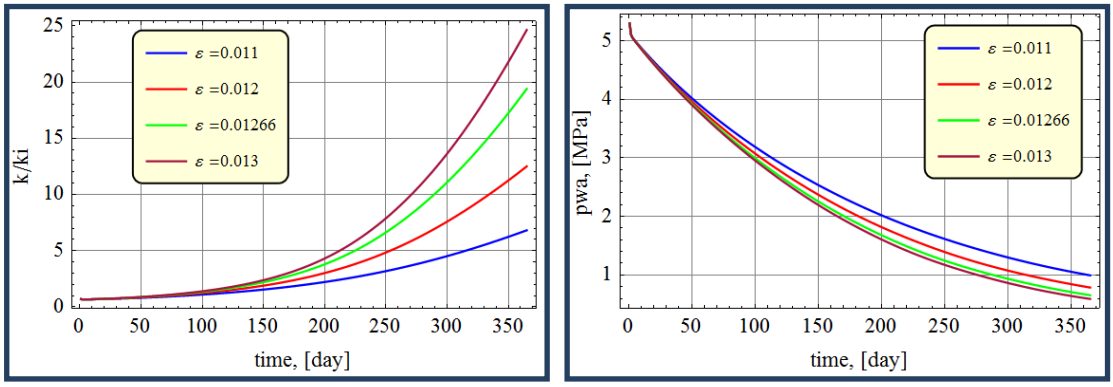

a) b)

Figure 32. Effect of Langmuir volumetric strain on a) absolute permeability; b) average water pressure

Effect of Poisson's Ratio

Poisson's ratio and Young's modulus are two independent parameters defining elastic properties of the material. Therefore their variation greatly affects the behavior of coal under stress. Axial tension of material is accompanied by lateral contraction. By definition Poisson's ratio is the relation of transversal contraction to longitudinal extension. If Poisson's ratio is known one can proportionally estimate volumetric changes of material under tension.

Value of Poisson's ratio can vary significantly for different ranks of coal. Therefore it is interesting to find out how sensitive production is to those elastic properties.

The effect of Poisson's ratio on production performance is represented in Figure 33 - Figure 35.

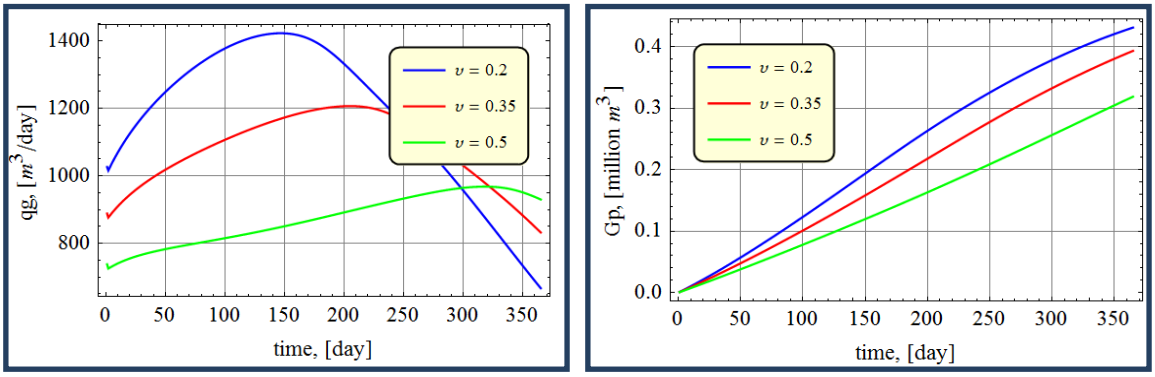

a) b)

Figure 33. Effect of Poisson's ratio on a) gas rate; b) cumulative gas production

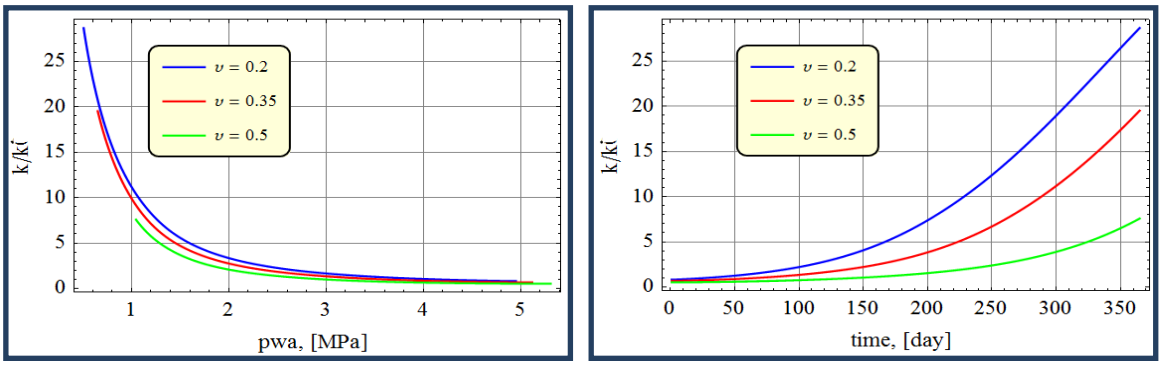

a) b)

Figure 34. Effect of Poisson's ratio on absolute permeability change as a function of a) average water pressure; b) time

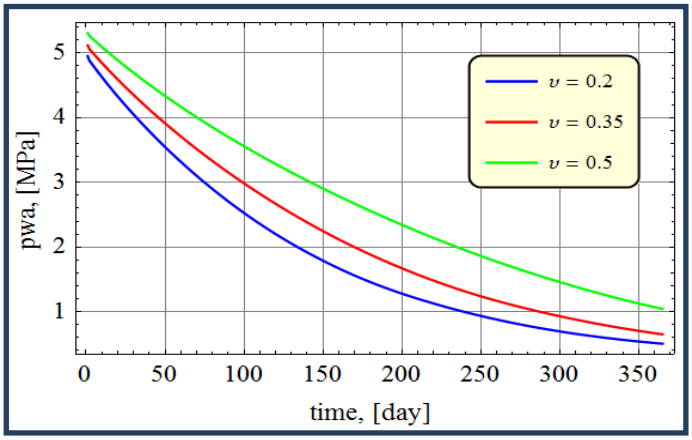

Figure 35. Effect of Poisson's ratio on average water pressure

Poisson's ratio is part of the compression term in strain and stress equations. At higher values of Poisson's ratio it becomes harder for the cleats to open, therefore it is harder for desorption effects to overcome negative effect of compression on horizontal stress. This meets common sense and the forecast performance.

As illustrated in Figure 33 - Figure 35 at higher values of Poisson's ratio relative permeability grows less intensively. This causes pressure drop rate to decline due to lower production rates. Therefore, the slower the pressure drops the longer production takes place, reaching the same cumulative value but later. Higher values of Poisson's ratio predetermine lower values of absolute permeability, since coal is more deformed under natural stress and high effective horizontal stress has negative impact on permeability.

Effect of Young's Modulus

Young's modulus is one of the parameters that have great effect on coalbed methane extraction. Being the second of two independent parameters describing elastic properties of material and directly affecting stress conditions in the formation it dramatically changes the curvature of gas rate plot. By definition Young's modulus is the relation of stress to lateral extension of the material. Effective horizontal stress values would therefore be greater for lower values of E. As a result we observe longer production period for a coal with low value of Poisson's ratio, since the permeabilities and gas rates are smaller in Figure 36 - Figure 38.

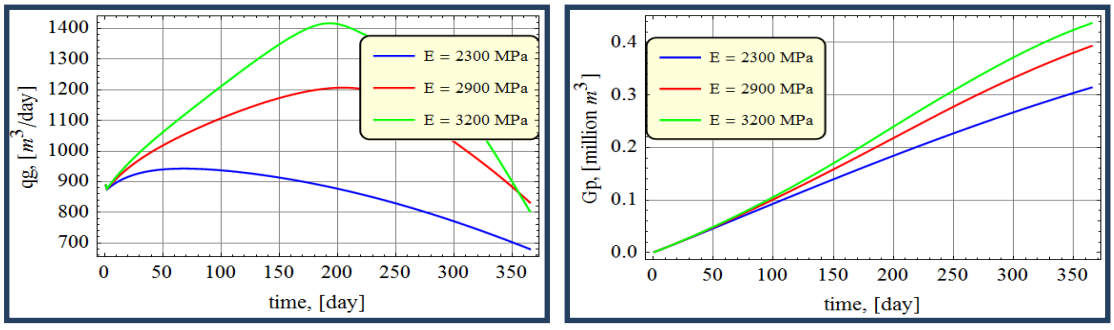

a) b)

Figure 36. Effect of Young's modulus on a) gas rate; b) cumulative gas production

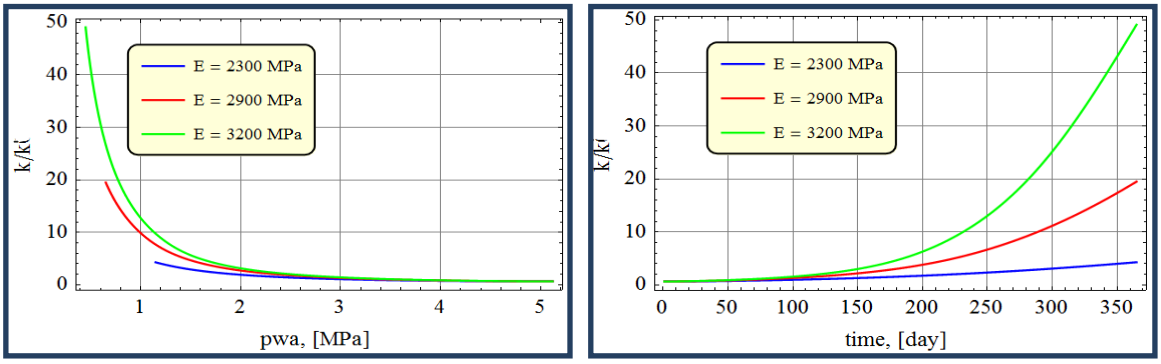

a) b)

Figure 37. Effect of Young's modulus on absolute permeability change as a function of a)average water pressure; b) time

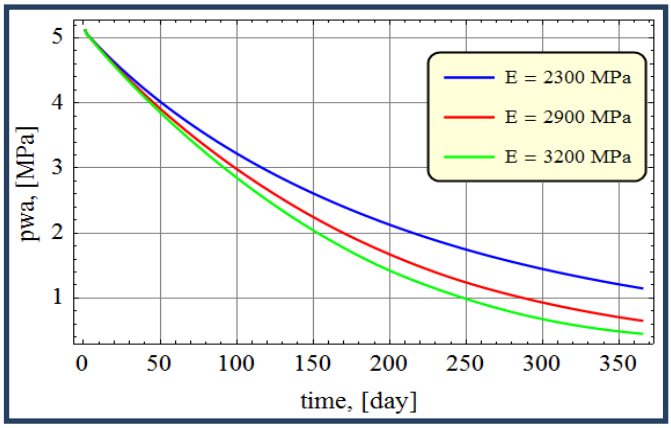

Figure 38. Effect of Young's modulus on average water pressure

Effect of Pore Size Distribution Index

Narrow range of pore sizes causes pore size distribution index, λ, to be high, while wide range of pore sizes results in lower values of that parameter. Theoretically, as comes from Brooks and Corey capillary pressure model, it can be any number greater than zero (Brooks and Corey, 1966). As in coal pore sizes are variable during methane recovery due to compression and matrix shrinkage effects, in Chen et al. (2013) pore

size distribution index value is corrected with porosity dependent shape factor, J-function. However, the initial value of pore size distribution index matters as demonstrated in Figure 39 - Figure 40.

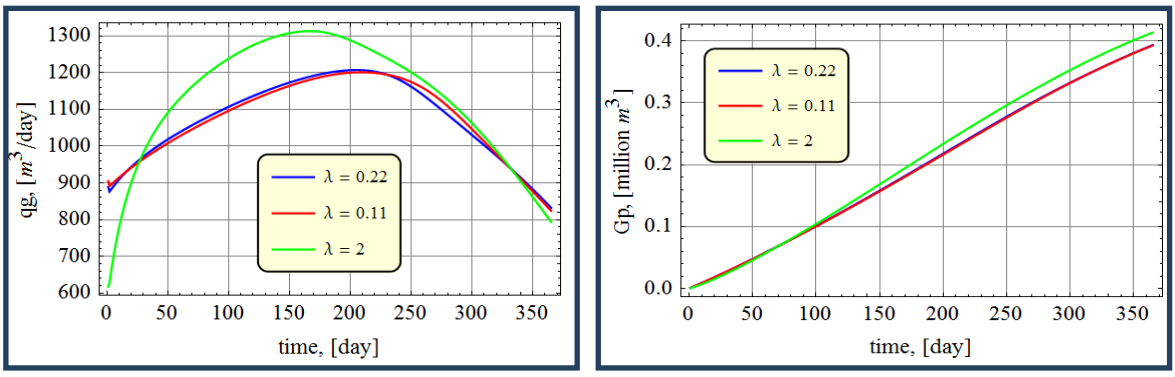

a) b)

Figure 39. Effect of pore size distribution index on a) gas rate; b) cumulative gas production

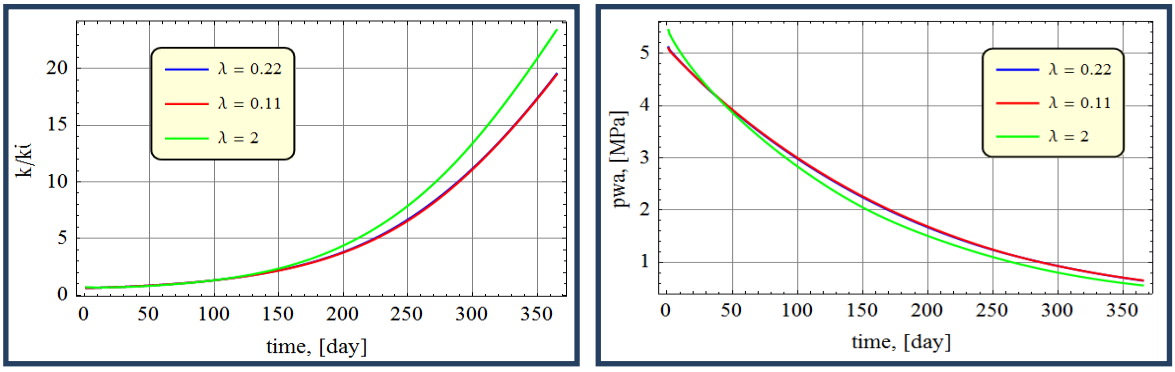

a) b)

Figure 40. Effect of pore size distribution index on a) permeability change; b) average water pressure

Since λ=0 would theoretically mean that porous medium has such distribution of pores that it cannot be desaturated regardless of the capillary pressure, it is intuitively clear that growth of pore size distribution index makes it easier for the fluids to flow. This results in faster pressure drawdown and earlier production termination.

Effect of Initial Absolute Permeability

In this work coal permeability was considered to be variable, defined by modified Shi and Durucan permeability model as a function of pore pressure, deformation and adsorbed gas content. Figure 41 - Figure 43 represent the changes that occur with varying initial absolute permeability value for coal. The magnitude of change being studied is from 1 mD to 8 mD significantly reduces the time to reach peak gas rate and enhances the production performance.

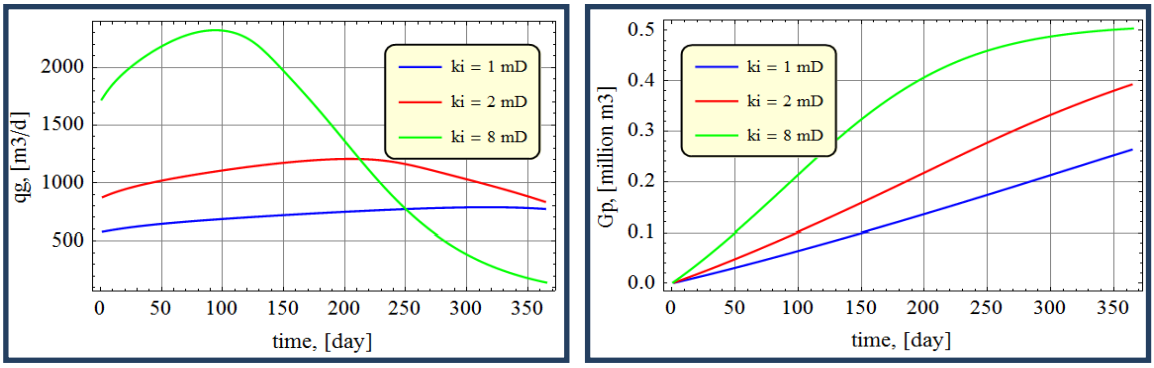

a) b)

Figure 41. Effect of initial absolute permeability on a) gas rate; b) cumulative gas production

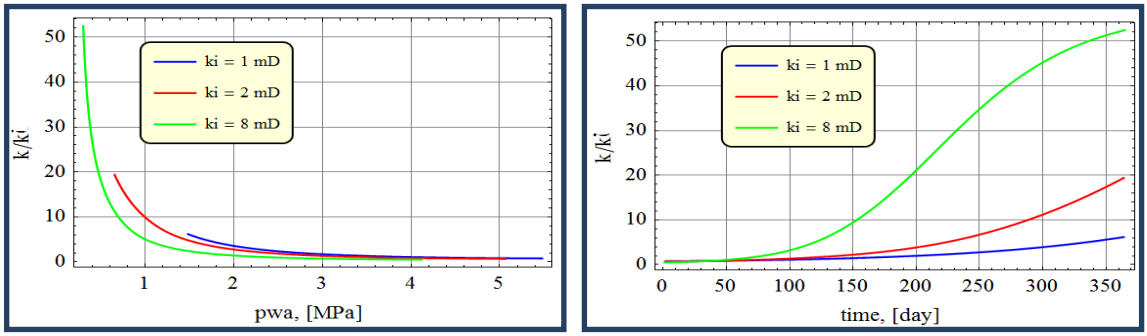

a) b)

Figure 42. Effect of initial absolute permeability on absolute permeability change as a function of a) average water pressure; b) time

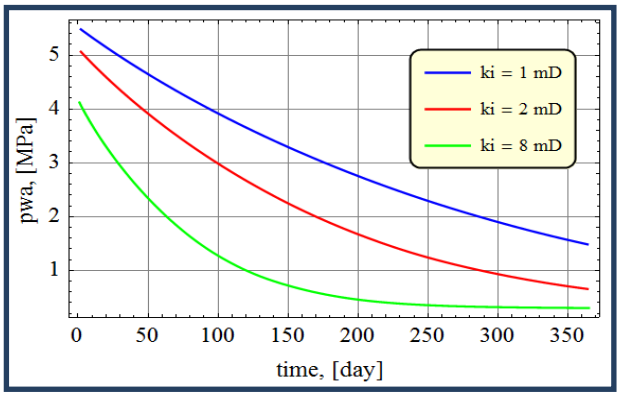

Figure 43. Effect of initial absolute permeability on average water pressure

Effect of Initial Residual Water Saturation

Lower values of residual water saturation create favorable conditions for water flow. On the contrary, higher residual water saturations cause gas relative permeability to increase steeper as water saturation decreases.

Figure 44 - Figure 47 show how CBM reservoir performance is affected by the changes in initial residual water saturation. In our case peak gas rate and the cumulative

production for the same time period are the highest for the maximum simulated S_{wr} as a result of a more intense pressure decline.

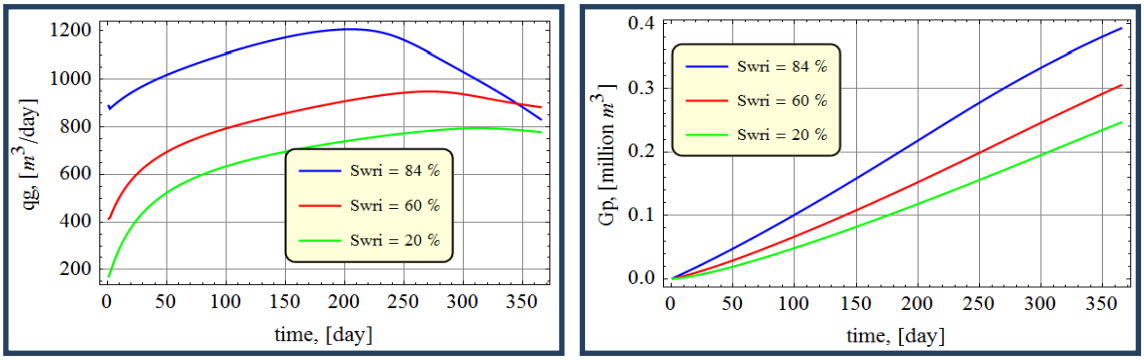

a) b)

Figure 44. Effect of initial residual water saturation on a) gas rate; b) cumulative gas production

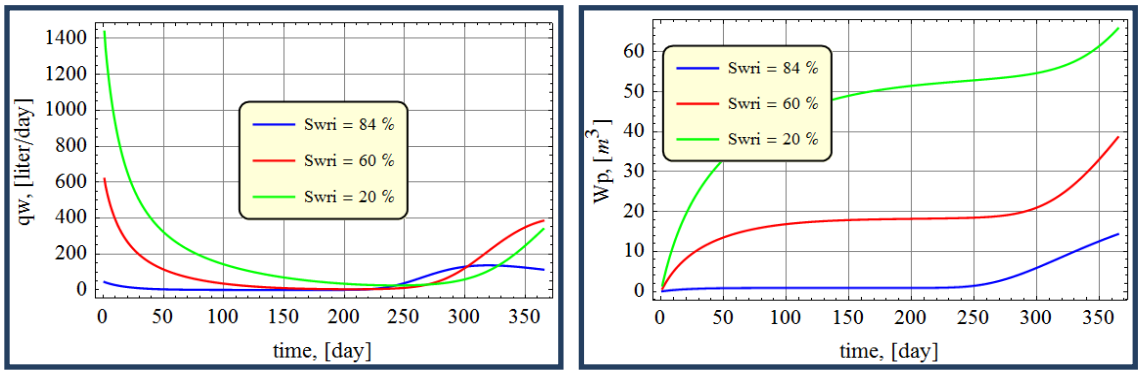

a) b)

Figure 45. Effect of initial residual water saturation on a) water rate; b) cumulative water production

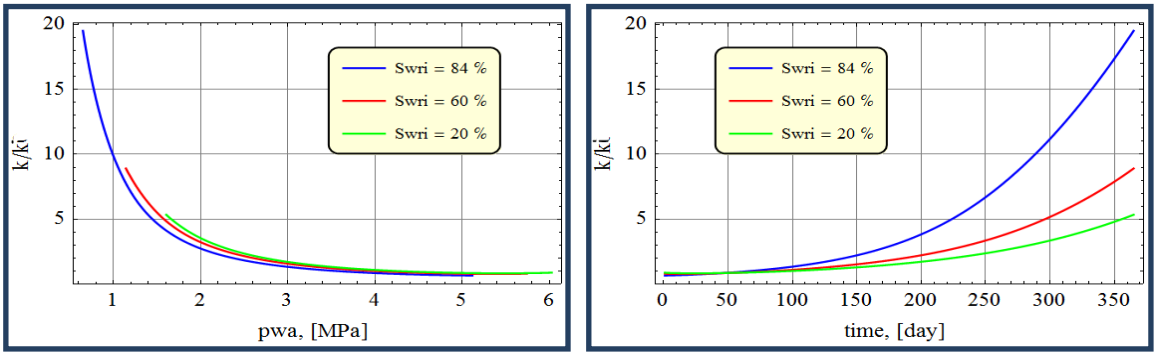

a) b)

Figure 46. Effect of initial residual water saturation on absolute permeability change as a function of a) average water pressure; b) time

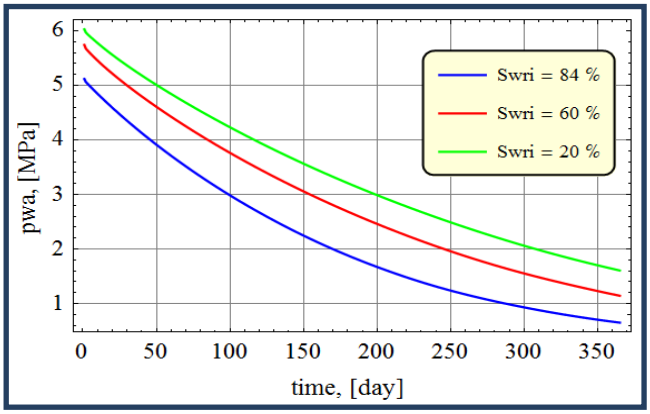

Figure 47. Effect of initial residual water saturation on average water pressure

However, it should not be misunderstood that water production is negligible for all CBM reservoirs. Often water production is a necessary to initiate gas desorption.

Effect of Dimensionless Productivity Index

The above described factors characterize the coal and cannot be controlled, but rather predetermine the conditions of production. Wellbore radius, skin-factor and

bottomhole pressure are the engineering parameters under the engineer's control. Different well completions may also affect the effectiveness of depletion process.

Wellbore Radius

Wellbore radius and skin-factor influence the dimensionless productivity index defined in equation 3.49, which influences the production rates.

The comparison of production forecasts for different wellbore radius values may be done basing on the results of runs illustrated in Figure 48 - Figure 50.

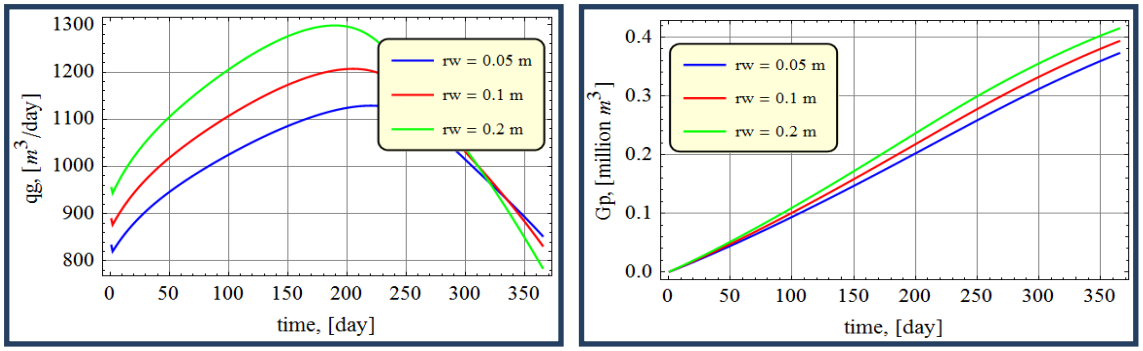

a) b)

Figure 48. Effect of wellbore radius on a) gas rate; b) cumulative gas production

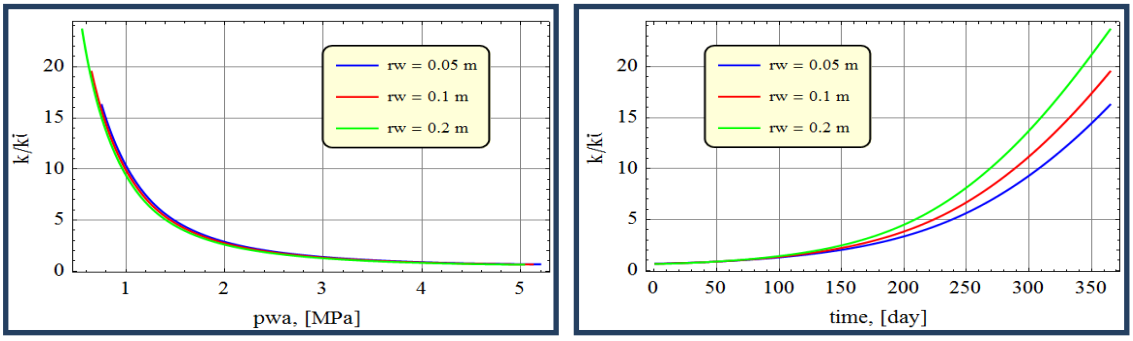

a) b)

Figure 49. Effect of wellbore radius on permeability change as a function of a) average water pressure; b) time

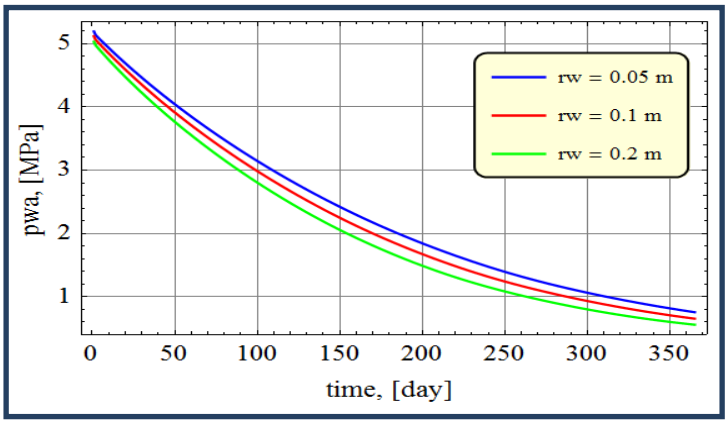

Figure 50. Effect of wellbore radius on average water pressure

Increase in wellbore radius has a positive influence on production rates. However, final wellbore radius and well completion selection is determined by a number of factors, including the properties of lifted fluids and economic criteria.

Skin-factor

Skin-factor allows engineers to simulate the degree of contamination of the near-wellbore area as well as various well stimulation treatments, such as hydraulic fracturing. Negative values of skin-factor imitate increased formation conductivity,

resulting from a successful creation of a long hydraulic fracture for example. The effect of skin-factor on CBM production is shown in Figure 51 - Figure 53.

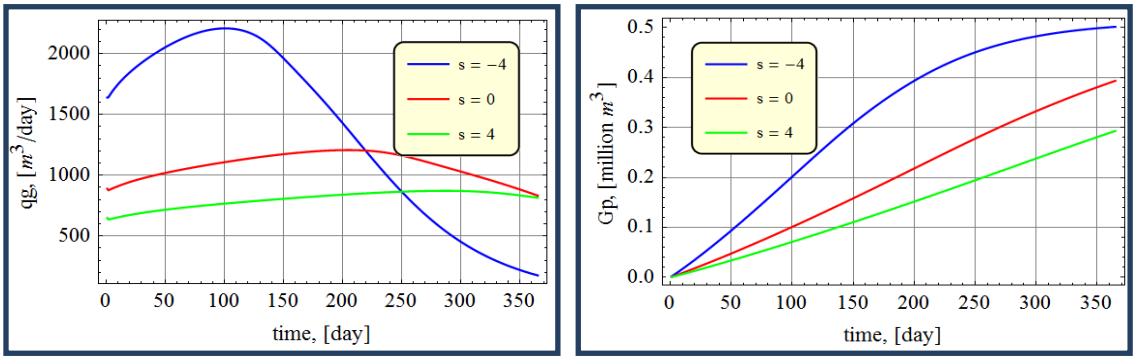

a) b)

Figure 51. Effect of skin-factor on a) gas rate; b) cumulative gas production

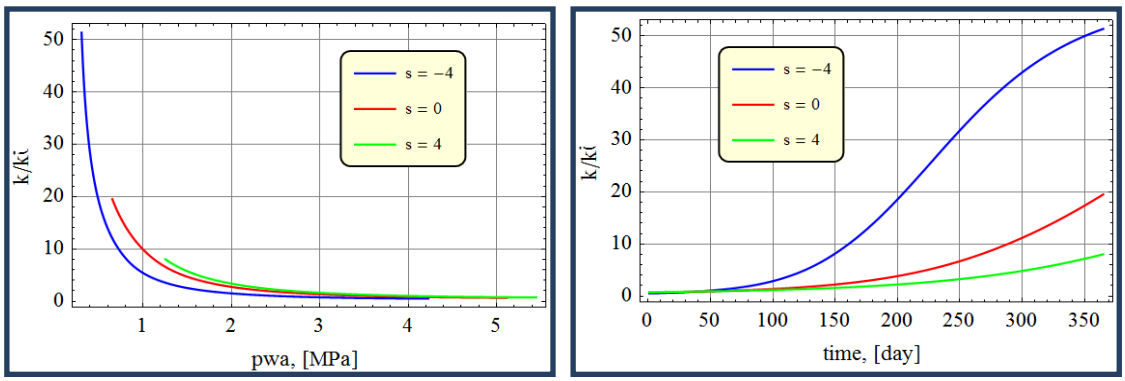

a) b)

Figure 52. Effect of skin-factor on permeability change as a function of a) average water pressure; b) time

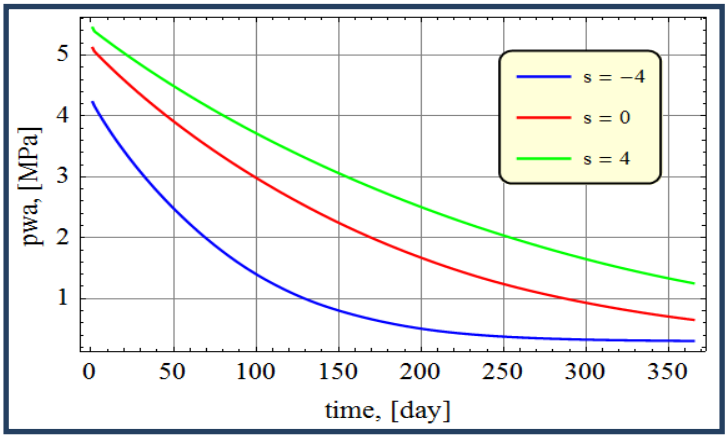

Figure 53. Effect of skin-factor on average water pressure

As well becomes more productive, possibly due to various reasons, the rates are higher from very beginning, resulting in faster pressure drop. As a result methane extraction process is more effective.

Effect of Wellbore Flowing Pressure Selection

In our model we are constraining the production according to bottom hole pressure, therefore the higher bottomhole pressure is the higher abandonment pressure. High abandonment pressure results in more significant amount of gas left in the formation, therefore total producible gas value lowers.

Other effects of wellbore flowing pressure may be observed on Figure 54 - Figure 55.

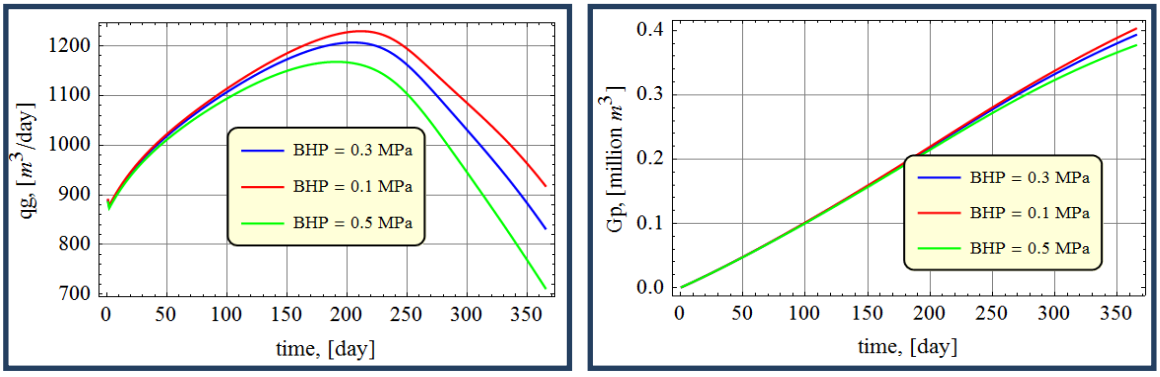

a) b)

Figure 54. Effect of wellbore flowing pressure on a) gas rate; b) cumulative gas production

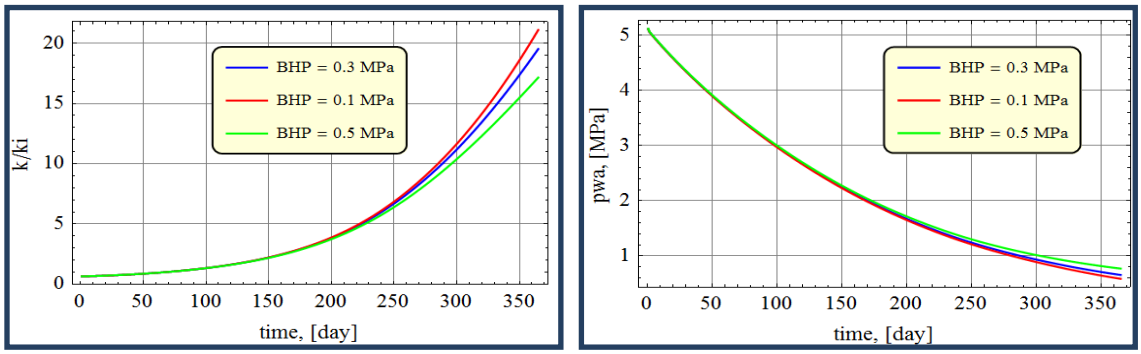

a) b)

Figure 55. Effect of wellbore flowing pressure on a) permeability change; b) average water pressure

The magnitude of changes is not very significant, therefore at the beginning the resulting gas production is similar due to close pressure gradient values. The small difference in gas rates causes at every step causes a slightly bigger pressure drop for lower wellbore flowing pressures, which causes more gas to desorb.

Sensitivity Summary

The effect of sensitivity can be classified into groups according to how it changes the appearance of production profiles. Table 7 presents a summary of the studied sensitivity effects.

Table 7. Sensitivity summary

Type of effect	Parameter	Effect magnitude
Time to peak gas	Coal cleat compressibility	Large
	Poisson's ratio	Large
	Young's modulus	Medium
	Langmuir volumetric strain	Small
	Diffusion time	Large
	Initial residual water saturation	Medium
	Pore size distribution index	Small
	Initial permeability	Large
	Dimensionless productivity index	Large
Peak gas value	Coal cleat compressibility	Large
	Poisson's ratio	Large
	Young's modulus	Large
	Langmuir volumetric strain	Large
	Diffusion time	Large
	Initial residual water saturation	Medium
	Pore size distribution index	Small
	Initial permeability	Large
	Dimensionless productivity index	Very large
Curvature	Coal cleat compressibility	Small
	Poisson's ratio	Medium
	Young's modulus	Small
	Langmuir volumetric strain	Small
	Diffusion time	Medium
	Initial residual water saturation	Small

Table 7. Continued

Type of effect	Parameter	Effect magnitude
Curvature	Pore size distribution index	Small
	Initial permeability	Small
	Dimensionless productivity index	Small

Possibility for Application in Optimization

It is possible to apply the program in order to assess the production from wells and choose optimum strategy that would allow maximum recovery subject to cost constrains or minimum cost subject to required recovery. As mentioned above, engineers may control the wellbore flowing pressure and perform various well stimulation treatments.

For optimization purposes we select a two-year time horizon, a fixed abandonment pressure and consider various production strategies in order to maximize the methane recovery.

Comparing production profiles over the two-year period with application of various wellbore flowing pressure profiles indicates that there is no significant difference in recovery as long as abandonment pressure is the same: the final gas recovery values are very similar. It would be more profitable to have large drawdowns if there were no additional limitations, since gas would be produced in a more efficient way. The comparison is illustrated in Figure 56.

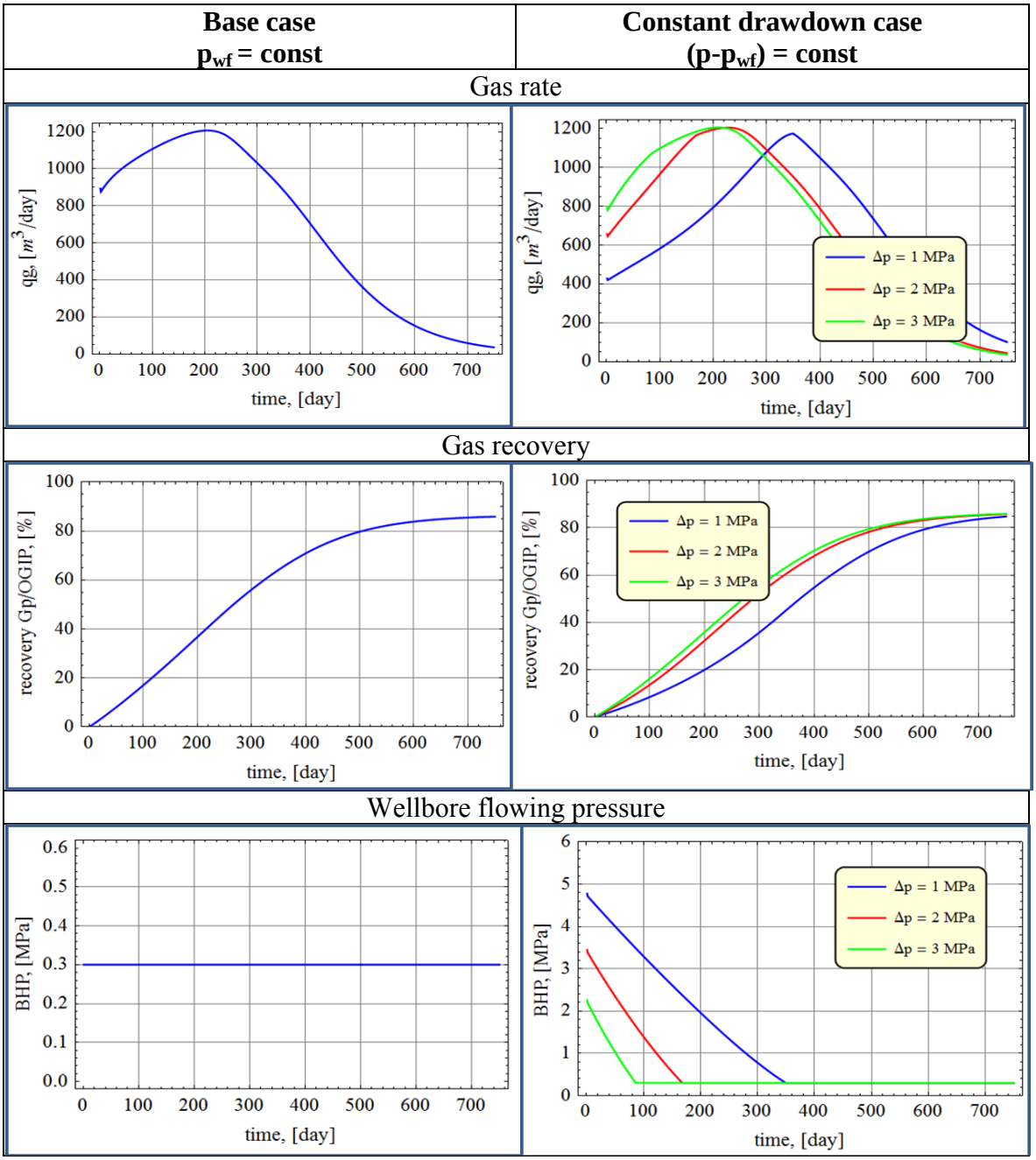

Figure 56. Wellbore flowing pressure optimization

If one also considers the time value of money, the advantage of increased productivity is even more evident.

Successful well stimulation treatments, such as hydraulic fracturing, result in an increase in dimensionless productivity index J_D. The effect of skin factor has been described in the sensitivity study section. Since hydraulic fractures are frequently modeled directly through dimensionless productivity index, the results can be directly translated to varying J_D. Maximum theoretically achievable dimensionless productivity index is $6/\pi$ and $J_D = 0.18$ roughly corresponds to zero skin factor in the base case. The results are presented in Figure 57.

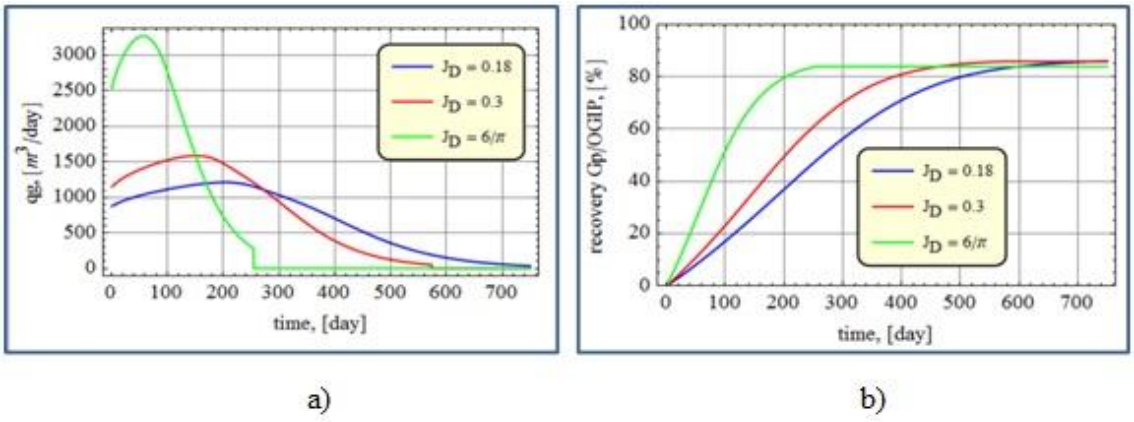

Figure 57. Effect of dimensionless productivity index on a) gas rate; b) gas recovery

It can be seen that although the production rates are increasing and time to peak gas is decreasing simultaneously with increase in dimensionless productivity index, the total recovery is larger for smaller productivity index. However, a realistic abandonment rate would completely reverse the picture and the stimulated case would have higher recovery.

In addition, in market economies the reduction of the necessary two-year production time to one year might make all the difference. In the case of coal-bed methane, time might be also constrained by the subsequent coal mining operation. A more detailed optimization would consider all these factors together with the cost of achieving a certain well productivity (that is the cost of the fracture stimulation treatment).

Results of Comparison Runs with F.A.S.T. CBM and the Proposed Single-Well Analytical Model

As previously mentioned, we will be comparing the results of simulation done in F.A.S.T. CBM software and in our program.

Since commercial software considers instantaneous diffusion and constant relative permeability curves some of the input parameters described in base case are not needed (e.g. tortuosity coefficient η, diffusion time τ, pore size distribution index λ, entry capillary pressure p_e) and other have to be applied (parameters for generalized Corey relative permeability curves construction: residual gas saturation S_{gr}; residual water saturation S_{wr}; n_g – gas exponent; n_w – water exponent). We chose to use $S_{gr} = 0$ %; $S_{wr} = 70$ %; $n_g = 1.5$; $n_g = 3$. The value of S_{wr} is consistent with that variable S_{wr} calculated with our model that is closer to the end of production period.

In order to justify the differences between F.A.S.T. CBM and single-well analytical model proposed performances a number of specific cases were run, showing that in some cases more similar results may be acquired.

Inputting Langmuir Isotherm and initial pressure data into F.A.S.T. CBM interface results in calculation of the Langmuir isotherm from initial pressure to zero that is presented in Figure 58 together with one constructed in the proposed software. The results are consistent.

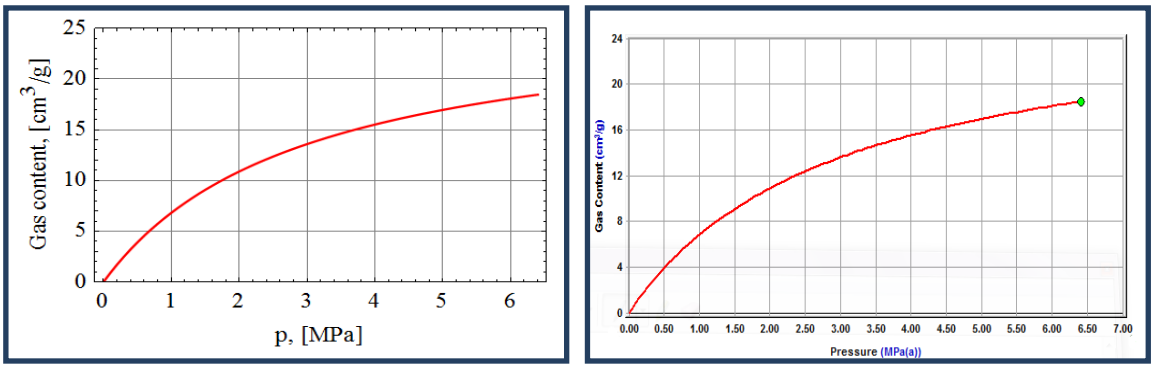

a) b)

Figure 58. Langmuir isotherms constructed in a) proposed single-well analytical model; b) F.A.S.T. CBM

When matrix shrinkage option is chosen and all the necessary data (coal cleat compressibility c_f, Poisson's ratio ν, Young's modulus E, Langmuir volumetric strain ε_L and pressure at ½ Langmuir volumetric strain P_ε) is input F.A.S.T. CBM produces the permeability change graph, as in Figure 59. The result is identical to Figure 17, showing permeability ratio calculated with Shi and Durucan model considering the matrix shrinkage with equilibrium desorption.

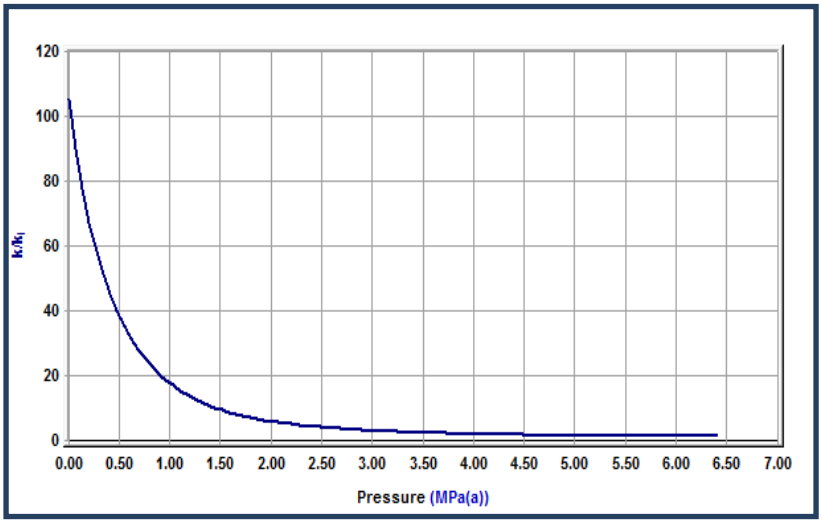

Figure 59. Permeability ratio constructed in F.A.S.T. CBM

Relative permeability curves used in F.A.S.T. CBM simulation runs can be found in Figure 60.

After we additionally input skin-factor value, initial permeability value, wellbore flowing pressure and drainage area the production forecast and OGIP estimation may be performed. The estimated OGIP values are presented in Table 8.

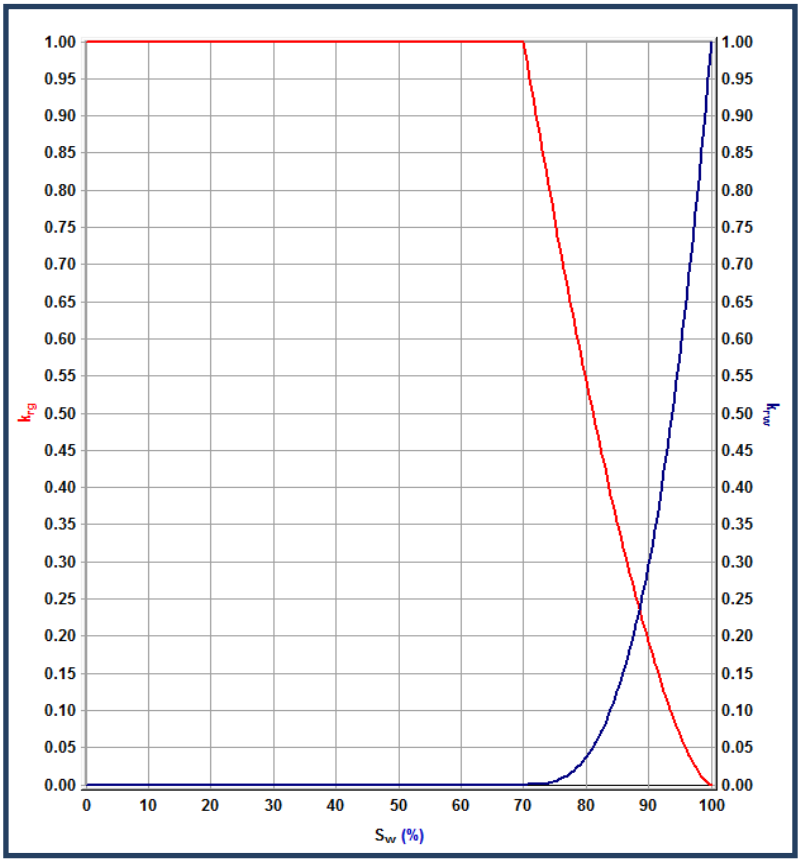

Figure 60. Relative permeability applied in F.A.S.T. CBM simulation runs

Table 8. OGIP estimations

Units	The proposed single-well analytical model	F.A.S.T. CBM
m^3	593 000	591 000
MMSCF	20.9	20.9

The F.A.S.T. CBM simulation results are presented in Figure 61 - Figure 62. They may be compared to results of base case in the proposed single-well analytical model (Figure 9, Figure 12).

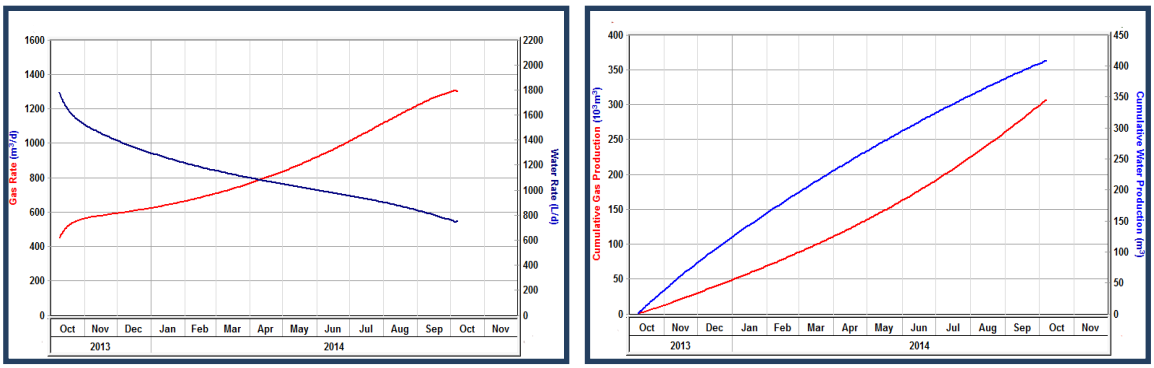

a) b)

Figure 61. F.A.S.T. CBM production forecast: a)gas and water rates; b) cumulative gas and water production

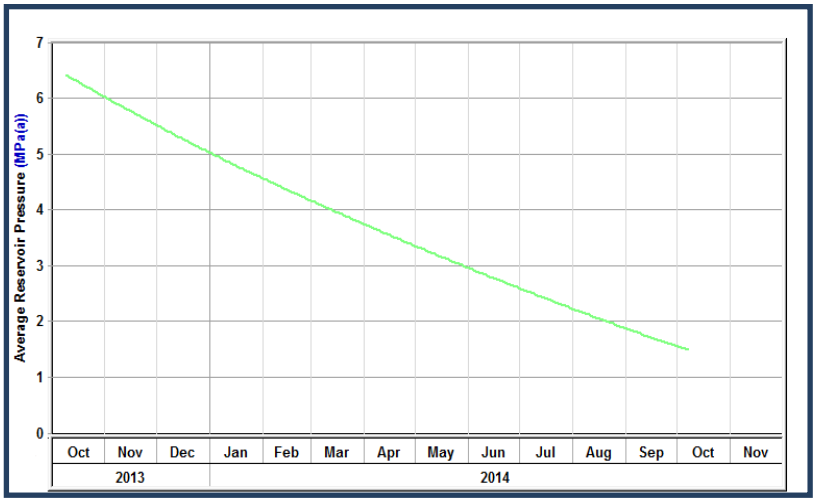

Figure 62. F.A.S.T. CBM production forecast: average reservoir pressure

The behavior of production curves is very different from the ones acquired in the proposed program. We see an increase in gas rate and, the forecast is terminated for later in life of the well and cannot be continued, probably due to computation problems arising from the use of the base data set (great permeability increase due to large c_f).

The difference in results may be referred to:

- F.A.S.T. CBM considers equilibrium desorption, therefore tau is not applied (gas transfer from matrix to cleats is instantaneous);
- Relative permeability curves in F.A.S.T. CBM are functions of water saturation ignoring the effects of porous media deformation;
- Accounting for water compressibility in F.A.S.T. CBM;
- F.A.S.T. CBM performs calculations in field units that are converted to metric system only on special command, the conversions applied and rounding of the input may cause insignificant differences in the results.

We tried matching the forecasted values of F.A.S.T. CBM by adjusting the parameters of the relative permeability model in the proposed single-well analytical model. Changing pore size distribution index λ and tortuosity coefficient η resulted in the range of gas rate predictions that are plotted in Figure 63 together with F.A.S.T. CBM performance. Zero tortuosity coefficient represents straight coal cleats, it's increase describes the cleats becoming more tortuous and relative permeability decreases. The effect of pore size distribution index has been described earlier. No satisfactory match was achieved.

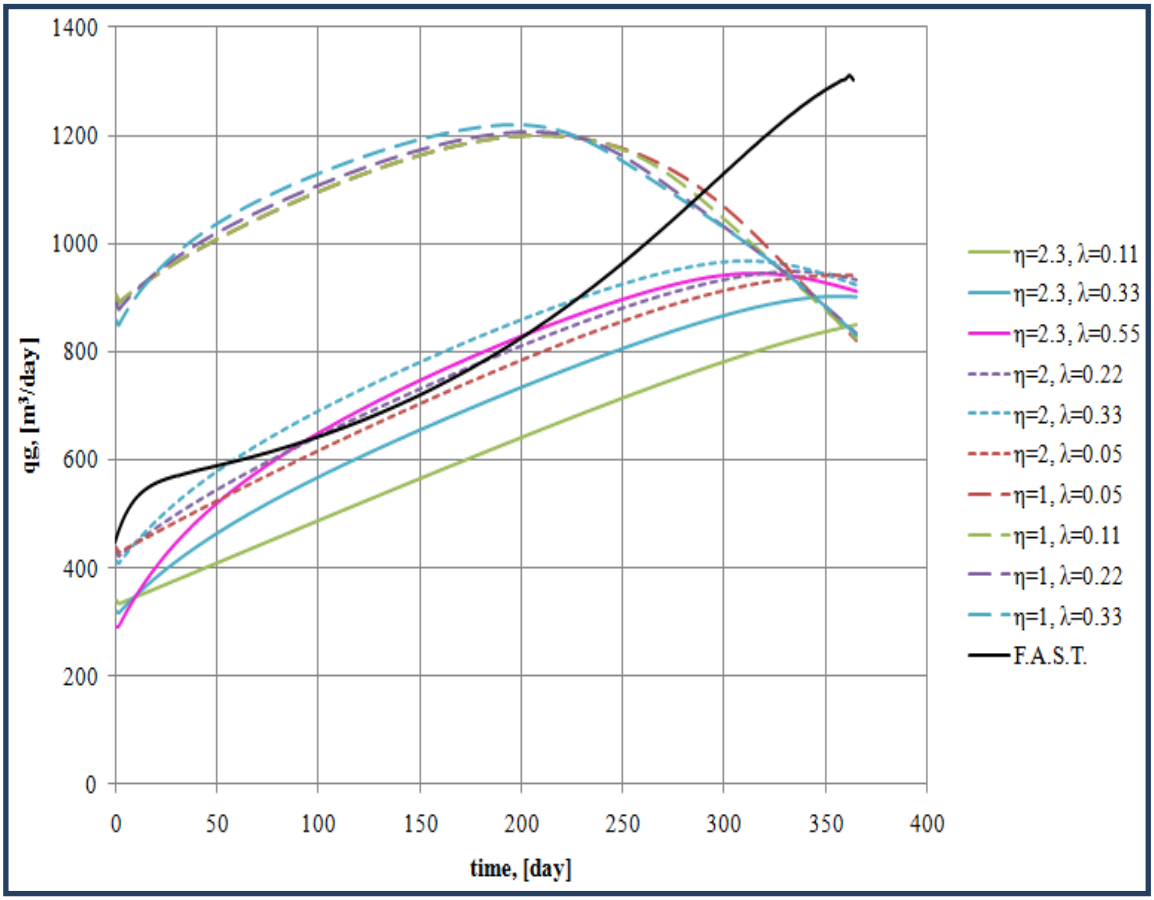

Figure 63. Forecasted gas rate: F.A.S.T. CBM comparison with different runs of the single-well analytical model (variable τ, λ, η)

In order to see if the difference can be addressed to non-equilibrium nature of desorption that is not accounted for in F.A.S.T. CBM we performed another series of runs, the results are presented in Figure 64. It those runs in addition to parameters previously modified we investigated the changes that occurred at smaller diffusion times. It can be seen that the faster diffusion occurs, the closer result is to F.A.S.T. CBM values.

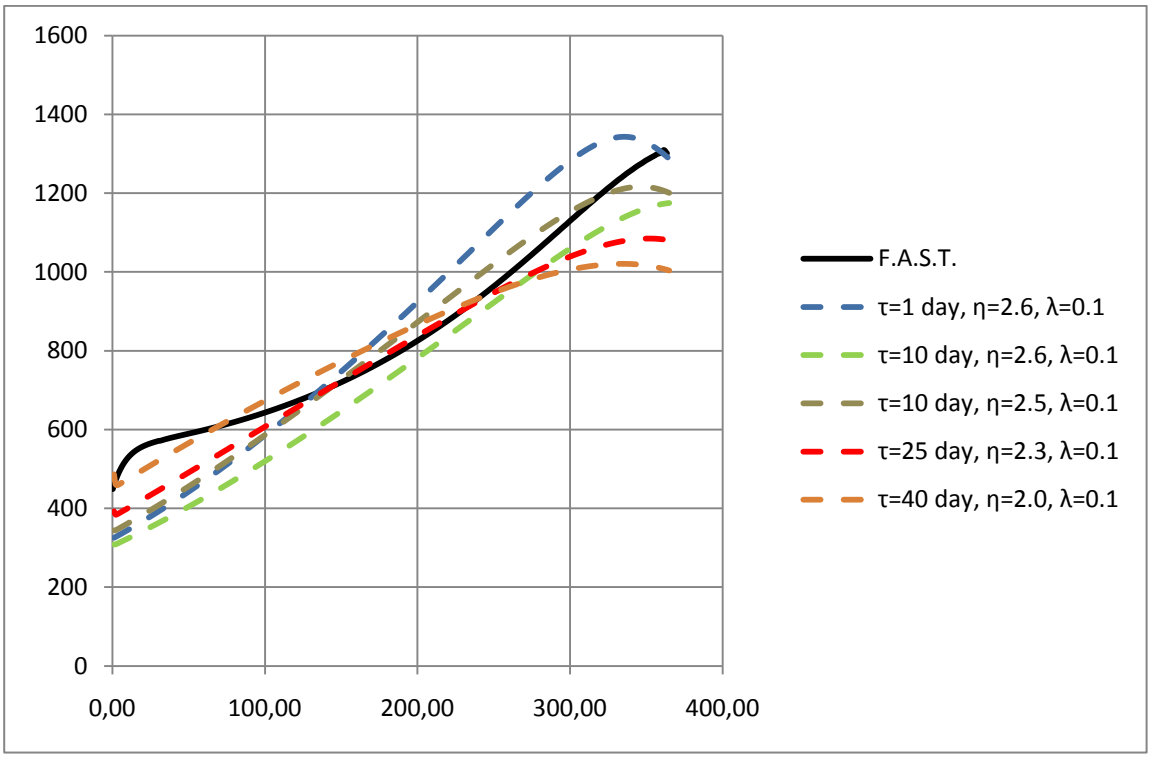

Figure 64. Forecasted gas rate: F.A.S.T. CBM comparison with different runs of the single-well analytical model (variable τ, λ, η)

F.A.S.T.CBM is sensitive to the input parameters and constrains the possiblility of forecasting with highly compressible coals. Coal cleat compressibility and elastic properties of coal control the absolute permeability ratio k/k_i and the solutions are more stable when coal conductivity change is not dramatic. Therefore, it is easier to compare the solutions acquired under the application of coal cleat compressibility value of 0.1 MPa^{-1}, which is closer to the default in F.A.S.T. CBM software.

Figure 65 shows permeability change with pressure drawdown, that is applied in F.A.S.T. CBM for the run with $c_f = 0.1$ MPa^{-1}.

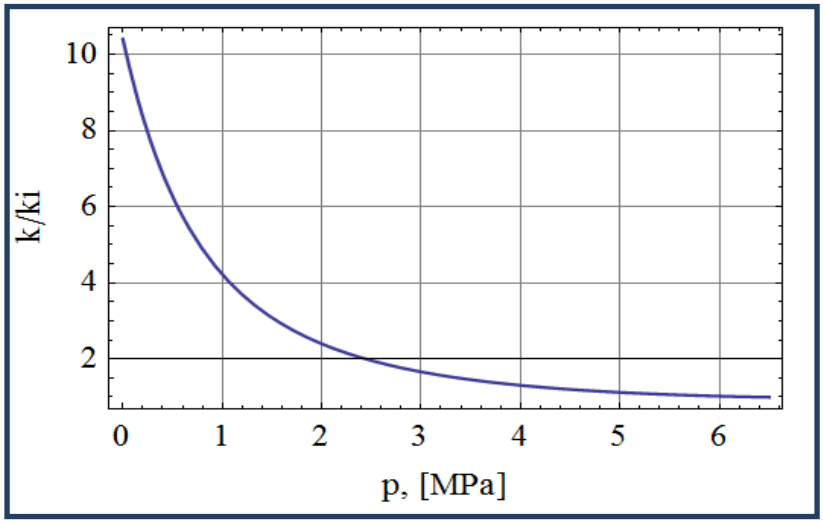

Figure 65. Permeability change with pressure drawdown applied in F.A.S.T. CBM for run with c_f=0.1 MPa^{-1}

In order to achieve closer result the following values were changed in our single well analytical model:

- η=1;
- λ=1;
- c_f=0.1 MPa^{-1}.

The resulting gas and water rates for both programs can be found in Figure 66.

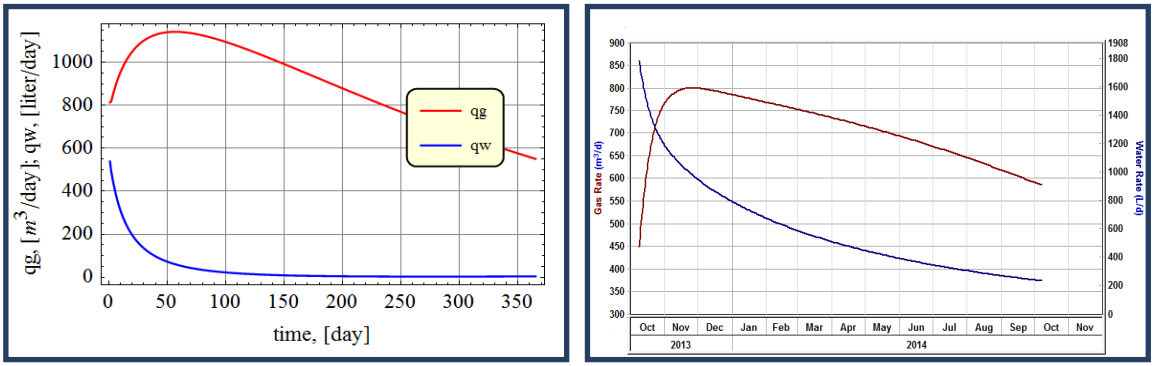

a) b)

Figure 66. Gas and water rates for c_f=0.1 MPa^{-1} runs predicted in a) the proposed single-well analytical model; b) F.A.S.T. CBM

The resulting form of the production rate curves is similar. However, the rates do not correspond. The predicted peak gas production in F.A.S.T. CBM is lower than the one predicted in the proposed single-well analytical model.

Discussion

Work on the description of the process of extracting methane from coal seams is still under continuous development. In particular, the existing numerical and analytical models describe the process from different approaches, emphasizing some aspects and neglecting others. No model provides an exhaustive description of all the phenomena occurring during CBM production.

Models coupling production performance with geomechanical effects are complex and highly sensitive to minor formulation differences. Such complicated interrelations of parameters and nonlinearity of functions make CBM modeling a very difficult experience, and on some occasions, may bring unexpected results impossible to

foresee without the actual model runs. Therefore, the research results illustrate the importance of appropriate coal property models and consistent reservoir characterization to be used in modeling CBM.

Permeability and porosity models need significant adjustments to meet the actual experimental values. However, even fitting the experimental values with the models does not guarantee successful field application. Since various analytical models are based on limited pressure data they yield different results when exposed to different conditions and extended. Therefore a "perfect" model is yet to be proposed.

A significant improvement in the CBM production forecasting methodology presented in Chen et al. (2013) is including the non-equilibrium nature of gas desorption in the geomechanical effects induced by fluid extraction processes. Our model improves the description of all changes related to volumetric strain, because instead of the pore pressure it considers the actual adsorbed gas amount, as the state variable. The proposed model of porosity change is based on a combination of one-dimensional deformation caused by the non-equilibrium desorption and the expression for the one-dimensional compression deformation of coal under the influence of developing effective vertical compressive stress in the absence of lateral displacement.

The research has shown that non-equilibrium nature of desorption has a significant effect on CBM production. Overestimating the sorption induced strain can bring significant mistakes to production forecasting, therefore, the proposed model is theoretically more appropriate, especially for reservoirs with large diffusion times.

An assessment of the sensitivity of the results to the input parameters made it possible to observe how the gas flow rates may vary depending on the properties of the reservoir, rock mechanics and on the selected completion method. The calculations illustrate the effects of these parameters on the gas production rates and allow the engineer to select an optimum recovery strategy, once the parameter values are known. Thus, it is shown that the diffusion time, which is not included in the analytical commercial simulators, for example F.A.S.T. CBM, has a significant impact on CBM production; the impact of changes in the residual water saturation due to lowering reservoir pressure on gas and water production is shown. From the managing and engineering point of view the calculations for different values of the well radius, skin factor and pressure gradient have been performed. The results obtained in this study showed that the applied method allows performing forecasts that will not conflict with physical meaning.

The complexity of numerical solutions, commercial value and limited descriptions of commercial software makes it difficult to identify the potential drawbacks, while our approach is based on the material balance equation, is relatively simple and at the same time more flexible in terms of adapting to the actual production data and changing the mathematical description of the processes.

CONCLUSIONS

CBM extraction process description is hard to model both numerically and analytically. The CBM production rates are controlled by the interaction of multiple processes triggered by gas and water production itself. Those interactions are accounted for through defining a number of coal properties as variable and the coal characteristics that lie in the basis of mathematical models make significant differences to the results.

CBM production models coupled with geomechanical effects are very sensitive to minor formulation differences. It is important to use consistent reservoir properties and models in order to expect reliable results. Further work is needed to develop theoretically sound and field applicable models of permeability and porosity. Current models are possible for application with heavy and time consuming adjustment.

In this work, the most widely known models of changes in the properties of the coal seam were considered. We used the Shi and Durucan (2003c) formulation of absolute permeability and the relative permeability model proposed by Chen et al. (2013). A flexible single-well tank model was built the software package Mathematica (by Wolfram Research) to investigate the effect of various assumptions and model parameters quickly and effectively. The approach allows engineers to perform production forecasts and analyze the change in production behavior due to varying values of reservoir properties, including the most influential rock-mechanics parameters. The results obtained in this study showed that the applied method allows performing forecasts that will not conflict with physical meaning.

Non-equilibrium nature of desorption has a significant effect on CBM production. Considering equilibrium sorption induced strain may cause overestimation of gas production.

A sensitivity study was performed. An assessment of the sensitivity of the results to the input parameters made it possible to observe how the gas flow rates may vary depending on the properties of the reservoir, rock mechanics and on the selected completion method.

Diffusion time has a significant impact on CBM production.

The possibility to perform optimization based on maximum recovery values has been illustrated. It has suggested that for the studied combination of data the variation of wellbore flowing pressure does not affect the final gas recovery, but only the time it is achieved. Creating long hydraulic fractures increases well productivity, which leads to shortened production period and slightly lower total gas recovery. Lower gas recovery can be attributed to fast reservoir pressure decline. However, since the difference in recovery is not large, the final decision has to be made based on economics.

The simplicity and flexibility of the proposed model makes it beneficial for application in new mathematical models assessment.

The recommendations for work development include validation and adaptation of the program to cases where both laboratory and field data are available; changing the inflow formulae applied, for example, by considering horizontal well geometry.

NOMENCLATURE

USA	United States of America
CBM	Coalbed Methane
UK	United Kingdom
TOC	Total Organic Carbon
ASTM	American Society for Testing and Materials
V_E	Gas Storage Capacity per one kilogram
P; p	Pressure
V_L	Langmuir Volume Constant
P_L	Langmuir Pressure Constant
ELI	Extended Langmuir Isotherm
F	Diffusion Flux
D	Diffusion Coefficient
C	Concentration
a	Warren and Root Shape Factor; Cleat Spacing
t	Time
S	Spacing Between Cleats
τ	Diffusion time
ARI	Advanced Resources International, Inc.
k	Permeability
c_f	Cleat Volume Compressibility

σ	Horizontal Stress; Hydrostatic Stress
p_s	Equivalent Sorption Pressure
ν	Poisson's ratio
E	Young's modulus
ε_s	Volumetric Strain; Strain Caused by Equivalent Sorption Pressure
ϕ	Porosity
C_p	Pore Volume Compressibility
C_m	Matrix Shrinkage Compressibility
P_d ; p_d	Desorption Pressure
ε	Strain Due to Matrix Shrinkage
B	Langmuir Constant
ε_L	Langmuir Volumetric Strain
P_ε	Pressure at ½ ε_L
E_F	Analog of Young's Modulus for a Fracture
ΔS	Change in Adsorbate Mass
α	Volumetric Swelling Coefficient; Rate of Change in Fracture Compressibility
M	Constrained Axial Modulus
K	Bulk Modulus
K_p	Modulus of Pore Volume
ε_v	Sorption Induced Volumetric Strain
w	Cleat Width

ε_{max}	Linear Strain at Infinite Pore Pressure on Unconstrained Sample
G_p	Cumulative Gas Produced at Standard Conditions
$OFGIP$	Original Free Gas in Place
G_D	Cumulative Volume of Desorbed Gas
G_F	Free Gas in Cleats
B_g	Gas Formation Volume Factor
Z	Compressibility Factor
T_{res}	Reservoir Temperature
T_{st}	Temperature at Standard Conditions
p_{st}	Pressure at Standard Conditions
A	Area
h	Thickness
S_w	Water Saturation
S_g	Gas Saturation
V_p	Cleat Volume
V_w	Water Content
W_p	Cumulative Water Production
p_g	Gas Pressure
m_c	Coal Mass
ρ_c	Coal Bulk Density
G_A	Gas Volume Adsorbed at Equilibrium
$OGIP$	Original Gas in Place

G	Gas Volume Adsorbed at Equilibrium at Initial Pressure
G_{ads}	Gas Volume Adsorbed by Matrix at Non-Equilibrium
V_{ads}	Gas Volume Adsorbed by 1 kilogram of Coal at Equivalent Pore Pressure Corresponding to Current Adsorbed Content
p_{ads}	Equivalent Pore Pressure Corresponding to Current Adsorbed Content
ρ_{g-l}	Density of Adsorbed Gas in Pseudo-Liquid State
V_{Lg-l}	Langmuir Volume of Gas in Pseudo-Liquid State in 1 Kilogram of Coal
ρ_g	Gas Density
V_{pore}	Minimum Necessary Pore Volume in 1 Kilogram of Coal
l	Length
d	Diameter
$\Delta\varepsilon_1$	Axial Strain
$\Delta\varepsilon_2$	Lateral Expansion
sol	Fraction of Volume Occupied by Solid
S_{wr}	Residual Water Saturation
S_{gr}	Residual Gas Saturation
S_w^*	Normalized water Saturation
p_c	Capillary Pressure
p_e	Entry Capillary Pressure
λ	Pore size Distribution Index

J	Shape factor
p_w	Water Pressure
k_{rw}	Water Relative Permeability
k_{rg}	Gas Relative Permeability
η	Tortuosity Coefficient
k_{rw}^*	End-point Water Relative Permeability
k_{rg}^*	End-point Gas Relative Permeability
m	Gas Pseudopressure
μ_w	Viscosity of water
μ	Viscosity
J_D	Dimensionless Productivity Index
p_{wf}	Wellbore Flowing Pressure
q_g	Gas Rate
q_w	Water Rate
r_e	Drainage Radius
r_w	Wellbore Radius
s	Skin Factor
PVT	Pressure Volume Temperature

Subscripts

i	initial
0	initial

REFERENCES

Airey, E.M. 1968. Gas Emissions from Broken Coal: An Experimental and Theoretical Investigation. *International Journal of Rock Mechanics and Mining Science* **5**: 475–494.

Al-Hussainy, R., Ramey , H.J., Jr., Crawford, P.B. . 1966. The Flow of Real Gases Through Porous Media. *Journal of Petroleum Technology* **15** (5): 625-636.

Al-Jubori, A., Johnston, S., Boyer, C., Lambert, S.W., Bustos, O.A., Pashin, J.C., Wray, A. 2009. Coalbed Methane: Clean Energy for the World. *Oilfield Review* **21** (2): 4-13.

Aminian, K. , Ameri, S., Bhavsar, A., Sanchez, M., Garcia, A. 2004. Type Curves for Coalbed Methane Production Prediction. SPE Eastern Regional Meeting, Charleston, West Virginia. SPE 91482.

Ayers, W.B. Jr. 2002. Coalbed Gas Systems, Resources, and Production and a Review of Contrasting Cases from the San Juan and Powder River Basins. *AAPG Bulletin* **86** (11): 1853-1890.

Billemont, P., Coasne, B., De Weireld, G. 2013. Adsorption of Carbon Dioxide, Methane, and Their Mixtures in Porous Carbons: Effect of Surface Chemistry, Water Content, and Pore Disorder. *Langmuir* **29** (10): 3328-3338.

Boyer, C.M., Kelafant, J.R., Kuuskraa, V.A., Manger, K.C. 1990. *Methane Emissions from Coal Mining: Issues and Opportunities for Reduction*. U.S. Environmental Protection Agency, Washington, District of Columbia.

Brooks, R.H., Corey, A.T. 1966. Properties of Porous Media Affecting Fluid Flow. *Journal of the Drainage and Irrigation Division, American Society of Engineering* **92** (2): 61-88.

Cervik, J. 1967. Behavior of Coal-Gas Reservoirs. SPE Eastern Regional Meeting, Pittsburgh, Pennsylvania. SPE 1973-MS.

Chen, D., Liu, J., Pan, Z., Connell, L.D. 2012. Forecast of Gas Production From Coal Seams: The Impact of Effective Permeability. 46th U.S. Rock Mechanics/Geomechanics Symposium, Chicago, Illinois. ARMA-2012-332.

Chen, D., Pan, Z., Liu, J., Connell, L.D. 2013. An Improved Relative Permeability Model for Coal Reservoirs. *International Journal of Coal Geology* **109–110** (0).

Clarkson, C. R., Jordan, C. L., Gierhart, R. R., Seidle, J. P. 2008. Production Data Analysis of Coalbed-Methane Wells. *SPE Reservoir Evaluation & Engineering* **11** (2). SPE 107705-PA.

Clarkson, C.R., Rahmanian, M.R., Kantzas, A., Morad, K. 2010. Relative Permeability of CBM Reservoirs: Controls on Curve Shape. Canadian Unconventional Resources and International Petroleum Conference, Calgary, Alberta, Canada. SPE 137404-MS.

Connell, L.D., Detournay, C. 2009. Coupled Flow and Geomechanical Processes During Enhanced Coalseam Methane Recovery Through CO_2 Sequestration *International Journal of Coal Geology* **77** (1-2): 222-233.

Cui, X., Bustin, R.M., Dipple, G. 2004. Selective Transport of CO_2, CH_4 and N_2 in Coals: Insights from Modeling of Experimental Gas Adsorption Data. *Fuel* **83** (3): 293-303.

Cui, X. J., Bustin, R. M. 2005. Volumetric Strain Associated with Methane Desorption and its Impact on Coalbed Gas Production from Deep Coal Seams. *AAPG Bulletin* **89** (9): 1181-1202.

Dabbous, M.K., Reznik, A.A., Mody, B.G., Fulton, P.F., Taber, J.J. 1976. Gas-Water Capillary Pressure in Coal at Various Overburden Pressures. *Society of Petroleum Engineers Journal* **16** (5): 261-268. SPE 5348-PA.

Dabbous, M.K., Reznik, A.A., Taber, J.J., Fulton, P.F. 1974. The Permeability of Coal to Gas and Water. *Society of Petroleum Engineers Journal* **14** (6): 563-572. SPE 4711-A.

Dake, L. 1983. *Fundamentals of Reservoir Engineering*. Elsevier, Amsterdam, Netherlands.

Dake, L. 2001. *The Practice of Reservoir Engineering*. Elsevier, Amsterdam, Netherlands.

Daniels, F., Alberty, R.A. 1957. *Physical Chemistry*. J.Wiley, New York.

Derickson, J.P., Horne, J.S., Fisher, R.D., Stevens, S.H. 1998. Huaibei Coalbed Methane Project, Anhui Province, People's Republic of China. SPE International Oil and Gas Conference and Exhibition, Beijing, China. SPE 48886.

Dontsov, K.M. 1977. *The Development of Oil Fields [Разработка нефтяных месторождений]*. Nedra, Moscow, Russia.

Economides, M.J., Hill, A.D., Ehlig-Economides, C., Zhu, D. 2013. *Petroleum Production Systems*, 2nd edition. Prentice Hall, Upper Saddle River, New Jersey.

Economides, M.J., Kenneth, G.N. 2000. *Reservoir Stimulation*. J.Wiley, New York.

Fick, A. 1855. On Liquid Diffusion. *Philisophical Magazine* **10** (63): 30-39.

Gates, J.I., Lietz, W.T. 1950. Relative Permeabilities of California Cores by the Capillary Pressure Method. API-50-285.

Geilikman, M., Wong, S.-W. 2012. A New Model of CBM Permeability and Sorption-Induced Strain Based on Open-System Geomechanics. AAPG International Convention and Exhibition, Singapore. Search and Discovery Article #80262.

Gimatudinov, Sh.K. 1983. *Reference Manual for the Design and Development of Oil Fields [Справочное руководство по проектированию разработки и эксплуатации нефтяных месторождений]*. Nedra, Moscow, Russia.

Gray, I. 1987. Reservoir Engineering in Coal Seams: Part 1. The Physical Process of Gas Storage and Movement in Coal Seam. *SPE Reservoir Engineering* **2** (1): 28-34. SPE 12514-PA.

Grishin, F.A. 1985. *Commercial Evaluation of Oil and Gas Fields [Промышленная оценка месторождений нефти и газа]*. Nedra, Moscow, Russia.

Gu, F. 2009. Reservoir and Geomechanical Coupled Simulation of CO_2 Sequestration and Enhanced Coalbed Methane Recovery. PhD Ph.D dissertation, University of Alberta, Edmonton, Alberta, Canada.

Gu, F., Chalaturnyk, R. 2010. Permeability and Porosity Models Considering Anisotropy and Discontinuity of Coalbeds and Application in Coupled Simulation. *Journal of Petroleum Science and Engineering* **74** (3-4): 113-131.

Guo, X., Du, Zh., Li, Sh. 2003. Computer Modeling and Simulation of Coalbed Methane Reservoir. SPE Eastern Regional Meeting, Pittsburgh, Pennsylvania. SPE 84815-MS.

Halliburton Company. 2012. Coalbed Methane: Principles and Practices, http://www.halliburton.com/public/pe/contents/Books_and_Catalogs/web/CBM/CBM_Book_Intro.pdf (downloaded 02.02 2012).

Harpalani, S. 1999. Compressibility of Coal and its Impact on Gas Production from Coalbed Reservoirs. Rock Mechanics for Industry Conference, Balkema, Rotterdam. ISBN 90 5809 0523.

Harpalani, S. , Schraufnagle, R. A. 1990. Influence of Matrix Shrinkage and Compressibility on Gas Production from Coalbed Methane Reservoirs. SPE Annual Technical Conference and Exhibition, New Orleans, Louisiana. SPE 20729.

Harpalani, S., Chen, G. 1995. Estimation of Changes in Fracture Porosity of Coal with Gas Emission. *Fuel* **74** (10): 1491-1498.

Harpalani, S., McPherson, M.J. 1986. Mechanism Of Methane Flow Through Solid Coal. The 27th U.S. Symposium on Rock Mechanics (USRMS), Tuscaloosa, Alabama. ARMA-86-0690.

Harpalani, S., Parity, U.M. 1993. Study of Coal Sorption Using a Multi-Component Gas Mixture. International Coalbed Methane Symposium, Tuscaloosa, Alabama.

Harpalani, S., Prusty, B.K., Dutta, P. 2006. Methane/CO_2 Sorption Modeling for Coalbed Methane Production and CO_2 Sequestration. *Energy & Fuels* **20** (4): 1591-1599.

Hower, T.L. 2003. Coalbed Methane Reservoir Simulation: An Evolving Science. SPE Annual Technical Conference and Exhibition, Denver, Colorado. SPE 84424-MS.

Jalali, J., Mohaghegh, Sh.D. 2004. A Coalbed Methane Reservoir Simulator Designed and Developed for the Independent Producers. SPE Eastern Regional Meeting, Charleston, West Virginia. SPE 91414-MS.

Jensen, D., Smith, L.K. 1997. A Practical Approach to Coalbed Methane Reserve Prediction Using a Modified Material Balance Technique. International Coalbed Methane Symposium, Tuscaloosa, Alabama.

Karacan, C. Ö. 2008. Evaluation of the Relative Importance of Coalbed Reservoir Parameters for Prediction of Methane Inflow Rates During Mining of Longwall Development Entries. *Computers & Geosciences* **34** (9): 1093-1114.

Kim, A.G. 1977. Estimating Methane Content of Bituminous Coalbeds from Adsorptive Data. U.S. Bureau of Mines, Washington, District of Columbia.

King, G.R. 1985. Numerical Simulation of the Simultaneous Flow of Methane and Water Through Dual Porosity Coal Seams During the Degasification Process. PhD Dissertation, Penn State University, State College, Pennsylvania.

King, G.R. 1993. Material-Balance Techniques for Coal-Seam and Devonian Shale Gas Reservoirs With Limited Water Influx. *SPE Reservoir Engineering* **8** (1): 67-72. SPE 20730-MS.

King, G.R. 1990. Material Balance Techniques for Coal Seam and Devonian Shale Gas Reservoirs. SPE Annual Technical Conference and Exhibition, New Orleans, Louisiana. SPE 20730-MS.

King, G.R., Ertekin, T. 1991. State-of-the-Art Modeling for Unconventional Gas Recovery. *SPE Formation Evaluation* **6** (1): 63-71. SPE 18947-PA.

King, G.R., Ertekin, T., Schwerer, F.C. 1986. Numerical Simulation of the Transient Behavior of Coal-Seam Degasification Wells. *SPE Formation Evaluation* **1** (2): 165-183. SPE 12258-PA.

Kolesar, J.E., Ertekin, T. 1986. The Unsteady-State Nature of Sorption and Diffusion Phenomena in Micropore Structure of Coal. SPE Unconventional Gas Technology Symposium, Louisville, Kentucky. SPE 15233-PA.

Law, D. H.-S., Van der Meer, L.G.H., Gunter, W.D. . 2002. Numerical Simulator Comparison Study for Enhanced Coalbed Methane Recovery Processes, Part I: Pure Carbon Dioxide Injection. SPE Gas Technology Symposium, Calgary, Alberta, Canada. SPE 75669-MS.

Leverett, M. C. 1941. Capillary Behavior in Porous Solids. *Transactions of the AIME* **142** (1): 152-169. AIME 941152-G.

Levine, J.R. 1996. Model Study of the Influence of Matrix Shrinkage on Absolute Permeability of Coal Bed Reservoirs. In *Coalbed Methane and Coal Geology*, ed. R. Gayer and T. Harris: 197-212. Geology Society, Cardiff, United Kingdom.

Levy, J., Day, S.J., Killingley, J.S. 1997. Methane Capacity of Bowen Basin Coals Related to Coal Properties. *Fuel* **74** (9): 813-819.

Liu, S., Harpalani, S. 2012. Gas Production Induced Strain and Permeability Variations in Coalbed Methane Reservoirs. 46th US Rock Mechanics/ Geomechanics Symposium, Chicago, Illinois.

Ma, Q. A., Harpalani, S., Liu, S. M. 2011. A Simplified Permeability Model for Coalbed Methane Reservoirs Based on Matchstick Strain and Constant Volume Theory. *International Journal of Coal Geology* **85** (1): 43-48.

Mavor, M.J. 1997. Increasing Absolute Permeability in the San Juan Basin Fruitland Formation. International Coalbed Methane Symposium, Tuscaloosa, Alabama.

Mavor, M.J., Gunter, W.D. 2004. Secondary Porosity and Permeability in Coal vs. Gas Composition and Pressure. SPE Annual Technical Conference and Exhibition, Houston, Texas. SPE 90255.

Mavor, M.J., Paul, G., Saulsberry, L., Schafer, S., Scraufnagel, A., Sparks, P., Zuber, M. 1996. A Guide to Coalbed Methane Reservoir Engineering. Chicago, Illinois. GRI-94/0397.

McKee, C.R., Bumb, A.C., Koenig, R.A. 1988. Stress-Dependent Permeability and Porosity Coal and Other Geologic Formations. *SPE Formation Evaluation* **3** (1): 81-91. SPE 12858-PA.

McKee, C.R., Hanson, M.E. 1975. Explosively Created Permeability from Single Charges. *SPE Journal* **15** (6): 495-501. SPE 5414-PA.

Moore, T.A. 2012. Coalbed Methane: A Review. *International Journal of Coal Geology* **101** (0): 36-81.

Morad, K., Mireault, R., Dean, L. 2008. Reservoir Engineering for Geologists: Coalbed Methane Fundamentals. *Reservoir* **9**: 23-26.

Olague, N.E., Smith, D.M. 1989. Diffusion of Gases in American Coals. *Fuel* **68** (11): 1381-1387.

Palmer, I.D. 2004. Permeability changes in a CBM reservoir during production: an update, and implications for CO2 injection. International Coalbed Methane Symposium, Tuscaloosa, Alabama.

Palmer, I.D., Mansoori, J. 1996. How Permeability Depends Upon Stress and Pore Pressure in Coalbeds: a New Model. SPE Annual Technical Conference and Exhibition, Denver, Colorado. SPE 24906.

Pan, Zh., Connell, L.D., Camilleri, M. 2010. Laboratory Characterisation of Coal Reservoir Permeability for Primary and Enhanced Coalbed Methane Recovery. *International Journal of Coal Geology* **82** (3–4): 252-261.

Patching, T.H. 1965. Variations in Permeability of Coal. Rock Mechanics Symposium, Toronto, Canada.

Paul, G.W., Sawyer, W.K., Dean, R.H. 1990. Validation of 3D Coalbed Simulators. SPE Annual Technical Conference and Exhibition, New Orleans, Louisiana. SPE 20733.

Pekot, L.J., Reeves, S.R. 2003. Modeling the Effects of Matrix Shrinkage and Differential Swelling on Coalbed Methane Recovery and Carbon Sequestration. International Coalbed Methane Symposium, Tuscaloosa, Alabama.

Purcell, W.R. 1949. Capillary Pressures - Their Measurement Using Mercury and the Calculation of Permeability Therefrom. *Journal of Petroleum Technology* **1** (2): 39-48.

Reeves, S., Pekot, L. 2001. Advanced Reservoir Modeling In Desorption-Controlled Reservoirs. SPE Rocky Mountain Petroleum Technology Conference, Keystone, Colorado. SPE 71090.

Remner, D. J., Ertekin, T., Sung, W., King, G.R. 1986. A Parametric Study of the Effects of Coal Seam Properties on Gas Drainage Efficiency. *SPE Reservoir Engineering* **1** (6): 633-646. SPE 13366-PA.

Reznik, A.A., Dabbous, M.K., Fulton, P.F., Taber, J.J. 1974. Air-Water Relative Permeability Studies of Pittsburgh and Pocahontas Coals. *Society of Petroleum Engineers Journal* **14** (6): 556-562. SPE 004711-B.

Roadifer, R.D., Moore, T.A., Raterman, K.T., Farnan, R.A., Crabtree, B.J. 2003. Coalbed Methane Parametric Study: What's Really Important to Production and When? SPE Annual Technical Conference and Exhibition, Denver, Colorado. SPE 84425-MS.

Robertson, E. P., Christiansen, R. L. 2007. Modeling Laboratory Permeability in Coal Using Sorption-Induced-Strain Data. *SPE Reservoir Evaluation & Engineering* **10** (3): 260-269. SPE 97068-PA.

Robertson, E. P., Christiansen, R. L. 2008. A Permeability Model for Coal and Other Fractured, Sorptive-Elastic Media. *SPE Journal* **13** (3): 314-324. SPE 104380-PA.

Ruckenstein, E., Voidyanthan, A.S., Youngquist, G.R. 1971. Sorption by Solid Bidisperse Pore Structure. *Chemical Engineering Science* **26** (9): 1305-1381.

Ruthven, R.E. 1984. *Principles of Adsorption and Adsorption Processes*. J.Wiley, New York.

Sawyer, W. K., Paul, G. W., Schraufnagle, R. A. 1990. Development and Application of a 3D Coalbed Methane Simulator. International Technical Meeting CIM/SPE, Calgary, Canada. SPE 12316.

Sawyer, W. K., Zuber, M.D., Kuuskraa, V.A., Horner, D.M. 1987. Using Reservoir Simulation and Field Data to Define Mechanisms Controlling CBM Production. Coalbed Methane Symposium, Tuscaloosa, Alabama.

Schilthuis, R.J. 1936. Active Oil and Reservoir Energy. *Transactions of the AIME* **118** (1): 33-52. AIME 936033-G.

Seidle, J. P. 1999. A Modified p/Z Method for Coal Wells. SPE Rocky Mountain Regional Meeting, Gillette, Wyoming. SPE 55605-MS.

Seidle, J. P., Arri, L.E. 1990. Use of Conventional Reservoir Models for Coalbed Methane Simulation. Intrernational Technical Meeting, Calgary, Canada. CIM-90/SPE 21599.

Seidle, J.P., Huitt, L.G. 1995. Experimental Measurement of Coal Matrix Shrinkage Due to Gas Desorption and Implications for Cleat Permeability Increases. SPE International Meeting on Petroleum Engineering, Beijing, China. SPE 30010.

Seidle, J.P., Jeansonne, M.V., Erickson, D.J. 1992. Application of Matchstick Geometry to Stress Dependent Permeability in Coals. SPE Rocky Mountain Regional Meeting, Casper,Wyoming. SPE 24361.

Shi, J.-Q., Durucan, S. 2003a. A Bidisperse Pore Diffusion Model for Methane Displacement Desorption in Coal by CO_2 Injection. *Fuel* **82** (10): 1219-1229.

Shi, J.-Q., Durucan, S. 2003b. Gas Storage and Flow in Coalbed Reservoirs: Implementation of a Bidisperse Pore Model for Gas Diffusion in Coal Matrix. SPE Annual Technical Conference and Exhibition, Denver, Colorado. SPE 84342.

Shi, J.-Q., Durucan, S. 2003c. Changes in Permeability of Coalbeds During Primary Recovery - Part 1: Model Formulation and Analysis. International Coalbed Methane Symposium, Tuscaloosa, Alabama.

Shi, J.-Q., Durucan, S. 2004. Drawdown Induced Changes in Permeability of Coalbeds: A New Interpretation of the Reservoir Response to Primary Recovery. *Transport in Porous Media* **56** (1): 1-16.

Shi, J.-Q., Durucan, S. 2005. A Model for Changes in Coalbed Permeability During Primary and Enhanced Methane Recovery. *SPE Reservoir Evaluation & Engineering* **8** (4): 291-299.

Shi, J.-Q., Durucan, S. 2009. Exponential Growth in San Juan Basin Fruitland Coalbed Methane Permeability with Reservoir Drawdown - Model Match and New Insights. SPE Rocky Mountain Petroleum Technology Conference, Denver, Colorado. SPE 123206.

Shi, J.-Q., Durucan, S. 2010. Exponential Growth in San Juan Basin Fruitland Coalbed Permeability With Reservoir Drawdown: Model Match and New Insights. *SPE Reservoir Evaluation & Engineering* **13** (6): 914-925. SPE-123206-PA.

Shi, J.-Q., Durucan, S., Fujioka, M. 2008. A Reservoir Simulation Study of CO_2 Injection and N_2 Flooding at the Ishikari Coalfield CO_2 Storage Pilot Project, Japan. *International Journal of Greenhouse Gas Control* **2** (1): 47-57.

Siemons, N., Busch, A., Bruining, H., Kroos, B. 2003. Assessing the Kinetics and Capacity of Gas Adsorption in coals by a Combined Adsorption/Diffusion Method. SPE Annual Technical Conference and Exhibition, Denver, Colorado. SPE 84340.

Smith, D.M., Williams, F.L. 1984. Diffusional Effects in the Recovery of Methane from Coalbeds. *SPE Journal* **24** (5): 529-535. SPE 10821-PA.

Somerton, W.H. 1975. Effect of Stress on Permeability of Coal. *International Journal of Rock Mechanics and Mining Science* **12** (5-6): 129-145.

Sparks, D.P., McLendon, T.H., Saulsberry, J.L., Lambert, S.W. 1995. The Effects of Stress on Coalbed Reservoir Performance, Black Warrior Basin, U.S.A. SPE Annual Technical Conference and Exhibition, Dallas, Texas. SPE 30743.

Spencer, S.J., Somers, M.L., Pinczewski, W.V., Doig, I.D. 1987. Numerical Simulation of Gas Drainage From Coal Seams. SPE Annual Technical Conference and Exhibition, Dallas, Texas. SPE 16857-MS.

Tan, T. 2002. Advanced Large-Scale Coalbed Methane Modelling Using a Conventional Reservoir Simulator. SPE Gas Technology Symposium, Calgary, Alberta, Canada. SPE 75672-MS.

Wang, G.X., Massarotto, P., Rudolph, V. 2009. An improved Permeability Model of Coal for Coalbed Methane Recovery and CO2 Geosequestration. *International Journal of Coal Geology* **77** (1-2): 127-136.

Wang, X., Ward, C. 2009. Experimental Investigation of Permeability Changes with Pressure Depletion in Relation to Coal Quality. International Coalbed Methane Symposium, Tuscaloosa, Alabama.

Warpinski, N.R., Teufel, L.W. 1990. Determination of the Effective-Stress Law for Permeability and Deformation in Low-Permeability Rocks. SPE Annual Technology Conference and Exhibition, New Orleans, Loisiana.

Warren, J.E., Root, P.J. 1963. The Behavior of Naturally Fractured Reservoirs. *SPE Journal* **3** (3): 245-255. SPE 426-PA.

Wei, X.R., Wang, G.X., Massarotto, P., Golding, S.D., Rudolph, V. 2007. A Review on Recent Advances in Numerical Simulation for Coalbed Methane Recovery Process. *SPE Reservoir Evaluation & Engineering* **10** (6): 657-666. SPE 93101-PA.

Wei, Zh., Zhang, D. 2010. Coupled Fluid-Flow and Geomechanics forTtriple-Porosity/Dual-Permeability Modeling of Coalbed Methane Recovery. *International Journal of Rock Mechanics and Mining Sciences* **47** (8): 1242-1253.

Young, G.B.C., McElhiney, J.E., Paul, G.W., McBane, R.A. 1991. An Analysis of Fruitland Coalbed Methane Production, Cedar Hill Field, Northern San Juan Basin. SPE Annual Technical Conference and Exhibition, Dallas, Texas. SPE 22913-MS.

Young, G.B.C., Paul, G.W., McElhiney, J.E., McBane, R.A. 1992. A Parametric Analysis of Fruitland Coalbed Methane Reservoir Producibility. SPE Annual Technical Conference and Exhibition, Washington, District of Columbia. SPE 24903-MS.

Zhdanov, M.A. 1962. *Oil and Gas Geology [Нефтегазопромысловая геология]*. State Scientific and Technical Publishing of Oil, Mining and Fuel Literature, Moscow, Russia.

Zheltov, Yu.P. 1985. *Collection of Problems in the Development of Oil Fields [Сборник задач по разработке нефтяных месторождений]*. Nedra, Moscow, Russia.

Zheng, Sh., Lili, X. 2011. Modeling and Simulation of a New Dual Porosity CBM Reservoir Model with an Improved Permeability Model through Horizontal Wells. SPE Middle East Unconventional Gas Conference and Exhibition, Muscat, Oman. SPE 141118-MS.

Zuber, M.D., Olszewski, A.J. 1992. The Impact of Errors in Measurements of Coalbed Methane Reservoir Properties on Well Production Forecasts. SPE Annual Technical Conference and Exhibition, Washington, District of Columbia. SPE 24908-MS.

Zuber, M.D., Sawyer, W.K., Schraufnagel, R.A., Kuuskraa, V.A. 1987. The Use of Simulation and History Matching To Determine Critical Coalbed Methane Reservoir Properties. Low Permeability Reservoirs Symposium, Denver, Colorado. SPE 16420-MS.

APPENDIX

CODE FOR BASE CASE IN MATHEMATICA SOFTWARE PACKAGE

Thesis Project:
Single-well Modeling of Coalbed Methane Production
Elena Martynova
2013

Initialization

```
(*Number format*)
Off[NumberForm::"sigz"]
nf2[x_]=NumberForm[x,2];
nf3[x_]=NumberForm[x,3];
nf4[x_]=NumberForm[x,4];
SetAttributes[{nf2,nf3,nf4},Listable]

(*Color*)
Maroon=RGBColor[0.65,0.08,0.25];

(*Conversion factors and constants*)
SpeedOfLightInVacuum=299792458;
NewtonianConstantOfGravitation=6.6742 10^-11;
ElementaryCharge=1.60217653 10^-19;
AvogadroConstant=6.022141510^23;
AtomicMassConstant=1.6605388610^-27;
gr=9.8066;
Ru=8.3145;
tera=10^12;
giga=10^9;
mega=10^6;
kilo=1000;
centi=0.01;
milli=0.001;
micro=10^-6;
nano=10^-9;
minute=60.;
hour=60. minute;
day=3600 24.;
```

```
year=365.25 day;
month=year/12;
mile=1609.3;
inch=2.54 10^-2;
ft=0.3048;
yard=0.915248;
cm=0.01;
mm=0.001;
acre=4046.9;
gal=0.00378541;
ounce=gal/128;
bbl=0.1589873;
lbm=0.4535924;
lbf=4.448222;
atm=101325.0;
torr=mmHg=133.3224;
psi=6894.757;
cp=0.001;
hp=745.7;
bpm=bbl/minute;
bpd=bbl/day;
gpm=gal/minute;
ppga=lbm/gal;
mcf=1000 ft^3;
mmcf=10^6 ft^3;
bcf=10^9 ft^3;
tcf=10^12 ft^3;
mcfd=1000 ft^3/day;
mmcfd=10^6 ft^3/day;
md=9.869233 10^-16;
darcy=kilo md;
Tsc=288.706;psc=14.65 psi;(*standard TX*);
Tnc=293.15;pnc=atm;(*normal*);
Mair=0.02897;
rhoairsc=psc/(Tsc Ru/Mair);
rhoairnc=pnc/(Tnc Ru/Mair);
muair=0.018 cp;
rhowat=1000.0;
muwat=1 cp;
rhowatnc=997.95;
(*temperature scales*)
degR=1/1.8;
KfrC[deg_]:=273.15+deg;
CfrK[deg_]:=-273.15+deg;
```

```
FfrR[deg_]:=-459.67+deg;
RfrF[deg_]:=459.67+deg;
KfrR[deg_]:=deg degR;
RfrK[deg_]:=1.8 deg;
KfrF[deg_]:=KfrR[RfrF[deg]];
FfrK[deg_]:=FfrR[RfrK[deg]];
CfrF[deg_]:=RfrK[KfrF[deg]];
FfrC[deg_]:=FfrK[KfrC[deg]];

(*Gas functions*)
(* use common gas data:
     - gas_gravity (w.r.t.air);
       - 3 mole fractions:yn2,yco2,yh2s;
       - absolute temperature (K);
       - pressuire (Pa);*)
(*Z-factor and viscosity*)
zmg[gg_?NumberQ,yn2_:0,yco2_:0,yh2s_:0][tabs_?NumberQ,ppa_?NumberQ]:=Modul
e[{a0=-2.462,a1=2.97,a2=-0.2862,a3=0.008054,a4=2.808,a5=-3.498,a6=0.3603,a7=-
0.01044,a8=-0.7933,a9=1.396,a10=-0.1491,a11=0.00441,a12=0.08393,a13=-
0.1864,a14=0.02033,a15=-
0.0006095,tran,p,ppc,tpc,ppr,tpr,m1hc,m1n2,m1co2,m1h2s,m1,mr,mg,E0,F0,D0,A0,B0,
C0,z},tran=tabs/degR;
  p=ppa/psi;
  ppc=678-50*(gg-0.5)-206.7*yn2+440*yco2+606.7*yh2s;
  tpc=326+315.7*(gg-0.5)-240*yn2-83.3*yco2+133.3*yh2s;
  ppr=p/ppc;
  tpr=tran/tpc;
  E0=9(tpr-1);
  F0=0.3106-0.49 tpr+0.1824 tpr^2;
  D0=10^F0;
  A0=1.39(tpr-0.92)^0.5-0.36 tpr-0.1;
  B0=(0.62-0.23 tpr)ppr+(0.066/(tpr-0.86)-0.037)ppr^2+0.32 ppr^6/10^E0;
  C0=0.132-0.32 Log[10,tpr];
  z=A0+(1-A0)Exp[-B0]+C0 ppr^D0;
  m1hc=8.188 10^-3-6.15 10^-3 Log[10,gg]+(1.709 10^-5-2.062 10^-6 gg) (tran-460);
  m1n2=(9.59 10^-3+8.48 10^-3 Log[10,gg])yn2;
  m1co2=(6.24 10^-3+9.08 10^-3 Log[10,gg])yco2;
  m1h2s=(3.73 10^-3+8.49 10^-3 Log[10,gg])yh2s;
  m1=m1hc+m1n2+m1co2+m1h2s;
  mr=a0+a1 ppr+a2 ppr^2+a3 ppr^3+tpr(a4+a5 ppr+a6 ppr^2+a7 ppr^3)+tpr^2(a8+a9
ppr+a10 ppr^2+a11 ppr^3)+tpr^3(a12+a13 ppr+a14 ppr^2+a15 ppr^3);
  mg=m1/tpr Exp[mr];
  {z,mg cp}];
(*rho density of gas at pressure*)
```

```
rhog[gg_?NumberQ,yn2_:0,yco2_:0,yh2s_:0][tabs_?NumberQ,ppa_?NumberQ]:=Modu
le[{z},z=zmg[gg,yn2,yco2,yh2s][tabs,ppa][[1]];
  ppa/(Ru/(Mair gg) z tabs)]
(*viscosity of gas at pressure*)
mug[gg_?NumberQ,yn2_:0,yco2_:0,yh2s_:0][tabs_?NumberQ,ppa_?NumberQ]:=zmg[g
g,yn2,yco2,yh2s][tabs,ppa][[2]]
(*compressibility factor of gas at pressure*)
zfg[gg_?NumberQ,yn2_:0,yco2_:0,yh2s_:0][tabs_?NumberQ,ppa_?NumberQ]:=zmg[gg
,yn2,yco2,yh2s][tabs,ppa][[1]]
(*compressibility of gas at pressure*)
cg[gg_NumberQ,yn2_:0,yco2_:0,yh2s_:0][tabs_NumberQ,ppa_NumberQ]:=Module[{rh
op},(rhop=rhog[gg,yn2,yco2,yh2s][tabs,ppa];(rhop-rhog[gg,yn2,yco2,yh2s][tabs,ppa-
10^3])/(rhop 10^3))]
```

Theory

```
Clear[p,Vads,Eyoung,υ,Vl,Pl,ε,Pε,pwi,pgi,εsi,ϕi,mcoal,cf,pe ,sw,swstar,ρgperρgi]
εsf[p_]=(ε*p)/(p+ Pε); (* total volumetric swelling/shrinkage strain - zero at pw=0 *)
△εsf[p_]=εsf[p]-εsi; (* total volumetric swelling/shrinkage strain change - zero at pw=0
*)
Vadsf[p_]=(Vl*p/(Pl+p)); (* Langmuir Isotherm  - volume adsorbed by 1 kg at
equilibrium *)
pVadsf[Vads_]=Pl Vads/(Vl-Vads); (*Inverse of Langmuir isotherm *)
△σf1[p_]=(-(υ/(1-υ)))*(p-pwi);   (* Lateral stress change from pore pressure 1 - direct
poroelastic effect *)
△σf2[p_]=(Eyoung*△εsf[p])/(3*(1-υ));      (* Lateral stress change from pore pressure 2
indirect effect of swelling/shrinkage *)

kpkif[p_,Vads_]=Exp[-3*cf*(△σf1[p]+△σf2[pVadsf[Vads]])];(* permeability ratio*)
kf[p_,Vads_]=ki kpkif[p,Vads]; (* absolute permeability *)
Jf[p_,Vads_]=0.1821*(kpkif[p,Vads])^2-0.7465*(kpkif[p,Vads])+1.5643; (* shape
factor *)
Lf[p_]=Vadsf[p]*mcoal; (* volume adsorbed at equilibrium by the coal mass being
drained *)
pcf[p_,swstar_,Vads_]:=pe(swstar^(-1/Jf[p,Vads])); (* capillary pressure pc=pg-pw *)
pgf[pw_,swstar_,Vads_]:=pw+pcf[pw,swstar,Vads]; (* pressure in gas phase *)
Swrf[p_,Vads_]=Swri/porosityperporosityif[p,Vads]; (* residual water saturation *)
Sgrf[p_,Vads_,ρgperρgi_]=Sgri/(porosityperporosityif[p,Vads]*ρgperρgi);  (* residual
gas saturation *)
Swstarf[p_,sw_,ρgperρgi_,Vads_]:=Clip[(sw-Swrf[p,Vads])/(1-Swrf[p,Vads]-
Sgrf[p,Vads,ρgperρgi]),{10^-6,1}]; (* normalized water saturation (movable water) *)
krwf[p_,sw_,ρgperρgi_,Vads_]:=krwstar*(Swstarf[p,sw,ρgperρgi,Vads])^(η+1+2/(Jf[p,
Vads]*λ));(* relative water permeability *)krgf[p_,sw_,ρgperρgi_,Vads_]:=krgstar*((1-
```

```
Swstarf[p,sw,ρgperρgi,Vads])^η)*(1-
(Swstarf[p,sw,ρgperρgi,Vads])^(1+2/(Jf[p,Vads]*λ))); (* relative gas permeability *)


solvoli=1-ϕi; (* fraction of volume occupied by solid at initial state*)
solvolf[p_,Vads_]=(solvoli+△εsf[pVadsf[Vads]]+(p-pwi)/(Eyoung*(1-υ)/((1+υ)(1-
2υ))))/(1+(p-pwi)/(Eyoung*(1-υ)/((1+υ)(1-2υ))));
porosityperporosityif[p_,Vads_]=(1-solvolf[p,Vads])/ϕi;(* porosity ratio *)
porecompressf[p_]=- D[porosityperporosityif[p,Vadsf[p]],p]//Simplify;
 (* pore compressibility as a derivative of  porosity change with pore pressure *)

(* gas pseudopressures *)
makefuns[gasGamma_, yn2_,yco2_,yh2s_,Tgas_]:=
 Module[{minpr,maxpr,np,ptab,p,z,mu,pzmtab,mtab},
  minpr=1 psi;maxpr=10000 psi; np=150;
  ptab=Exp[Range[ Log[minpr],Log[maxpr],Log[maxpr/minpr]/np]];
  pzmtab=Table[ {z,mu}= zmg[gasGamma, yn2,yco2,yh2s][Tgas, p]; p/(z mu),{p,ptab}
];
  pzmufun[p_]=Interpolation[{ptab,pzmtab}ᵀ,p];
  mtab=2  Table[ Integrate[pzmufun[pprime],{pprime,minpr,p}],{p,ptab}];
  Bgp[p_]:=(Tgas/Tsc)   (psc/p)  zfg[gasGamma, yn2,yco2,yh2s][Tgas,p];
  mfrompfun[p_]=Interpolation[{ptab,mtab}ᵀ,p];

  pfrommfun[m_]=Interpolation[{mtab,ptab}ᵀ,m];
  ];
```

```
Input
Data Input
{
 (* reservoir *)

 A=10000, (* Area of the model 100*100 - [m2] *)
 h=2 , (* Height of the model - [m] *)
 Swi=0.95, (* Initial water saturation *)
 ρc=1600, (* Density of coal - [kg/m3]*)

 (* gas property input *)

 Tres=305.15 , (* Temperature - [K] *)
 gasGamma=0.55,(* Gas gravity for pure methane (relative to air)*)
 Vl=0.027,(* Gas Langmuir volume constant - [m3/kg] *)
```

```
Pl=2.96 mega,(* Gas Langmuir pressure constant at 1/2 VL - [MPa] *)
ρch4liquid=414,(* Methane density in a liquid state, [kg/m3] *)

(* flow flow *)

pwi= 6.41 mega,  (* Initial average reservoir pressure for water phase - [MPa] *)
pe=0.006 mega,(* Entry capillary pressure - [MPa] *)
pwf=0.3 mega,   (* BHP - [MPa]*)
rw=0.1, (* Wellbore radius - [m] *)
s=0, (* skin-factor *)

Swri=0.84, (* Initial residual water saturation *)
Sgri=0, (* Initial residual gas saturation *)
krwstar=1, (* End-point relative permeability of water *)
krgstar=1, (* End-point relative permeability of water *)

η=1, (* Tortuosity coefficient *)
λ=0.22,(* Pore size distribution index *)

μw=6.5*10^-4, (* Viscosity of water - [Pa*s] *)
tau=50  day,(* diffusion time*)
ki=2  md, (* permeability, [mD] *)


(* Elastic properties *)

Eyoung=2900 mega,(* Young's modulus - [MPa] *)
υ=0.35,(* Poisson's ratio *)
ε=0.01266, (* Subscript[ε, L] - Langmuir volumetric strain constant *)
Pε=4.31 mega, (* Langmuir pressure constant at 1/2 Subscript[ε, L] - [MPa] *)
cf=0.2/mega,(* coal cleat compressibility, [1/MPa] *)


(* loop *)

deltat=0.25 day,
endday=365;
};
```

Calculation of some basic constants

```
makefuns[gasGamma, 0,0,0,Tres]; (* gas pseudopressure *)
endtime=endday day;
```

mcoal=A h ρc; (* mass of coal being drained *)
re=$\sqrt{\text{A}\,|\,|}$; (* drainage radius *)
JD=1/(Log[re/rw]-0.75+s); (* Dimentionless productivity index *)

(* minimum necessary porosity at initial state - from Langmuir Isotherm *)

ch4kgpercoalkg=(Vl*rhoairsc gasGamma) ;(* 1 kg of coal contains that mass in kg of gaseous methane *)
minimumporosityatpzero=(ch4kgpercoalkg/ρch4liquid)/(1/ρc) ;
(* part of volume that liquid methane would occupy = minimal porosity; in liquid state that mass of gas occupies ch4kgpercoalkg/ρch4liquid volume in [m3] *)
ch4kgpercoalkgpwi=Vadsf[pwi](rhoairsc gasGamma);
ϕi=((ch4kgpercoalkg-ch4kgpercoalkgpwi)/ρch4liquid)/(1/ρc); (* initial porosity for the adsorbed amount of gas that we currently have *)

Other initial values
εsi=εsf[pwi]; (* volumetric strain at initial pressure *)
pgi1=pgf[pwi,Swi,Vadsf[pwi]];
Vadsi1=Vadsf[pgi1];
swstari=Swstarf[pwi,Swi,1,Vadsi1];
pgi=pgf[pwi,swstari,Vadsi1]; (* initial gas pressure *)
Vadsi=Vadsf[pgi]; (* initial adsorbed gas per kg coal *)
swstari=Swstarf[pwi,Swi,1,Vadsi]; (* normalized water saturation at initial pressure and water saturation *)
Bgi=Bgp[pgi] ; (* gas volume factor at initial pressure *)
OFGIP=porvoli*(1-Swi)/ Bgi ; (* Original Free Gas in Place *)
adsini=Lf[pgi] ;(* Original adsorbed gas in place*)
porvoli=A*h*ϕi; (* initial pore volume *)
watvoli=porvoli*Swi;(* initial volume occupied by water *)
OGIP=OFGIP+adsini;
(* Original total gas in place expressed with standard conditions volume*)

Material balance module
Clear[pw,delt,ta, Wpo,Gpo,deso,matbal];

matbal[pw_,delt_,ta_,Wpo_,Gpo_,deso_]:=Module[{mb,

Sgrnew,sw,gasvol,gasscvol,rpri,swstar,pg,adsold,Vadsold,porosity,porvol,gasscvolnew,swstarnew,

qg,qwp,porositynew,porvolnew,pgnew,swnew,Gpnew,Wpnew,adsnew,desnew,gasvolnew,krwnew,krgnew,Swrnew,knew,zg,mg,Vads,rprinew},

```
  adsold=adsini-deso;(* gas volume adsorbed at equilibrium by total coal mass (state
before the deltat)*)
  Vadsold=adsold/mcoal; (* gas volume adsorbed by 1 kg of coal *)

  porosity= ϕi  porosityperporosityif[pw,Vadsold]; (* porosity at new pressure and
corresponding to volume of gas currently in matrix *)
  porvol= A h porosity;(* pore volume at new pressure and corresponding to volume of
gas currently in matrix *)

  Swrnew=Swrf[pw,Vadsold];(* residual water saturation *)
  knew=kf[pw,Vadsold]; (* permeability *)

  (*state before the deltat  to get saturation dependent quantities*)

  sw=(watvoli-Wpo)/porvol;(* current water saturation *)
  gasvol=porvol-(watvoli-Wpo); (* current volume available for gas at reservoir
conditions *)
  gasscvol=OFGIP-Gpo+deso;(* current gas volume at standard conditions *)
  rpri=Bgi/ (gasvol/gasscvol); (* gas density ratio ρg/ρgi=Bgi/Bg ???? *)
  Sgrnew=Sgrf[pw,Vadsold,rpri]; (* residual gas saturation *)
  swstar=Swstarf[pw,sw,rpri,Vadsold];(* normalized water saturation *)

  (*saturation dependent quantities*)

  krgnew=krgf[pw,sw,rpri,Vadsold]; (* relative permeability to gas *)
  krwnew=krwf[pw,sw,rpri,Vadsold]; (* relative permeability to water *)
  pg=pgf[pw,swstar,Vadsold]; (* pressure in gas phase *)
  (* {zg,mg}=zmg[gasGamma][Tres,(pg+pwf)/2]; *)

  (* gas rate *)
  (*qg=(π knew*krgnew h Tsc)/(psc Tres (zg mg) ) JD(pg^2-pwf^2);*)
  qg=π knew krgnew h  (Tsc/Tres)(1/psc) JD( mfrompfun[pg]-mfrompfun[pwf]);

  (* water rate *)
  qwp=(2π*knew*krwnew*h*JD/μw )*(pw-pwf);

  (* material balance *)

  Gpnew=Gpo+qg delt; (* cumulative gas production *)
  Wpnew=Wpo+qwp delt; (* cumulative water production *)
  desnew=deso+(adsold-Lf[pg] )delt/ta ;(* cumulative desorbed amount *)
  adsnew=adsini-desnew; (* adsorbed volume *)
```

```
  Vads=adsnew/mcoal; (* gas volume adsorbed by 1 kg of coal after deltat *)

  porositynew= ϕi  porosityperporosityif[pw,Vads]; (* porosity with new adsorbed
volume *)
  porvolnew= A h porositynew; (* pore volume with new adsorbed volume *)
  gasvolnew=porvolnew-(watvoli-Wpnew);
  gasscvolnew=OFGIP-Gpnew+desnew;
  rprinew=Bgi/ (gasvolnew/gasscvolnew);
  swnew=(watvoli-Wpnew)/porvolnew;
  swstarnew=Swstarf[pw,swnew,rprinew,Vads];
  pgnew=pgf[pw,swstarnew,Vads];

  mb=OFGIP+(desnew-Gpnew)-gasvolnew/ Bgp[pgnew];
  (* results *)

{mb,qg,qwp,porositynew,pgnew,swnew,Gpnew,Wpnew,adsnew,desnew,gasvolnew,krw
new,krgnew,Swrnew,knew,swstarnew}
  ];
```

```
Loop calculations
Clear[fun]
Dynamic[Row[{PaddedForm[t/day,{7,1}],"day",PaddedForm[Gpnew/OGIP,{5,3}],Padd
edForm[Gpnew/OGIP2,{5,3}]},"    "]]//Panel
xfact=1-10^Range[-3.05,-0.05,0.2];

(*First for calculating the first timestep we need initial state parameters *)
Gpold=0;Wpold=0;desold=0;pwold=pwi;tab={};
t=0;
Do[
 t=t+ deltat;
 pwsol=0;
 pw=.;
 fun[pw_?NumberQ]:=matbal[pw,deltat,tau,Wpold,Gpold,desold][[1]];

 mbold=Check[
             fun[pwold],
                  Print[{"Check 1","t/day",t/day,"pwold",pwold,"mbold",mbold}];Break[]
            ];
 (*bad cases*)
 If[ mbold≥0,pwsol=pwold;
  If[  i<10,
```

```
   Print[{"Positive mb old","i:",i,"t=",t/day,"mbold > 0, cannot be unless depleted, use
smaller deltat "}];
   Break[]
   ]
  ];

 (*mbold negative - good case*)
 pwfact=Cases[xfact pwold,l_/;l>pwf];
 pwpre=pwold;mblowpre=mbold;
  Do[
  mblow=Check[
    fun[pw],
    wrch=True;
    Print[{"Check 2","i:",i,"t/day",t/day,"pw",pw,"mb",mblow}];Break[]
    ];
  (* mblow >= 0 good *)
  If[mblow>0,
   pwlow=pw;pwup=pwpre;
   sol=FindRoot[ fun[pw],{pw,pwlow,pwup},AccuracyGoal→6,MaxIterations→50];
   pwsol=pw/.sol;Break[];
   ];
  (* mbold < 0 and mb is further decreasing: bad  *)
  If[mblow<mblowpre,pwsol=pwold; If[ i<10,
    Print[{"mbold<0 and mb is
decreasing","i:",i,"t/day",t/day,"pw,mblow:",pw,mblow}]];
   Break[]
   ];
  pwpre=pw;mblowpre=mblow;
  ,{pw,pwfact}];
 If[wrch,Print["We could not pass check, try smaller deltat"];Break[]];

 If[pwsol>pwf,

{mb,qg,qwp,porositynew,pgnew,swnew,Gpnew,Wpnew,adsnew,desnew,gasvolnew,krw
new,krgnew,Swrnew,knew,swstarnew}=matbal[pwsol,deltat,tau,Wpold,Gpold,desold];
  (* save *)

AppendTo[tab,{t/day,qg,qwp,pwsol,porositynew,pgnew,swnew,Gpnew,Wpnew,adsnew,
desnew,gasvolnew,krwnew,krgnew,Swrnew,knew/ki,swstarnew,mbold,mb}];
  (* rename cumulative values for use in next loop round *)
  Gpold=Gpnew;Wpold=Wpnew;desold=desnew;pwold=pwsol;
  ,
  qg=qwp=0;
```

```
AppendTo[tab,{t/day,qg,qwp,pwsol,porositynew,pgnew,swnew,Gpnew,Wpnew,adsnew,
desnew,gasvolnew,krwnew,krgnew,Swrnew,knew/ki,swstarnew,mbold,mb}];
  ];
 ,{i, endtime/deltat}
 ];
```

Plots in SI

```
frame[legend_]:=Framed[legend,RoundingRadius→10,FrameMargins→0,Background-
>LightYellow];
ip=IntegerPart[day/deltat];
dt=tab[[ip;;-1;;ip,1]];
qgt=tab[[ip;;-1;;ip,2]];
qwt=tab[[ip;;-1;;ip,3]];
Gpt=tab[[ip;;-1;;ip,8]];
pwt=tab[[ip;;-1;;ip,4]];
dest=tab[[ip;;-1;;ip,11]];
Wpt=tab[[ip;;-1;;ip,9]];
swt=tab[[ip;;-1;;ip,7]];
pgt=tab[[ip;;-1;;ip,6]];
krgt=tab[[ip;;-1;;ip,14]];
krwt=tab[[ip;;-1;;ip,13]];
Swrt=tab[[ip;;-1;;ip,15]];
desorbt=tab[[ip;;-1;;ip,11]];
kk0t=tab[[ip;;-1;;ip,16]];


pl1=Show[ListPlot[{{dt,Gpt/(1000)}ᵀ,{dt,Wpt}ᵀ},Joined→True,PlotStyle→{Red,Blue},P

lotRange→All,GridLines→Automatic,Frame→True,PlotMarkers→{""},FrameLabel→{"ti
me, [day]","Gp, [thousand m^3]; Wp,
[m^3]"},PlotLegends→Placed[LineLegend[{"Gp","Wp"},LegendFunction→frame,Legend
Layout→"Column",LabelStyle→8],{0.8,0.6}]]];

pl4=Show[ListPlot[{dt,swt*100}ᵀ,Joined→True,PlotStyle→{Blue},PlotRange→All,Grid

Lines→Automatic,Frame→True,PlotMarkers→{""},FrameLabel→{"time, [day] ", "Sw,
[%]"}]];

pl5=Show[ListPlot[{{dt,qgt/(1/day)}ᵀ,{dt,1000qwt/(1/day)}ᵀ},Joined→True,PlotStyle→{

Red,Blue},PlotRange→All,GridLines→Automatic,Frame→True,PlotMarkers→{""},Fram
eLabel→{"time, [day]","qg, [m^3/day]; qw,
[liter/day]"},PlotLegends→Placed[LineLegend[{"qg","qw"},LegendFunction→frame,Le
gendLayout→"Column",LabelStyle→8],{0.8,0.6}]]];
```

```
pl8=Show[ListPlot[{{dt,krgt}^T,{dt,krwt}^T},Joined→True,PlotStyle→{Red,Blue},PlotRan
ge→{0,1},GridLines→Automatic,Frame→True,PlotMarkers→{""},FrameLabel→{"time,
[day]", "kr, [-]
"},PlotLegends→Placed[LineLegend[{"krg","krw"},LegendFunction→frame,LegendLay
out→"Column",LabelStyle→8],{0.8,0.4}]]];

pl9=Show[ListPlot[{{swt*100,krgt}^T,{swt*100,krwt}^T},Joined→True,PlotStyle→{Red,B
lue},PlotRange→All,GridLines→Automatic,Frame→True,PlotMarkers→{""},FrameLabel
→{"Sw, [%]", "kr, [-]
"},PlotLegends→Placed[LineLegend[{"krg","krw"},LegendFunction→frame,LegendLay
out→"Column",LabelStyle→8],{0.8,0.5}]]];

pl10=Show[ListPlot[{{dt,Swrt*100}^T,{dt,swt*100}^T},Joined→True,PlotStyle→{Red,Blu
e},PlotRange→All,GridLines→Automatic,Frame→True,PlotMarkers→{""},FrameLabel→
{"time, [day]", "Sw, [%]
"},PlotLegends→Placed[LineLegend[{"Swr","sw"},LegendFunction→frame,LegendLay
out→"Column",LabelStyle→8],{0.8,0.7}]]];

pl12=Show[ListPlot[{dt,desorbt/mega}^T,Joined→True,PlotStyle→{Blue},PlotRange→All
,GridLines→Automatic,Frame→True,PlotMarkers→{""},FrameLabel→{"time, [day] ",
"V desorbed, [million m^3]"}]];

pl15=Show[ListPlot[{dt,kk0t}^T,Joined→True,PlotStyle→{Blue},PlotRange→All,GridLin
es→Automatic,Frame→True,PlotMarkers→{""},FrameLabel→{"time, [days]", "k/k0"}]];


pl17=Show[ListPlot[{{pwt/mega,qgt/(1/day)}^T,{pwt/mega,1000*qwt/(1/day)}^T},Joined
→True,PlotStyle→{Red,Blue},PlotRange→All,GridLines→Automatic,Frame→True,Plot
Markers→{""},FrameLabel→{"pwa, [MPa]","qg, [m^3/day]; qw,
[liter/day]"},PlotLegends→Placed[LineLegend[{"pg","pw"},LegendFunction→frame,Le
gendLayout→"Column",LabelStyle→8],{0.8,0.5}]]];


pl16=Show[ListPlot[{{dt,pgt/mega}^T,{dt,pwt/(mega)}^T},Joined→True,PlotStyle→{{Red,
Thick},Blue},PlotRange→All,GridLines→Automatic,Frame→True,PlotMarkers→{""},Fr
ameLabel→{"time, [day]","p,
[MPa]"},PlotLegends→Placed[LineLegend[{"pg","pw"},LegendFunction→frame,Legen
dLayout→"Column",LabelStyle→8],{0.8,0.7}]]];

Magnify[GraphicsRow[{pl5,pl1},ImageSize→500],2]//Panel
Magnify[GraphicsRow[{pl10,pl4},ImageSize→500],2]//Panel
Magnify[GraphicsRow[{pl8,pl9},ImageSize→500],2]//Panel
```

```
Magnify[GraphicsRow[{pl15,pl12},ImageSize→500],2]//Panel
Magnify[GraphicsRow[{pl17,pl16},ImageSize→500],2]//Panel
```